Dissecting the mechanism of HP1 mediated chromatin compaction

by
Madeline Keenen

DISSERTATION
Submitted in partial satisfaction of the requirements for degree of
DOCTOR OF PHILOSOPHY

in

Biochemistry and Molecular Biology

in the

GRADUATE DIVISION
of the
UNIVERSITY OF CALIFORNIA, SAN FRANCISCO

Approved:

DocuSigned by:
Barbara Panning
B18F20197C95417...

Barbara Panning
Chair

DocuSigned by:
David Agard
D2C1B9F[illegible]46A...

David Agard

DocuSigned by:
David Morgan
DAC[illegible]5472...

David Morgan

DocuSigned by:
Geeta Narlikar
B52[illegible]43B...

Geeta Narlikar

DocuSigned by:
A9C649A156A64AA...

Sy Redding

Committee Members

Acknowledgements

My life and this research has been shaped by the people I have had the privilege to work with. I would like to first thank my mentor Geeta Narlikar, whose incredibly precise mind taught me how to methodically think through a problem while still allowing time during each meeting to daydream about the crazy scientific possibilities we had no proof yet for. To my co-mentor Sy Redding, who provided the ideas to many of the experiments, funded much of the research, and from whom I've learned a lot.

To my committee, with whom this work would be a shell of what it was. David Morgan has been a constant advocate, and his faith in my scientific potential in my first year allowed me to begin to believe in it myself. David Agard's enthusiastic questioning in committee meetings was an honor that pushed me to be a more thoughtful and quantitative scientist, even as I was struggling to keep up. Barbara Panning, who has mentored me and countless others with compassion and kindness, is simultaneously one of the quickest scientists and deepest thinkers I have had the privilege to work with.

To my mentor Sue Kim, as without her early faith in me I would be on a completely different path. But you did, I grant you, warn me.

To Lucy Brennen, who allowed me to be both a human being and a scientist. You taught me physics with unhuman patience, built my confidence up when I was uncertain my experiments were worthwhile, and will remain one of my favorite people in the world to think about and do science with. It was a privilege to watch and learn from your compassionate leadership. To Luke Strauskulage, whose kind heart and generosity with his time reminded me what was important is people and silently challenged me to rearrange my priorities. Your methodical inquisitiveness as a scientist is a model I aim to follow in my post-doc. To Robbie Diaz, who combines a daring approach to life and science with the kindness of hearts. To Dana Kennedy, who is both brilliant and kind. To Adam Larson, who is an absolutely incredible scientist, for setting such a beautifully

high standard for this project. To Nathan Gamarra, for being the best rotation mentor ever and to Emily Wong, whose patience and kind heart was a huge source of joy.

I've been so lucky to have so many wonderful friends help me through graduate school. Eliza Nieweglowska, you are a joy to be around, a badass scientist, and slowly mentored me to be a more reliable, better friend. To my eternal roommates Paola Soto-Perez, who has a wonderful combination of self-confidence and kindness, and Rosa Rodriguez, who is quietly hilarious and brightens the day of everyone around her (so does Paola, sorry). I'll admit it here, I should have never moved out. Living and learning with you both was a highlight of my life. Although I'd next like to thank my new roommates and friends, Ben Barsi-Rhyne and Elise Muñoz, who were a complete joy and excellent at puzzles. To Dinara Azimova and Pedro Aguilar, whose generosity knows no bounds. You are two of the smartest, most enjoyable people I know. To countless other people, but most certainly including: Mitchell Lopez, Nat Hendel, Stephanie Johnson, Betsy Martin, Katie Augspurger, Lina Leon, Rebecca McGillivary, Leeanne Goodrich, Nick Sanchez, Rachel Greenstein, Henry Ng, Eric Simental, and Christopher Carlson.

To my best friends, in alphabetical order: Aliya, Emily, and Kaitie. You supported me through this journey, and all of the next ones and I am forever grateful.

To my brothers Jeffrey, Michael, and Bradley for reminding me that I am not my science. Finally, to my parents, who are my biggest role models. You bore the brunt of the anxiety and depression this phase of my life spurred, but often reminded me that every phase has an end and they'd be there to see me through it. This work would not have been possible without your support.

Acknowledgment of Previously Published and Submitted Work

Larson, A. G. *et al.* Liquid droplet formation by HP1α suggests a role for phase separation in heterochromatin. *Nature* **547**, 236–240 (2017).

Keenen M.M., Brown D, Brannan L.B., Renger R, Khoo H, Chrisotpher C.R., Huang B, Grill, S.W., Narlikar N.J., Redding S. HP1 proteins compact DNA into mechanically and positionally stable phase separated domains. *bioRxiv* 2020.10.30.362772; doi: https://doi.org/10.1101/2020.10.30.362772

Abstract

Dissecting the mechanism of HP1 mediated chromatin compaction

Madeline Keenen

Heterochromatin protein-1 (HP1) maintains condensed, stable heterochromatin domains throughout interphase despite the weak binding and rapid exchange of HP1 within heterochromatin. I utilize two methods, DNA curtains and liquid-liquid phase separation (LLPS) assays, to decode a mechanistic understanding of HP1 behavior and directly test if dynamic HP1 binding can maintain static DNA compaction *in vitro*. Within droplets, we find HP1α and DNA have distinct material properties: HP1α rapidly exchanges within and between droplets while simultaneously condensing DNA into stable domains within a droplet. Further, we show HP1α compacted DNA puncta are resistant to 40pN of force, over twice that required to stall RNA polymerase. I find the disordered regions of the three human HP1 paralogs - HP1α, HP1β, and HP1γ – dictate their DNA compaction and LLPS phenotypes. The HP1α hinge is necessary and sufficient for these activities, and we determine a network of hinge autoregulation within the N- and C- terminal extensions. I demonstrate dynamic HP1α binding primes droplets for regulation as the addition of HP1β, which exhibits minimal DNA compaction and LLPS behavior, invades and dissolves preformed HP1α droplets. Finally, I utilize chromatin substrates and find HP1 maintains separate domains of unmodified and H3K9me3 chromatin. Together this data describes how a pool of weakly bound HP1 proteins exploits both the collective behavior of proteins and the polymer properties of DNA to produce self-organizing domains that are simultaneously stable and fragile.

Table of Contents

List of Figures

List of Tables

Introduction

Every cell in the human body contains the exact same genetic information. However, these cells must differentiate into a wide variety of specialized cell types. This requires cells to selectively control which genes are transcribed and which are silenced. A major mechanism of transcriptional control in humans is the organization of the genome into transcriptionally inactive heterochromatic regions and transcriptionally active euchromatic regions. While over a century of research has allowed a detailed list of observations and proteins involved in heterochromatin formation, a cohesive mechanistic model to explain how (and even if) heterochromatin structure leads to transcriptional silencing remains elusive. This introduction will first delve into early observations of genomic organization and its relationship to transcriptional output, then describe some current models for how heterochromatin proteins mechanistically achieve gene inactivation.

Structure/function studies of heterochromatic domains in the 20th century

In the late 19th century progress made in light microscopy, cell fixation, and staining techniques allowed scientists to visualize chromatin in the nucleus. Careful observation of nuclei from over one hundred organismal species and technique development by Emil Heitz allowed him to make one of the first descriptions of chromatin organization. Heitz noticed two types of chromatin morphologies. Euchromatin was lightly stained by carmine acetic acid during interphase but transformed during mitosis into densely stained, compacted chromosomes. In contrast, heterochromatic regions maintained the densely stained, compacted structures throughout the cell cycle. Heitz determined that individual chromosomes can contain both heterochromatic and euchromatic regions, identified centromeres as heterochromatic, and found drosophila species with one euchromatic and one heterochromatic X chromosome. These studies underscore the importance of performing a detailed observation of a system: simply visualizing chromatin morphology during the cell cycle provided powerful observations that have led to entire subfields of chromatin biology.

There was no model system to understand the function of heterochromatin, however, until Muller discovered position effect variegation (PEV) in 1930. Muller found a translocation of the chromosome arm containing the *white* gene, which provides the red pigmentation of the fly eye. While this chromosome was abnormally arranged, it was present in the cell at the correct dosage. Instead of seeing either a normal or mutant phenotype, however, Muller saw these flies had molted eyes with patches of both red and white (Muller, 1930). The gene was therefore still functional in some cells, and scientists speculated the cells without the red pigment had somehow lost the DNA encoding the red gene (Schultz, Muller, others). Interestingly, this variegation phenotype was dependent on the temperature the flies were kept at. The translocation was soon mapped and shown that the *white* gene had been positioned adjacent to pericentric heterochromatin, which Heitz and others had found are inert, heterochromatic species (Schultz, 1936). Demerec and Slizynska showed that these position effect variegation patterns were actually reversible in an individual fly eye and this reversibility was dependent on the distance of the gene from the pericentric heterochromatin, indicating that the cells with white eye phenotype must still have a functional copy of the white gene. So how do you accomplish gene silencing in a position dependent manner?

The early hypothesis that PEV was caused by a change in the number of gene copies in certain cells was further disproven in the late 20th century and was instead suggested to be a product of transcriptionally regulation and not gene dosage (Heinikoff 1981, Tartof et al., 1984). Prokofyeva-Belgovskaya, a Russian female scientist, had detected examples of PEV both where euchromatin is translocated close to a heterochromatic site and became heterochromatinized, but also many examples of the reverse where a heterochromatic site is translocated to a euchromatic site and takes on the characteristics of diffuse euchromatin. Therefore, she speculated that the translocated chromatin took on the characteristics of nearby genomic regions (Prokofyeva-Belgovskaya, 1948). The idea was starting to form that heterochromatin could spread into adjacent regions and influence both the morphology and subsequent gene expression of the

region. This correlation was directly detected in the salivary gland cells of Drosophila that had a chromosome translocation of a locus important for polytene chromosome puffing into the vicinity of centromeric chromatin. Zhimulev found that in cells where this gene is phenotypically inactive, the reporter gene is packaged into a dense block of heterochromatin (Zhimulev et al., 1986), indirectly indicating gene packaging had an impact on transcriptional output (Heinikoff 1981). The cytological observation of dense heterochromatin packaging led to the idea that heterochromatin was less accessible than euchromatic regions. This hypothesis was tested at a molecular level by Wallrath and Elgin in 1995. They found a translocated gene placed next to pericentric regions had reduced accessibility to restriction enzyme digestion and more regular nucleosome spacing, directly relating structural changes in DNA accessibility to both the increased DNA density observed via microscopy and changes in gene expression during PEV. Advances in EM and super-resolution microscopy in the last few years has allowed visualization of nuclear DNA with unprecedented resolution and confirmed these early speculations that heterochromatic regions are indeed more densely compacted than the euchromatic regions of the genome (Boettiger et al., 2016 and Ou et al., 2017).

As the cytological and functional aspects of heterochromatin were being characterized, a hunt began for the proteins involved in achieving such phenotypes. Schultz and Spofford identified the first mutations that affected the variegation phenotype in 1950 and 1967, and these are now labeled suppressors of variegation (Su(var)) or enhancers of variegation (E(var)) (Elgin and Reuter, 2013). A major mediator of heterochromatin, heterochromatin protein-1 (HP1) was cloned in 1986 and a mutation in the HP1 gene found to be a suppressor of PEV (James and Elgin, 1986 and Eissenberg et al., 1990). It was later found the targeting of HP1 to an ectopic gene locus results in both transcriptional silencing and condensation of DNA *in vivo* (Verschure et al., 2005). These results are reminiscent of the correlative studies done by Zhimulez. While HP1 localization, DNA condensation, and transcriptional silencing are concurrent, a lack of mechanistic details into

HP1 function has made it challenging to definitively test whether it is the ability of HP1 to compact chromatin, or some other function, that leads to silencing.

Mechanism of compaction and transcriptional silencing

Biochemical studies have shown that HP1 proteins can oligomerize and compact chromatin (Yamada et al., 1999, Canzio et al., 2011&2103, Azzaz et al., 2014). These studies help explain how HP1 can contribute to stable chromatin compaction and to the ability of heterochromatin structures to spread across large genomic regions (Yamada et al., 1999, Canzio et al., 2011). On the other hand, fluorescence recovery after photobleaching (FRAP) experiments have demonstrated that human HP1 proteins bind transiently to heterochromatin, exchanging on the seconds timescale with other HP1 molecules in the nucleus (Cheutin et al., 2003, Festenstein et al., 2003). Such rapid exchange of HP1 molecules is consistent with micromolar oligomerization affinities of HP1 molecules. These studies can explain how rapid disassembly of heterochromatin could be enabled upon expression of specific transcriptional activators that can compete for sites in heterochromatin as HP1 exchanges (Cheutin et al. 2003). However, together these findings raise the central question of how a rapidly exchanging pool of weakly oligomerizing HP1 proteins can result in the stable compaction of DNA.

Dissection of the HP1 paralogs

The HP1 paralogs share a common domain architecture: three disordered regions interspaced by a chromodomain (CD) and a chromoshadow domain (CSD) (Grewal and Elgin, 2002). The CD binds to H3K9me (Platero et al., 1995), the CSD mediates HP1 dimerization and interactions with other nuclear proteins (Brasher et al., 2000 and Thiru et al., 2004), and the disordered hinge mediates binding to DNA (Sugimoto et al., 1996 and Zhao et al., 2000). Across the paralogs, both the CD and CSD show high conservation of sequence. Interestingly, the unstructured regions have diverged from one another, yet the charge character of each domain is conserved between HP1 paralogs, with only the C-terminal extension of HP1γ breaking this rule.

In the cell, HP1α is found at compacted heterochromatic regions bearing tri-methylation of histone 3 at lysine 9 (H3K9me3) and is thought to localize via direct recognition of histone methylation by the HP1 chromodomain (CD) (Platero et al., 1995). However, recruitment to these domains can occur prior to histone modification, implying that HP1α responds to additional molecular inputs (Yuan and O'Farrell 2016). Furthermore, while mutations that abolish H3K9me recognition disrupt genomic localization in cells, so do mutations within the unstructured hinge region of HP1α required for DNA binding (Muchardt et al., 2002 and Mishima et al., 2012). In fact, all three HP1 paralogs display unique nuclear localization patterns despite all bearing a well conserved CD, with HP1β and HP1γ often localizing to euchromatic regions lacking H3K9 methylation entirely (Smothers et al., 2000 and Dialynas et al., 2007). These observations raise the possibility that the diverging phenotypes of the HP1 paralogs observed *in vivo* arise in part from differential DNA binding, compaction, and phase separation activities seen *in vitro*.

Phase separation of chromatin proteins

It has been hypothesized that the cell takes advantage of phase separation to organize its genetic material (Hancock, 2014). Recent findings of liquid-liquid phase separation (LLPS) behavior by HP1 proteins provide a new perspective from which to address the questions raised above (Larson et al., 2017, Strom et al., 2017, Sanulli et al., 2019, Ackerman et al., 2019, Wang et al., 2019., Erdel et al., 2020). At a superficial level, LLPS has the potential to explain some of the seemingly contradictory properties of HP1-mediated heterochromatin. The emergence of two phases, one with a high concentration of molecules and the other low, is often mediated by weak and dynamic multivalent interactions in the high concentration phase, which would facilitate rapid competition by competitor proteins. At the same time, phase-separation can allow for stable sequestration of the molecules within the concentrated phase (Hyman et al., 2014, Alberti et al., 2019). Therefore, I wished to determine whether the phase separation of HP1 proteins could explain both the stable compaction and rapid dissolution of heterochromatic domains.

Chapter 2: Dynamic binding of HP1α maintains the static compaction of DNA domains

2.1 Introduction

Since the mid-20th century scientists studying heterochromatin have been debating a core enigma of the field: heterochromatin is an inert, stable structure while simultaneously being rapidly reversible. While the inert nature of heterochromatin was initially defined when visualizing the stable heterochromatic compaction throughout the cell cycle, recent work has demonstrated heterochromatic regions are positionally stable throughout interphase (Vasquez et al., 2001, Chubb et al., 2002, Gerlich et al., 2003). However, during cellular differentiation or DNA replication these stable structures need to be rapidly disassembled in response to environmental and development cues. The finding that HP1 molecules in these domains exchange within seconds provides some insight into how these domains can be dissolved, as competing molecules would be able to rapidly displace HP1 proteins from DNA (Cheutin et al., 2003, Festenstein et al., 2003, Kilic 2015). However, such models raise the fundamental question of how HP1 molecules, which are dynamic on the order of seconds, enable chromatin states that are stable on the order of hours. A challenge in the field has been developing assays that allow for real-time visualization of HP1-activity. Herein, I utilize DNA curtains, LLPS droplet assays, and optical trap experiments to visualize dynamic HP1 binding and test the stability of DNA compacted by HP1.

2.2 Results

A previous graduate student in the Narlikar lab, Adam Larson, found that HP1α shows the most robust phase-separation and DNA compaction abilities of all of the HP1 paralogs (Larson et al., 2017). I therefore used HP1α and DNA as a model system to dissect the steps involved in DNA compaction and phase-separation and to study the material properties of the resultant phases.

2.2.1 HP1α binds DNA globally but compacts DNA locally

To characterize DNA compaction by HP1α, I leveraged a single molecule DNA curtain approach (Figure 2.1A) (Greene et al., 2010). In this assay, ~50kbp molecules of DNA from bacteriophage λ are fixed to the surface of a microfluidic flowcell via a supported lipid bilayer. Visualization of DNA is achieved by labeling with the intercalating dye YOYO-1 and the end of the DNA strand is labeled with a fluorescent dCas9 (Figure 2.1A-B). Upon HP1α injection, a DNA puncta is first formed at the end of the DNA strand (Figure 2.1C-middle panel, E) and then rapidly and sequentially incorporates upstream DNA in a linear fashion until a single puncta lies at the top of the barrier (figure 2.1C, bottom panel, figure 2.1D, F, H). HP1α compaction is electrostatically mediated as a high salt wash (0.5M KCl) dissolves the DNA puncta (Figure 2.1D). The initial puncta formation at the DNA end could be explained by the lower tension exhibited at untethered DNA end. This allows the DNA to explore a larger distribution of conformational states that increases the probability that two non-adjacent DNA-sites will come into contact. HP1α could then capitalize on these conformations to bridge distal sites together, thus forming a puncta of DNA at the free end. Subsequent compaction of the HP1-DNA puncta would occur by further bridging sites at the puncta to that of upstream DNA. Compaction from the untethered end of λ DNA is in agreement with modeling from Ostrovsky and Bar-Yam and has been previously seen upon the addition of protamine, a protein containing arginine patches that facilitates compaction of sperm DNA into toroid structures in the mammalian spermatid (Ostrovsky and Bar-Yam, 1995 and Brewer et al., 1999). Similar to the protamine structure, HP1α contains three basic patches in the hinge domain which when mutated abrogate DNA binding. To test whether the basic patches are essential for compaction, the lysine and arginine residues of one basic patch in HP1α was mutated to alanines (BPm). Indeed, the BPm severely abrogated DNA compaction (Figure 2.1H), consistent with an electrostatically mediated compaction process.

Interestingly, protamine compaction is thought to be dependent on the complete coverage of the protein along the length of the DNA molecule upstream of the puncta site (Brewer et al.,

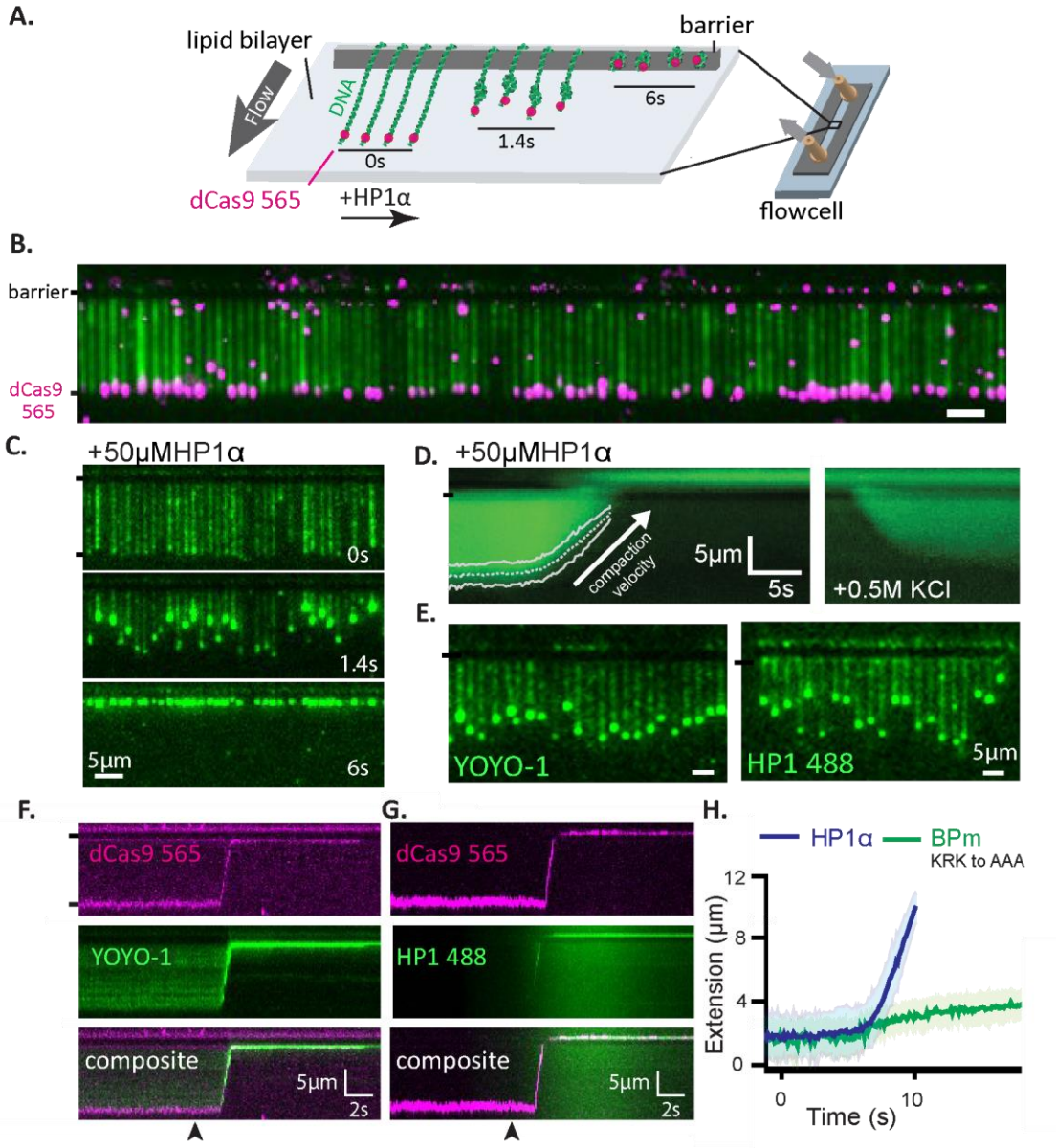

Figure 2.1. Characterization of DNA compaction by HP1α. **A.** Cartoon of the DNA curtains assay showing compaction of DNA. **B.** DNA curtain end-labeled with fluorescent dCas9 (C-). The dCas9 is targeted to a site 750bp from the untethered end of the DNA. **C.** Timestamped images of DNA labeled with YOYO-1 undergoing compaction by 50μM HP1α (unlabeled) shown before, during, and after compaction. **D.** Average kymograph DNA labeled with YOYO-1 and compacted over time with 50μM HP1α overlayed with the fit for average compaction (dashed line) and standard deviation (solid line). Upon full compaction of the DNA strand the buffer was changed to include 0.5M KCl and de-compaction visualized. **E.** Still images during DNA compaction of either DNA labeled with YOYO-1 (top) or HP1α-488 (bottom). **F. and G.** Kymograms of DNA compaction by 50μM HP1α. **F.** DNA labeled with YOYO-1 (top), dCas9-565 (middle), and composite image (bottom). **G.** HP1α-488 (top), DNA labeled with dCas9-565 (middle), and composite image (bottom). Arrowheads represent approximate time of protein injection. **H.** Overlayed trajectories of DNA compaction by HP1α and HP1α basic patch mutant (BPm) with average shown with the solid line and standard deviation is shaded.

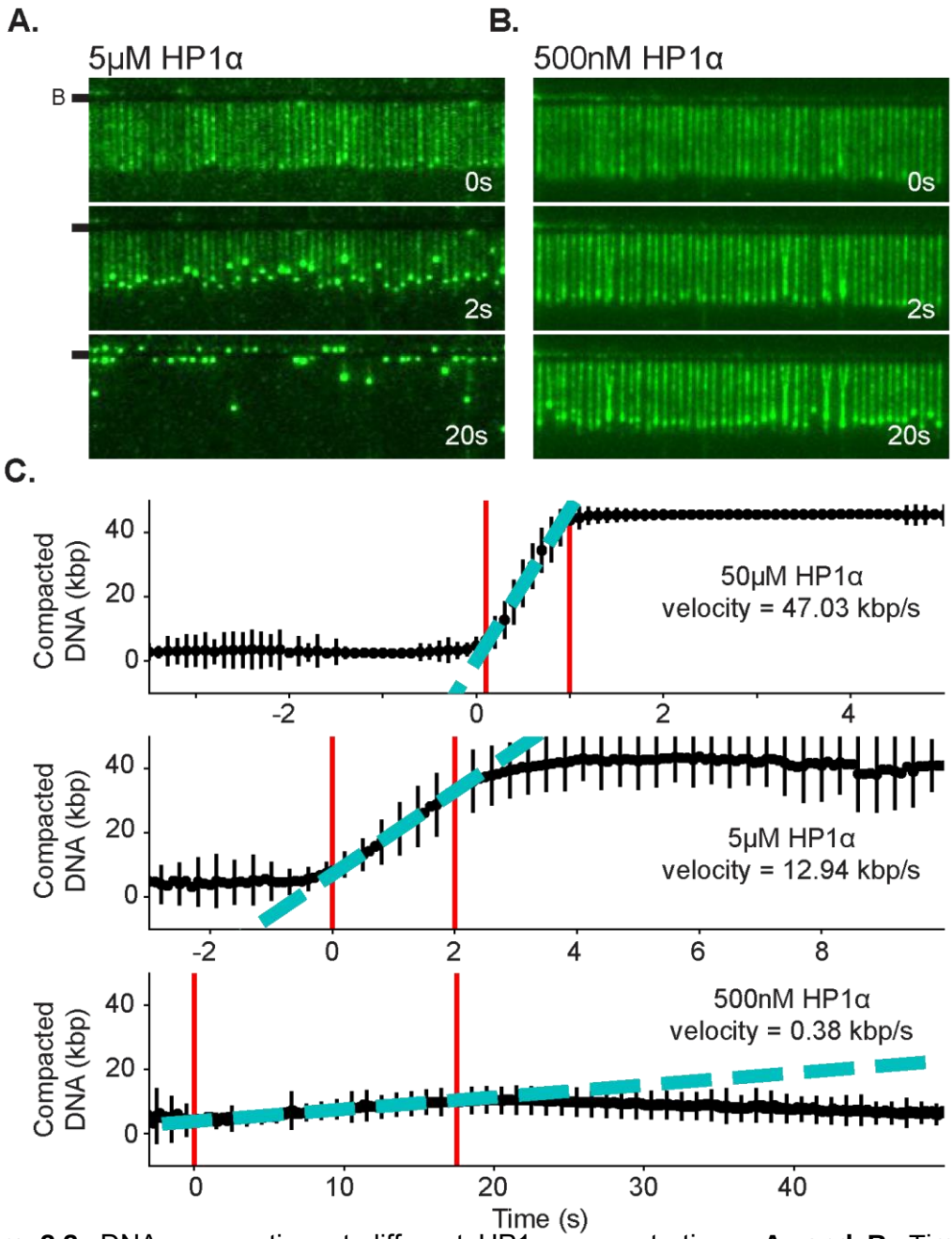

Figure 2.2. DNA compaction at different HP1α concentrations. **A. and B.** Timestamped images of DNA compaction by either **A.** 5μM or **B.** 500nM HP1α. DNA is labeled with YOYO-1. (B-) or (-) specifies location of the barrier. **C.** Average DNA compaction for 50μM, 5μM and 500nM HP1α. Compaction velocity estimated from linear fit to data (cyan). Fit constrained to the region within the two red lines.

1999). This global binding would facilitate bridging of the puncta to upstream DNA when natural DNA fluctuations occurred. To test the HP1α coverage along the DNA strand during the compaction process, I labeled HP1α with Atto-488 (HP1α-488). HP1α-488 initially localizes all across the DNA strand and then rapidly forms a puncta of HP1α molecules at the free DNA end (Figure 2.1E,G) identical in position to the DNA labelled puncta (Figure 2.1E-G). HP1α-488 coat the length of the DNA before a linear decrease in DNA length occurs as the puncta compacts up (Figure 2.1G, 50μM HP1α), consistent with the predictions of Ostrovsky and Bar-Yam. To test how protein occupancy affects compaction velocity, I performed experiments with varying HP1α concentrations and measured the decrease in DNA length over time (Figure 2.2A-C). We see an increase in DNA compaction rate as we raise the HP1α concentration, implying compaction rate is dependent on the amount of protein bound along the length of DNA. Interestingly, this model predicts that genomic regions with low HP1 affinity and occupancy of HP1 binding sites would not be incorporated into HP1 domains.

Together, this data suggests HP1α acts as an electrostatic, non-covalent tether to bridge DNA sites. The free DNA end exhibits less constrained diffusion, allowing it to sample a larger distribution of conformational states. HP1α can capitalize on these conformations to bridge distal sites together, thus forming a puncta of DNA at the free end. Experiments with fluorescent protein demonstrate HP1α is bound both within the puncta and along the length of the DNA strand. This HP1α coating would allow tethering to occur when the DNA puncta comes into close contact with a site of upstream uncompacted DNA, resulting in the linear compaction of the puncta up the length of the DNA strand in a protein concentration dependent fashion. Intrinsic to the DNA curtains experiments is visualization of single stands of DNA tethered on one end and isolated from adjacent DNA stands. I next wished to relax this constraint and visualize the ensemble HP1α behavior when it can bind to multiple strands of DNA at once in bulk solution.

2.2.2 Condensate formation is more sensitive to the concentration of HP1 than of DNA

To further uncover the molecular details of how HP1α organizes DNA, I initially use a short (147bp) dsDNA oligomer proportional to the persistence length of DNA to avoid overly complicated contributions of the polymer behavior, and titrated both DNA and protein to produce a phase diagram. As seen previously, at these buffer conditions (70mM KCl, 20mM Hepes, 1mM DTT) both HP1α and DNA alone are miscible in solution even at exceedingly high concentrations (400μM HP1α and 4μM 147bp DNA) (Figure 2.3A, left column and bottom row). However, when mixed at high concentrations (4μM 147bp DNA and 400μM HP1α, estimated 2 HP1α dimers bound per 147bp DNA) macroscopic droplets emerge (Figure 2.3A-top right corner, Figure 2.4B). The network of weak, multivalent interactions required to form phase-separated droplets is consistent with HP1α's ability to capture and stabilize distal segments of DNA leading to DNA compaction as discussed in the previous section.

One way to quantify the phase-separation capability of a molecule is through measurement of its critical concentration. Empirically, the critical concentration is defined as the concentration of the molecule above which the system separates into two phases. Theoretically, this transition occurs at the concentration at which the collective weak interactions of the system pay the entropic cost of de-mixing. In a two-component system, such as HP1α and DNA, each component may contribute differentially to condensation, and measuring the critical concentration of each component can provide insights into how the two components interact to form condensates.

As the concentration of HP1α is titrated down the HP1α critical concentration exhibits a sharp cutoff at 25-50μM of HP1α (Figure 2.3A). In contrast, upon varying DNA concentration there was a continuous rather than sharp transition in droplet appearance and size, such that droplet formation was not completely abrogated at a critical DNA concentration but rather the size of the droplets was gradually reduced (Figure 2.3A). Thus, we conclude while HP1α at these conditions

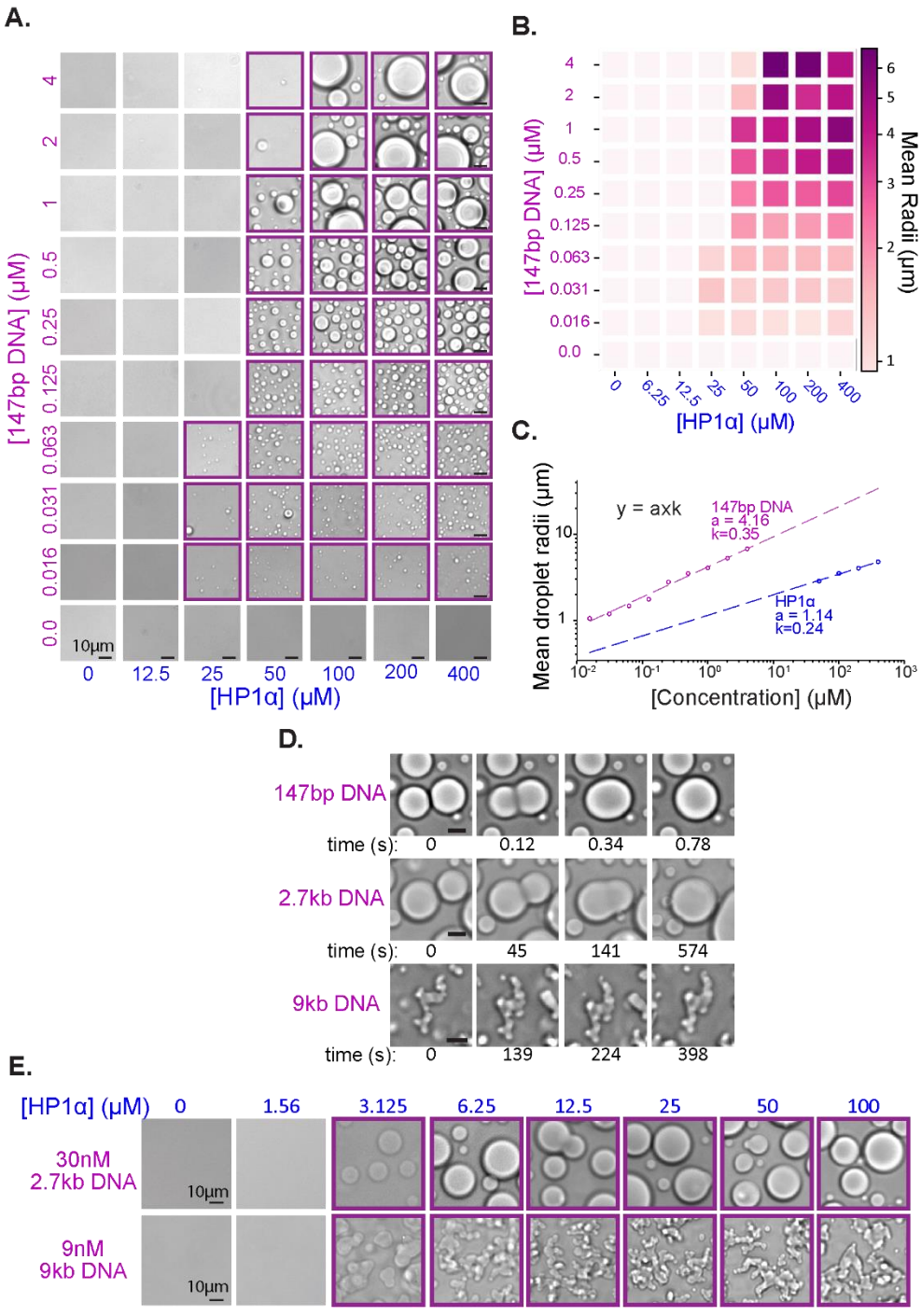

Figure 2.3 Characterization of HP1α-DNA condensate formation. **A.** Brightfield images of mixtures of HP1α and 147bp DNA. **B.** Heat map of the mean radius of condensates for each condition in (A). **C.** Mean condensate radius plotted against HP1α (blue) or 147bp DNA (magenta) concentration and fit to a power law. **D.** Time stamped brightfield images of 100μM HP1α and 147bp, 2.7kbp, or 9kbp DNA depicting fusion and coalescence behavior. **E.** Brightfield images of HP1α with either 30nM 2.7kb DNA (top) or 9nM 9kbp DNA (bottom). Throughout, purple boxes indicate presence of condensates.

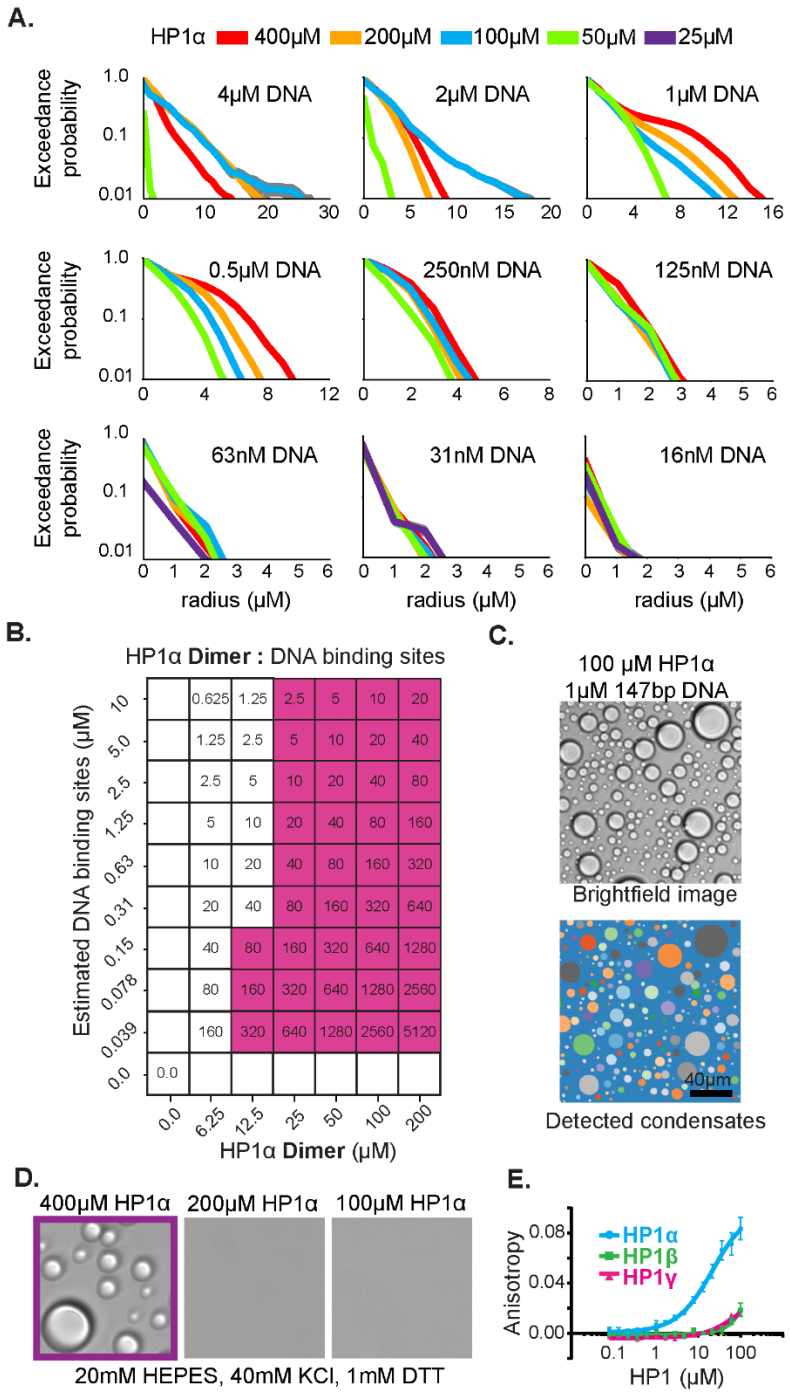

Figure 2.4. Characterization of HP1α condensates. **A.** Exceedance probability (number of condensates (y-axis) with radius exceeding indicated size (x-axis) for each concentration of HP1α and DNA in Figure 2A. Expectation values determined by integrating each curve are reported in Figure 2B-C. **B.** Ratio of HP1α dimer to estimated DNA binding sites for experimental conditions in Figure 2A (2 HP1α binding sites per 147bp DNA oligo). **C.** (top) Brightfield image of 100μM HP1α and 1μM 147bp DNA and (bottom) output of automated condensate detection. **D.** Brightfield images of HP1α dialyzed into low salt buffer (20mM HEPES pH7.5, 40mM KCl, and 1mM DTT). **D.** Normalized fluorescence anisotropy curves for each HP1 paralog.

requires DNA to form droplets, it is largely invariant to the concentration of DNA—even at sub-stochiometric ratios of DNA to HP1α macroscopic droplets still form (1:5000, Figure 2.4B).

The apparent equilibrium constant for HP1α interactions with ~60-200 bp DNA ranges from 0.3-10 μM (Figure 2.4E) (Nishibuchi et al., 2014) which means, for most of the conditions tested here where we observe macroscopic droplets, we expect that nearly all DNA molecules are fully bound by HP1α. Once a collection of HP1α molecules coat a single DNA, that DNA molecule and its associated HP1α can, on average, act as a single highly valent molecule, or proto-condensate, that acts as a liquid building block and aggregates with other HP1α-DNA proto-condensates as they encounter one another in solution. It is helpful to recall that DNA regions already bound by HP1α were readily incorporated into condensates in our curtain assay, and the same biophysical considerations above also apply here. Specifically, we hypothesize that condensate formation and growth are dependent on the concentration of HP1α and are the result bridging adjacent DNA sites together.

The ensuing aggregation process—proto-condensates clustering into large macroscopic condensates—should result in condensates sizes distributed according to a power law; where the power is set by molecular rates of diffusion and absorption (Brangwynne et al., 2011, Kilian et al., 1997, Vicsek et al., 1984). Specifically, this result comes about because increasing the HP1α or DNA concentration increases the rate of formation and total number of proto-condensates, which increases their encounter frequency in solution accelerating the process of diffusion-driven aggregation. To test this hypothesis, we measured the average radius of condensates as a function of DNA and HP1α concentration (Figure 2.3B-C, Figure 2.4A,C). We find the average droplet size versus concentration of both DNA and HP1α is in fact well described by a power law (Figure 2.3C), further connecting the formation of macroscopic liquid droplets to the microscopic processes of aggregation and DNA compaction.

While both the curtains and droplet assays suggest HP1α can act to bridge DNA, our assays do not provide a detailed lens into the mechanism of this bridging. Prior work by Adam

Larson detailing the phase separation behavior of phosphorylated HP1α showed higher-order oligomerization mediated by the N-terminal phosphorylation sites and the basic patches in the hinge (Larson et al., 2017). The weak, multivalent contacts required for phase separation led to the hypothesis that HP1α-HP1α oligomerization might contribute to DNA bridging in a similar manner to that seen with the phosphorylated protein. In support of this model, HP1α at low salt conditions (40mM KCl) forms macroscopic droplets even in the absence of DNA, indicating that the wild-type protein is capable of mediating multivalent contacts. Interestingly, the basic patches in the hinge that supported higher order oligomeric species in the phosphorylated protein also overlap as the site of DNA binding. If this mechanism of multivalency is conserved in the wild-type protein, as the concentration of DNA is increased eventually HP1α-DNA interactions will outcompete HP1α-HP1α interactions, resulting in a loss of condensation. However, an alternative, compatible explanation suggests that as DNA concentration is increased, each DNA molecule is not bound by a sufficient amount of HP1α to drive the aggregation of DNA strands together to form a macroscopic droplet. Consistent with both of these expectations, at concentrations approaching equimolar ratios of HP1α to DNA binding sites (assuming 60bp per HP1α dimer binding site (materials and methods)—50μM HP1α and 2-4μM 147bp DNA) droplet formation is abrogated (Figure 2A-B, figure supplement 2.2A). Future work is needed to dissect the mechanism of multivalency of this system.

Overall, the behavior of HP1α and DNA in this condensation assay is consistent with the compaction process we measure in our single molecule assay, and ultimately our results demonstrate that DNA and HP1α play qualitatively different roles in the formation of the HP1α-DNA condensates. In both assays, at suitable HP1α concentrations, HP1α condenses locally around a single DNA molecule. In the curtains assay, DNA is then compacted through lateral HP1α-DNA and possible HP1α-HP1α interactions *in cis,* whereas in the droplet assay, HP1α and DNA collectively condense into proto- and macroscopic condensates *in trans.* Additionally, both assays suggest that HP1α engaged with a single DNA molecule samples the same biophysical

states as HP1α molecules contained within compacted structures and large macroscopic phases. However, a key difference between these two assays is the length of DNA. We observe robust DNA condensation on curtains at concentrations lower than the critical concentration for HP1α-DNA LLPS measured here on short DNA oligomers, indicating changes in DNA length will affect the formation of condensates. Moreover, we expect that as DNA length is increased, the conformational constraints and increased binding site availability of longer polymers will also have profound effects on the formation and material properties of HP1α-DNA condensates.

2.2.3 The length of the DNA affects critical concentration and viscosity

The droplet assay above was designed using a short 147bp strand of DNA, proportional to the persistence length of DNA where robust DNA bending does not occur, meaning any HP1α tethering of two DNA sites would have to occur with separate strands. However, as the length of the DNA increases past its persistence length, the polymer can begin to bend and occupy a much larger distribution of conformational states. This means HP1α tethering and compaction can occur within an individual piece of DNA as well as linking adjacent strands together in trans. As long polymers of DNA are condensed into close proximity by HP1α the internal friction of the condensate increases. To determine how the polymer properties of this added DNA length affects condensate formation, we first increased the size of linear DNA from 147bp to 2,700bp (2.7kb). We saw an order of magnitude decrease in the critical HP1α concentration, from 50μM with 147bp to 3μM with 2.7kb (Figure 2.3E), consistent with polymer physics studies showing DNA length scales with a polymers ability to phase separate out of solution. However, when we increased the DNA length to 9kb, we saw the HP1α critical concentration plateaus at 3μM (Figure 2.3E). Notably, this lower limit is comparable to the HP1α-HP1α dimerization constant (Larson et al., 2017), suggesting dimerization is an important step in condensate formation. Moreover, as DNA length increases the condensate morphology becomes less uniform, with 9kb DNA-HP1α droplets producing elaborately digitated structures. As the length of heterochromatic domains *in vivo* are typically greater than 10kb long, the molecular interactions that produce these droplets with

oblong morphologies might more closely replicate heterochromatic domains in cells. Therefore, we wished to determine how DNA length affected both HP1-HP1 and HP1-DNA interactions and how these alter the mesoscale droplet properties of surface tension and viscosity.

Surface tension, or the propensity of a fluid to minimize surface area, occurs because the macromolecules in the concentrated phase are better solvated by self-self interactions over those with the surrounding solvent. Viscosity defines a fluids resistance to deformation, and as the internal friction of the fluid increases so does the viscosity. The molecules within a liquid have a high degree of motion, low internal friction, and prefer self-self interactions over those with the solvent. These molecular properties of a liquid manifest in bulk as low viscosity and high surface tension. Therefore, when two liquid condensates fuse the droplets rapidly coalesce into a spherical structure that minimizes surface tension and therefore interactions with the surrounding solvent. However, as either the viscosity of a condensate increases, or the surface tension decreases, the time it takes for two droplets to coalesce will increase and this can report on the nature of molecular interactions within the droplet.

To determine the effect of DNA length on coalescence time, and therefore viscosity and/or surface tension, I visualized droplet fusion at different lengths of DNA. Co-condensates formed with 147bp DNA rapidly minimized surface tension, forming a sphere within a second (Figure 2.3D). This implies liquid condensate characteristics, with a low viscosity and high surface tension. In contrast, co-condensates formed with 2.7kb DNA took minutes to become spherical while 9kb droplets were unable to complete coalescence within an hour. (Figure 2.3D). As the polymer length increases internal friction between segments of the DNA strand led to a higher viscosity of the solution. Therefore, the decrease in coalescence with 9kb DNA could be due to increased viscosity because the polymers internal friction produced as it is condensed into the high concentration condensate via HP1-DNA interactions. In theory, the viscosity of condensates should scale as a power of the molecular weight of the polymer (Li et al., 2012). However, under the solvent conditions tested here, and for DNA lengths < 3kbp, the scaling relationship between

intrinsic viscosity and DNA length is expected to be near linear, which has been confirmed experimentally (Rubinstein and Colby, 2003 and Ross and Scruggs, 1968). Thus, the increase in size of linear DNA from 147bp to 2.7kbp should approximately correspond to an order of magnitude change in viscosity. However, while coalescence was complete within one second for condensates formed with 147bp DNA, condensates formed with 2.7kbp DNA required several minutes to complete coalescence (Figure 2.3D). This greater than 100X increase in the rate of coalescence overshoots our expectations based solely on DNA length changes, demonstrating that HP1α-DNA interactions also contribute to the intrinsic viscosity of the condensate. Moreover, condensates formed with 9kbp DNA (~60X larger than 147bp) were unable to complete coalescence within an hour (Figure 2.3D). And while these condensates do exhibit a slow reduction in perimeter over time suggesting that coalescence is proceeding locally, at the whole condensate level, the morphology of these condensates remains aspherical. Therefore, it is possible that HP1 and DNA contribute differently to the bulk droplet properties, with the length of DNA contributing to the viscosity of the condensates and HP1-DNA and potential HP1-HP1 interactions dictating the surface tension.

2.2.4 HP1α dynamically binds to DNA while simultaneously maintaining stable DNA domains

To test whether HP1 and DNA contributed differently to condensate properties, I used fluorescence recovery after photobleaching (FRAP) in collaboration with David Brown. Interestingly, the rates of fluorescence recovery of HP1 measured after partial droplet photobleaching did not depend on DNA length (Figure 2.5A-C). Droplets with DNA lengths ranging from 147 bp to ~ 50Kb recovered HP1α fluorescence with a $t_{1/2}$ value of ~2s, despite obvious differences in droplet morphology as DNA length increased (Figure 2.5A-C, 2.3E).. Interestingly, the $t_{1/2}$ values that we measure in our reconstituted system are similar to the $t_{1/2}$ values determined previously from *in vivo* FRAP experiments (Cheutin et al., 2003, Festenstein et al., 2003). Additionally, photobleaching of the entire droplet formed with 147 bp DNA and HP1α

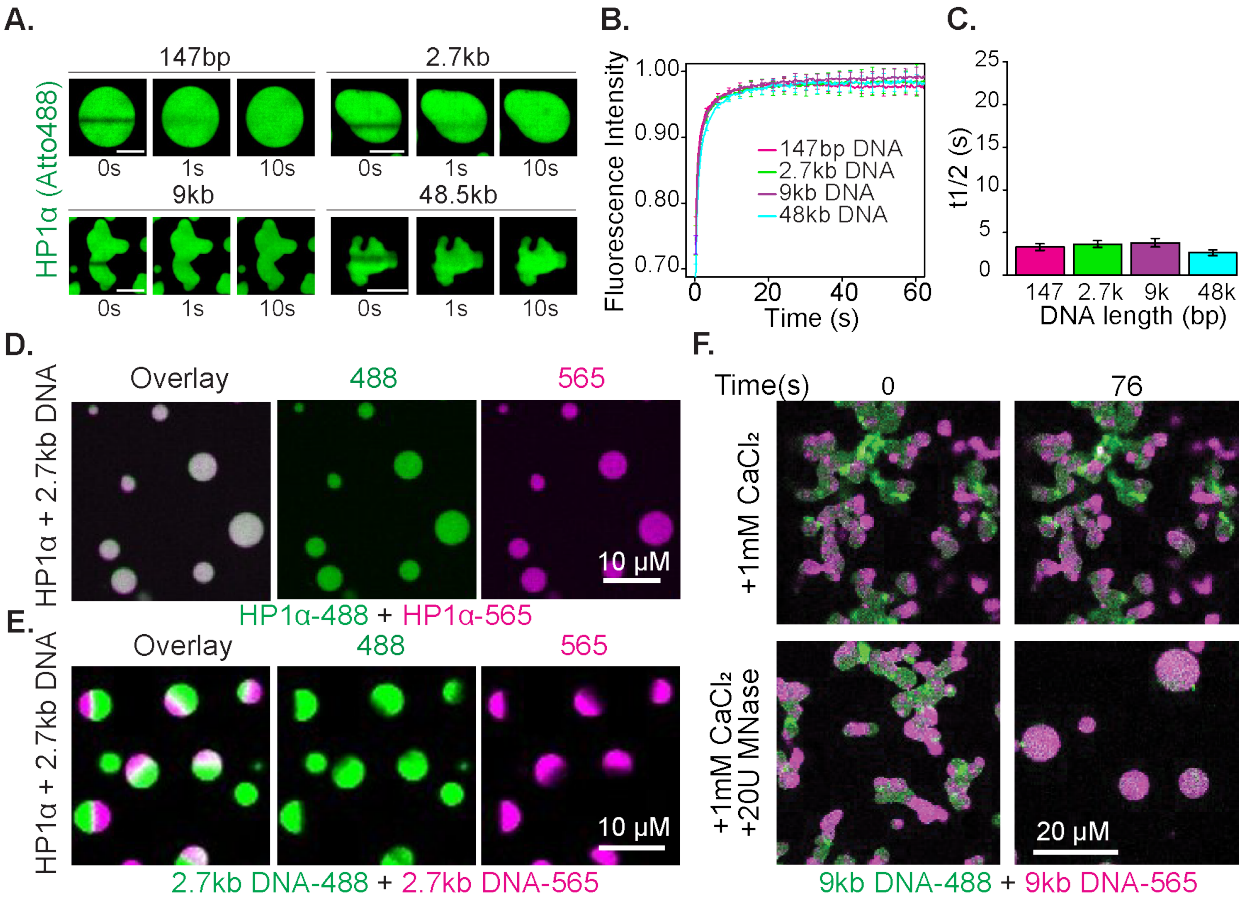

Figure 2.5 Distinct characteristics of HP1α and DNA in condensates. **A.** FRAP of HP1α in condensates. Timestamped images from FRAP experiments for fluorescent HP1α and four lengths of linear DNA (147bp, 2.7kbp, 9kbp, or 50kbp). Scale bar indicates 5μm. **B.** Recovery of HP1α fluorescence intensity and **C.** half-life of HP1α recovery plotted for each DNA length tested. **D.** Two color HP1α mixing experiments. Condensates formed separately with 2.7kbp unlabeled DNA and either HP1α-488 (green) or HP1α-565 (magenta) imaged 1.16 minutes after mixing. **E.** Two color DNA mixing experiments. Condensates formed separately with unlabeled HP1α and 2.7kbp DNA-488 (green) or 2.7kbp DNA-565 (magenta) imaged 4.4 minutes after mixing. **F.** MNase treatment of condensates. Mixed condensates formed separately with unlabeled HP1α and 9kbp DNA-488 (green) or 9kbp DNA-565 (magenta) treated with either 1mM $CaCl_2$ or 1mM $CaCl_2$ and 20U MNase. Images shown for both conditions before and 76 seconds after the treatment.

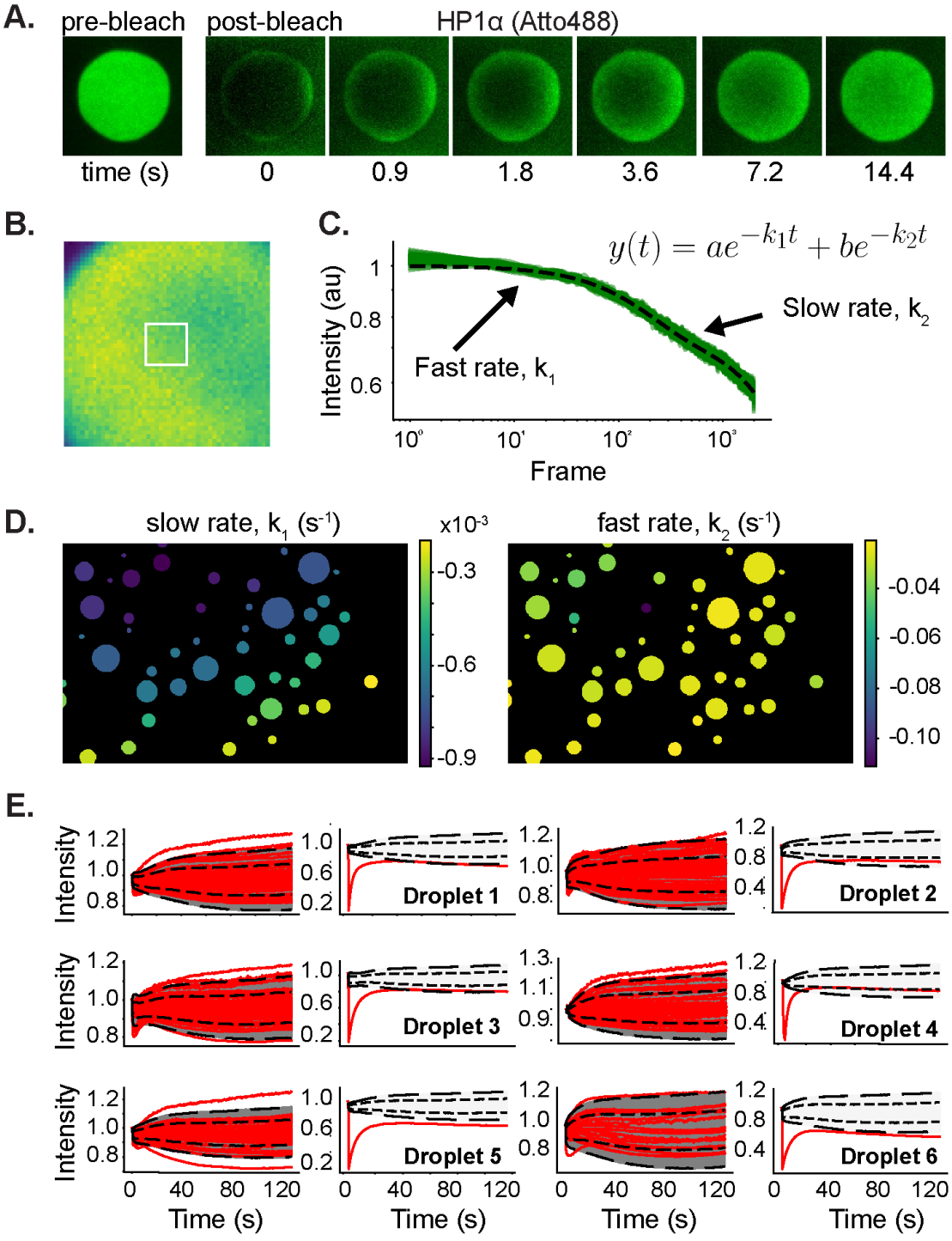

Figure 2.6. Whole droplet FRAP of HP1α-488 in HP1α-DNA condensates. **A.** Timestamped images of whole droplet HP1α-488 FRAP. **B. and C.** Time dependence of ambient fluorescence decay of HP1α-488 within **B.** sample unbleached condensate region (white box), **C.** fit to a bi-exponential decay. **D.** Sample images colored by average decay rates. **E.** Fluorescence recovery of unbleached condensates (left) versus the photobleached condensate for six FRAP experiments. Dotted lines indicate 1 and 2 standard deviations from the mean determined from the unbleached condensates.

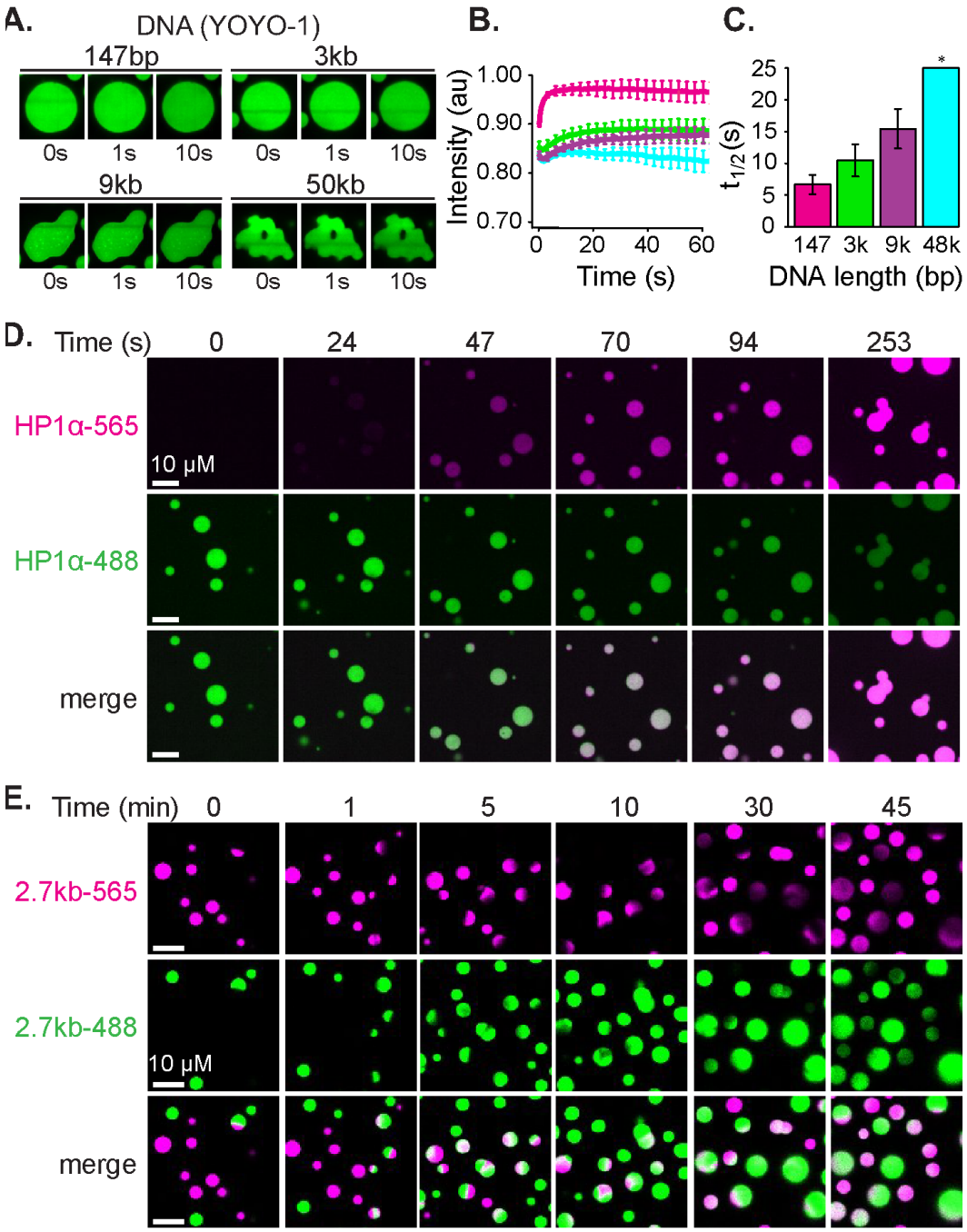

Figure 2.7. FRAP of DNA and mixing of HP1α and DNA in condensates. **A.** FRAP of YOYO-1 in condensates. Timestamped images from FRAP experiments for four lengths of linear DNA (147bp, 2.7kbp, 9kbp, or 50kbp). **B.** Recovery of YOYO-1 fluorescence intensity and **C.** half-life of recovery plotted for each DNA length tested. * indicates half-life not determined. **D.** Timestamped images of two color HP1α-DNA condensate mixing experiments. Condensates formed separately with 2.7kbp unlabeled DNA and either HP1α-488 (green) or HP1α-565 (magenta). **E.** Timestamped images of two color HP1α-DNA condensate mixing experiments. Condensates formed separately with HP1α and 2.7kbp DNA-488 (green) or 2.7kbp DNA-565 (magenta).

also results in similarly rapid recovery of fluorescence levels to their original values (Figure 2.6A-E). These results indicate fast diffusivity of HP1α *within* co-condensates and free and fast exchange of HP1α *between* droplet and solution populations. To further test the diffusivity of HP1α we mixed droplets pre-formed with two differentially labeled pools of HP1α (HP1α-488 or HP1α-565) and 2.7kbp DNA. After mixing, both HP1α-488 and HP1α-565 rapidly disperse equally into all droplets within seconds (Figure 2.5D, 2.7D). This rapid dispersion of fluorescent protein is in agreement with the fast exchange of HP1α between droplets seen in the FRAP experiments. The free and fast diffusion of HP1α mediates the surface tension of condensates formed with all DNA lengths: the preference of the bulk HP1α population to interact with DNA and other HP1α molecules rather than solution leads the droplets to minimize the surface area. Importantly, it does not stop any individual HP1α from diffusing freely in or out of a condensate. However, if HP1α is rapidly diffusing within solution and inside the droplets regardless of DNA length, the question still remains of what leads to the increased viscosity seen in droplets made with larger pieces of DNA.

To examine the diffusion of DNA within condensates we performed droplet mixing experiments using droplets formed with HP1α and 2.7kb DNA that was end labeled with either Atto488 (DNA-488) or Atto565 (DNA-565). Contrary to the observations with labeled HP1α, the labeled DNA did not rapidly mix between fused droplets and instead maintained large and long lived (> 1 hour) single color DNA domains (Figure 2.5E, 2.7E). Further, FRAP experiments of DNA labeled with YOYO-1 exhibit partial fluorescence recovery at a rate proportional to DNA length: the longer the DNA, the slower the recovery (Figure 2.7A-C). As pieces of an individual DNA strand are tethered together by HP1α the internal friction of molecule increases as it has less degrees of freedom as compared to a short DNA oligo, leading to the increased viscosity as a function of DNA length. Interestingly, HP1α tethers individual polymers into a static, condensed conformation that does not diffuse freely and interact with other DNA molecules in the condensate. To condense this DNA into a distinct domain, no individual HP1α molecule must statically bind for hours, but instead the bulk effect of a subset of HP1α proteins being bound at

any one time, combined with the internal friction of the DNA polymer, facilitate the stable compaction of DNA.

The dynamic exchange of HP1α is consistent with the protein dominating the surface tension of co-condensates, and we wished to directly test our hypothesis that the abnormal morphologies of co-condensates formed with longer DNA lengths are a consequence of higher DNA viscosity. Therefore, we altered the viscosity of the DNA polymer in real time by changing the average length of DNA with the addition of a non-specific DNA nuclease. Two color droplets formed with HP1α and 9kb DNA labelled with either Atto488 or Atto565 were allowed to settle, and then the nuclease MNase and the cofactor calcium were added to the well. As DNA is digested the irregularly shaped co-condensates coalesce into spheres and the two colors of DNA mix (Figure 2.5F). Although HP1α is rapidly diffusing within the droplets with 9kb DNA, it cannot fully compensate for the internal friction of the DNA polymer, leading to digitated morphologies. As the DNA length decreases with the nuclease addition, the friction of the polymer decreases and HP1α-DNA and HP1α-HP1α interactions can begin to mix the DNA within the droplet and minimize the surface tension. These results are consistent with a model of dynamic HP1α interactions maintaining the surface tension of condensates while DNA dominates the viscosity as a function of length.

Overall, these experiments reveal a remarkable character of HP1α-DNA co-condensates—a fast exchanging, liquid pool of HP1α can stably trap and organize kb long stretches of DNA into long lived domains. This is reminiscent of *in vivo* phenotypes, where heterochromatic domains are maintained in a fixed position within the nucleus throughout interphase, despite the dynamic exchange of HP1α. While the fast diffusion of HP1α and stable compaction of heterochromatin was often thought to be incompatible phenotypes, our minimal reconstituted system illustrates dynamic HP1α binding is sufficient to condense DNA into long lived domains, thus preliminarily resolving the perceived inconsistencies.

2.2.5 HP1α maintains compacted DNA at relatively high forces

Given the dynamic behavior of HP1α, we expected that condensed HP1α-DNA structures, although kinetically long-lasting, would be readily dissolved if subjected to biologically relevant forces. To test this hypothesis, I collaborated with Lucy Brennen and Roman Renger to investigate condensate stability against an externally applied force through optical trapping experiments combined with confocal microscopy (Figure 2.8A-B). In these experiments, we subject the DNA to stretch-relax cycles (SRC) (Figure 2.9C) and we measure the force required to extend the DNA to a given length, i.e. a force-extension curve (Figure 2.8C, 2.9A). Prior to adding HP1α, we first ensured that each tether was composed of a single strand of DNA and behaved as previously described (Figure 2.4C, black line)[46]. We then moved the trapped DNA molecule, held at an extension of ~5μm, to a chamber containing HP1α and observed the formation of compacted HP1α-DNA structures analogous to those observed on DNA curtains (Figure 2.1C, 2.8B). This initial incubation was sufficiently long to complete condensate formation (30s). Notably, in this assay, compacted DNA structures appear in the center of the DNA molecule rather than at the end, because, with the motion of both ends of the DNA constrained by their attachment to polystyrene beads, the largest DNA chain fluctuations occur in the middle of the molecule.

For our initial experiments, DNA tethers bearing internal HP1α-DNA condensates were stretched at constant velocity to a final force of 40pN, immediately relaxed, and then stretched again (Figure 2.8C, 2.9A). We observe a substantial deviation in the force extension curve for DNA in the presence of HP1α relative to DNA alone (Figure 2.8C, 2.9A). We verified that the shift to larger forces for DNA extended in the presence of HP1α is not a consequence of radiation driven cross-linking (Figure 2.9B). From this measurement, we identify three prominent features of HP1α-DNA interactions. First, sequestered DNA domains, measuring on average 10kbp, are able to resist disruption to an instantaneous force of 40pN (Figure 2.8C,D). However, smaller HP1α-DNA structures (~1-2kbps) are observed to rupture at lower forces ranging from 5-20pN, suggesting the stability of HP1α-compacted DNA scales by size (Figure 2.8C, 2.9A). Second, by

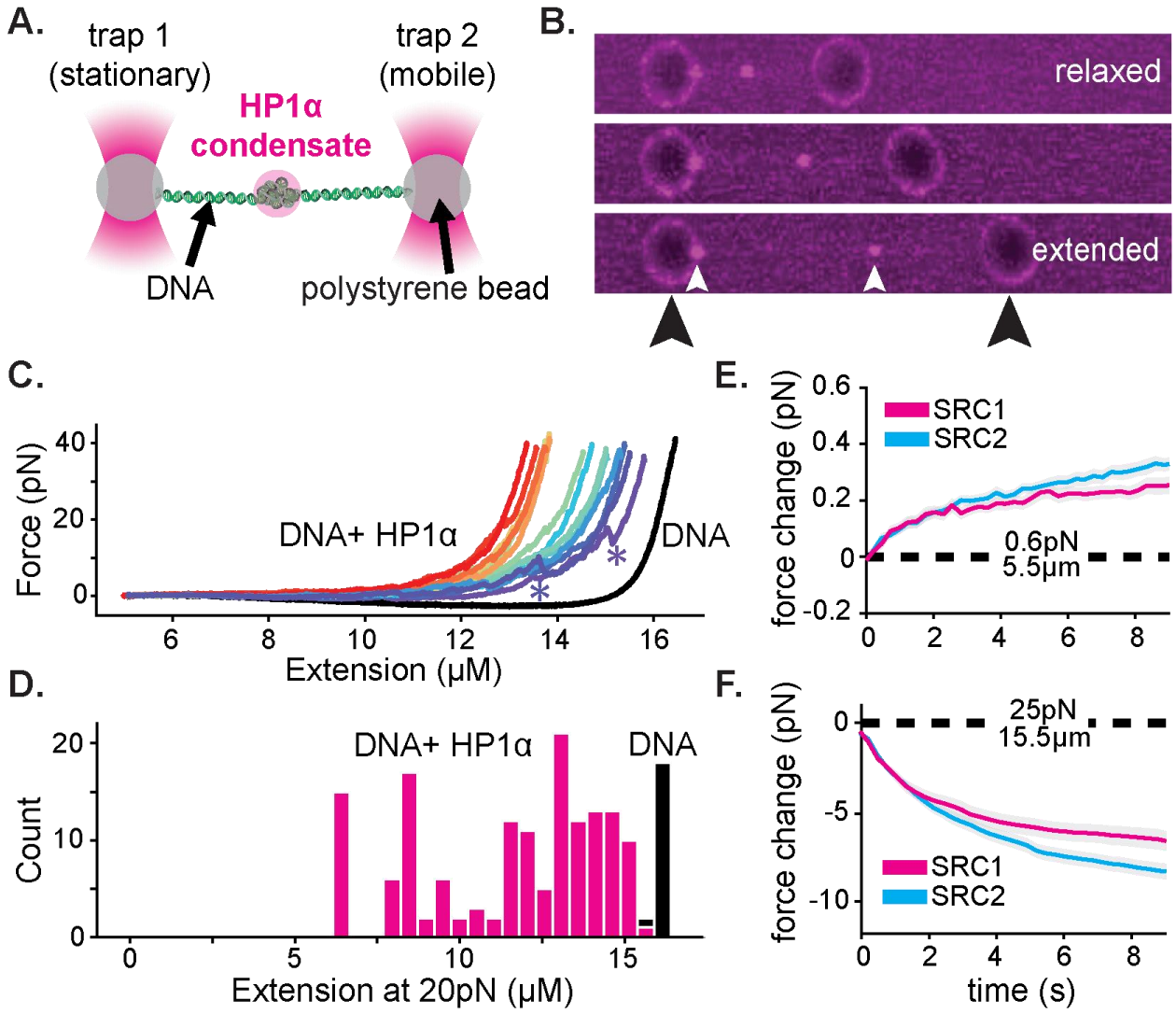

Figure 2.8. HP1α-DNA condensates resist disruptive forces and retain memory of past strain. **A.** Cartoon of optical trap experiments. **B.** Confocal images of relaxed, intermediate, and extended states of DNA (unlabeled) in the presence of HP1α (magenta). Black arrowheads indicate trapped beads and white arrowheads indicate HP1α-DNA condensates. **C.** Force extension curves for DNA in the absence (black line) or presence of HP1α (colored lines). Each trace represents a single stretch-relax cycle (SRC) of the same DNA strand. Traces are colored by pulling order from first extension (violet) to the final extension (red). ***** indicates rupture event. **D.** Histogram of DNA extension at 20pN in the absence (black) or presence of HP1α (magenta). **E. and F.** Force change for DNA incubated with HP1α in **E.** relaxed or **F.** extended conformation. Shown is the average of the first (magenta) and second (cyan) SRC.

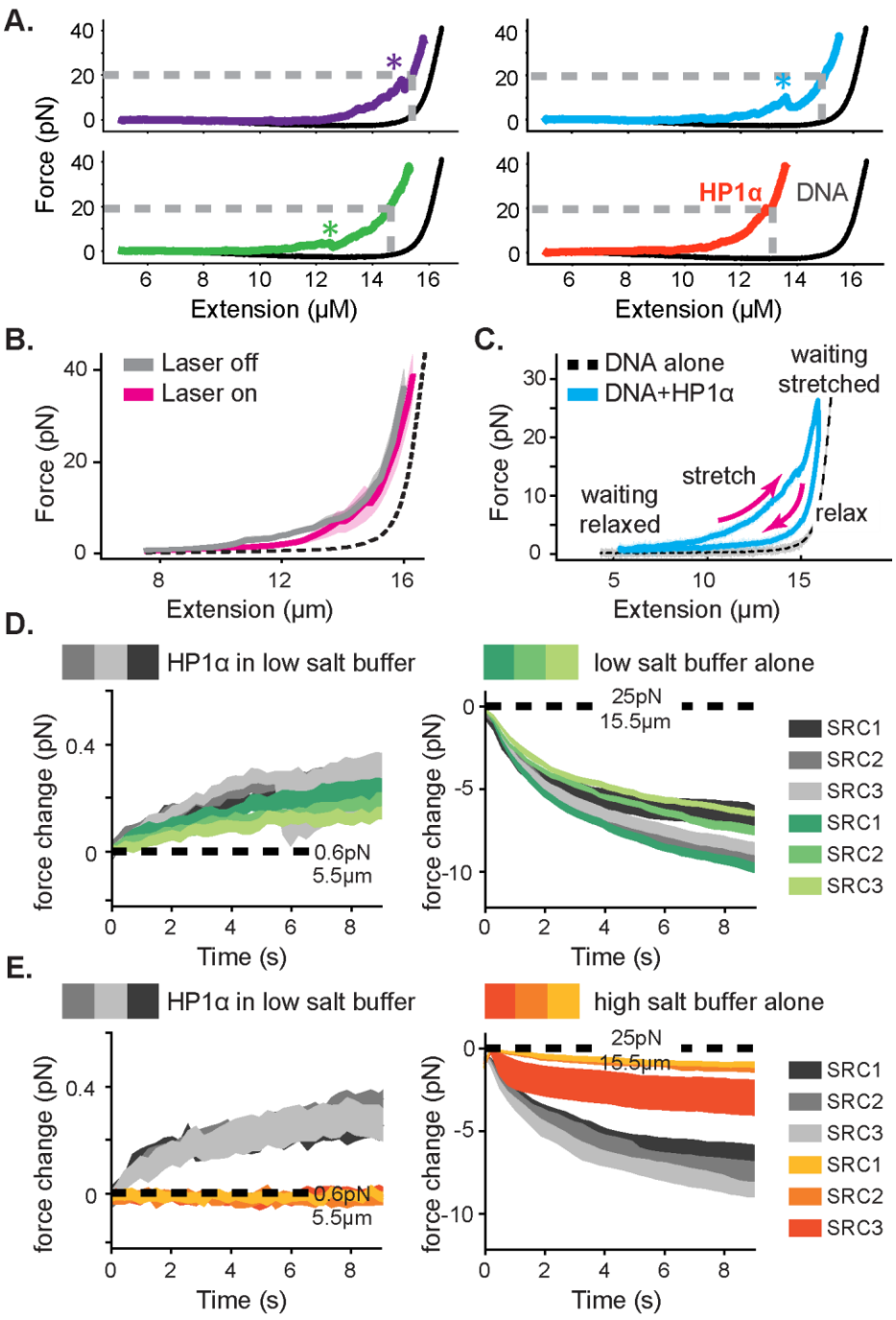

Figure 2.9. Representative traces and controls for optical trap experiments. **A.** Four representative traces from Figure 4C. All traces are separate pulls from the same DNA strand. * indicates rupture event. Grey dashed line indicates the DNA extension at 20pN force reported in Figure 4D. **B.** Average force extension curves for the second SRC either with (magenta) or without (gray) laser illumination. The force extension curve of DNA alone is shown in black. **C.** Force extension curve across a stretch-relax cycle including waiting periods in the extended or relaxed configurations. **D. and E.** Force change in the relaxed (left) and stretched (right) configurations in the presence (gray) and absence (green or orange) of HP1α. SRCs in the absence of protein performed in either **D.** low salt (70mM KCl) or **E.** high salt (500mM KCl) buffer.

integrating the area between the force-extension curves for DNA alone and in the presence of HP1α, we estimate that an average energetic barrier of ~1k_bT/bp of compacted DNA separates HP1α-compacted states of DNA from extended DNA states in the absence of HP1α (Figure 2.8C, 2.9A). Finally, we observed that each successive SRC resulted in more DNA stably sequestered by HP1α (Figure 2.8C). This surprising result shows that, after HP1α-DNA condensates are subjected to strain, polymer rearrangements and/or force-dependent selection of HP1α binding interactions provide a basis for further stable compaction of DNA by HP1α.

Next we asked whether or not HP1α-DNA condensates could compact DNA against force or maintain the compacted state when subjected to sustained force by performing consecutive SRCs that included waiting periods after complete relaxation (~5.5μm) and after stretching to 25pN (~15.5μm) (Figure 2.8E-F, 2.9C-E). During the waiting period after relaxation, we observe a steady force increase over time (Figure 2.8E, 2.9D-E). This result may be the product of either association of HP1α molecules from solution and/or rearrangements of DNA and already bound HP1α. To test whether low-force DNA compaction required a constant influx of HP1α binding, we moved the DNA tether from the chamber containing HP1α to a chamber containing only buffer and performed an additional three SRCs (Figure 2.9D). We find that even in the absence of free HP1α, the population of already bound HP1α molecules is sufficient to induce compaction in the low force regime (~1pN) (Figure 2.9D). Notably, compaction in the absence of free protein can be abrogated by increasing the ionic strength of the buffer (from 70mM to 0.5M KCl) (Figure 2.9E), consistent with salt-induced decompaction observed on DNA curtains[23].

When the DNA is held at a steady extension of 15.5μm following stretching, we observe a drop in measured force over time (Figure 2.8F, 3.9D-E). This relaxation indicates that HP1α-DNA condensates are biased toward disassembly during sustained higher forces. This result is potentially due to force-dependent changes in the kinetics of HP1α binding and/or the reduction in DNA strand fluctuations required by HP1α to induce compaction. To test whether HP1α in solution could affect the stability of the condensate, through a facilitated exchange mechanism[47],

we again performed an additional three SRCs in the absence free HP1α (Figure 2.9D-E). We find that the disassembly of HP1α-DNA condensates at higher forces proceeds at the same rate irrespective of the presence of HP1α in solution (Figure 2.9D).

Notably, during both waiting periods—before and after stretching—we measure changes in HP1α-DNA condensation activity in later SRCs (Figure 2.8E-F, 2.9D-E). In the relaxed configuration, during low-force compaction, we observe more robust compaction during the second SRC relative to the first (Figure 2.8E). In comparison, we observe more rapid disassembly while waiting at higher forces during the second SRC (Figure 2.8F). These strain-induced effects on HP1α behavior can have important consequences for how HP1α-organized genetic material responds to cellular forces. For example, RNA polymerase ceases to elongate when working against forces as low as 7.5-15pN[48]. Our experiments show that short transient bursts by polymerase are unlikely to disassemble and may even strengthen HP1α-compacted structures above the force threshold for efficient transcription. However, repeated, sustained efforts by polymerase might be sufficient to relax HP1α-compacted structures and allow for transcription to proceed.

Moreover, these data suggest that a dynamic network of HP1α-DNA and potential HP1α-HP1α interactions can both account for increased viscosity and stabilization of global condensate structure. In general, we propose that such properties arise from a mean-field activity of an exchanging population of HP1α molecules that constrain the DNA at any given time. That is, regardless of the stability of any individual HP1α molecule, the average character of the HP1α-DNA network is maintained in condensates at a pseudo steady state.

While the measured stability of HP1α-DNA condensates is consistent with a role for HP1α as a mediator of transcriptional repression, it is hard to reconcile this activity with dynamic chromatin reorganization when cellular cues necessitate the disassembly of heterochromatin. These data also raise the question of which molecular features of HP1α allow it to realize its many functions in condensates and on single DNA fibers.

2.3 Discussion

Heterochromatic domains are transcriptionally inert and positionally stable throughout interphase. While HP1 is known to be a major mediator of heterochromatic structure and function *in vivo*, experiments detailing their rapid diffusion raised the critical question of how a dynamic binding protein can mediate stable condensation. Within this chapter, I've found that HP1α is capable of rapidly compacting 50kb stretches of DNA and forming macromolecular phase separated droplets when incubated with DNA. Within the droplet system, HP1 recapitulates the dynamic binding seen in cells. Further, HP1-DNA droplets maintain static compaction of individual DNA domains and can withstand up to 40pN of force when condensation stability is tested on an individual DNA strand. These experiments utilize a minimally reconstituted system of simply HP1 and DNA but show that the bulk action of many HP1molecules in solution can capitalize on properties of long DNA polymers to create static, stable domains similar to heterochromatic properties seen *in vivo*. These findings have important implications for both the initiation and dissolution of heterochromatic domains as will be discussed below.

2.3.1 Implications for the initiation of heterochromatin domains

The DNA curtains experiments present three regulatable steps in which HP1 captures and compacts DNA. (1) Local assembly of HP1α along DNA prior to DNA condensation; (2) initiation of DNA compaction through bridging of proximal DNA fluctuations via HP1α-DNA and potentially HP1α-HP1α interactions to form a puncta, and (3) progression of DNA compaction through inclusion of uncompacted DNA into the growing condensate via HP1α-DNA and HP1α-HP1α interactions. For the initiation of heterochromatin in cells, therefore, this work implies HP1 must coat the length of the domain and capitalize on polymer fluctuations to tether a growing puncta to upstream sites of DNA. In cells, many variables would contribute to the success of this heterochromatin spread including nucleosome positioning, linker length, histone modifications, boundary elements, RNA polymerase activity, and protein occupancy (Allshire et al., 2018).

Therefore, it is important to note that HP1 concentration is not the only variable responsible for growing of condensates in cells, as the DNA curtains suggest any barriers to HP1 binding would result in the stuttering of compaction (suggested in Erdel et al., 2020). This insufficiency of HP1 alone to regulate condensate size is further seen in the droplet assays. While increasing the concentration of HP1 does have an impact on condensate size, it is modest in comparison to the affect of increasing the concentration of DNA in solution (Figure 2.3A-C). In cells, this might manifest as a major driver of the size of heterochromatic domains being the availability of DNA sites bound by HP1, and not the total concentration of HP1 in solution.

An interesting finding in the heterochromatin field is the even spacing of nucleosomes in heterochromatic regions of the genome (Bloom et al., 1982, Cartwright et al., 1983, Funk et al., 1989). While this spacing was initially thought essential for the organization of the 30nm fiber (Grigoryev et al., 2012), recent work has suggested heterochromatic nucleosomes appear disordered in structure despite their even spacing (Horng et al., 2017). I'll have a little fun and speculate wildly. Perhaps this even spacing is important for initial compaction of DNA into heterochromatic domains, and not the downstream organization of them. As HP1 spreads along a DNA domain, it is bridging these nucleosomes that are closely spaced with just enough linker length to promote binding until it has created a puncta of condensed chromatin (Mishima et al., 2012). But then it finds the upstream DNA of this growing puncta is a dessert of unevenly spaced nucleosomes with proteins bound all over the naked DNA, stuttering any further spread. The puncta would stop growing until some remodelers are recruited in and clean up the dessert, kicking off the proteins bound to the naked DNA and organizing the chromatin into nice step sizes that promote the probability of looping into the growing condensate (Shimada et al., 1984 and Mirny 2011). Having done their job, the remodelers will be on their way and HP1 will gobble up the nicely spaced chromatin into the growing condensate until it reaches the next dessert and stutter once again until it reaches an insurmountable barrier (like an active gene wildly transcribing) and reach a happy equilibrium until cellular conditions change. End scene.

Finally, the sequence and structural characteristics of constitutive heterochromatic regions has interesting implications on how HP1 would spread based on our model. Satellite sequences are typically AT-rich, highly repetitive, and often show evidence of DNA curvature (Radiac et al., 1987, Martinez-Balbas et al., 1989, Benfante et al., 1989, and Fitzgerald et al., 1994). This increased bendability of DNA would increase the probability of looping, therefore allowing HP1 to bridge adjacent sites more readily. This sequence bias could enable constitutive heterochromatic domains to initiate and maintain HP1-compacted heterochromatic structures more readily than gene rich regions. Interestingly, instances of position effect variegation often occur when a euchromatic gene is translocated close to sites of constitutive heterochromatin, particularly at centromeres. The increased curvature of these sites could increase the contact probability of the heterochromatin with the newly transposed euchromatic gene. An intriguing variable of PEV is the increased efficiency of gene silencing upon lowering the temperature the flies are grown at. This is a fascinating parallel to the phase separation of HP1: lower temperatures often decrease the critical concentration necessary to form droplets (Alberti et al., 2019). Perhaps the temperature dependence of PEV lies in the promotion of multivalent interactions at lower temperatures, leading to an increased ability of the constitutive chromatin to spread into the adjacent euchromatic domains.

2.3.2 Implications for the dissolution of heterochromatic domains

A conserved property of heterochromatic regions in cells is their late replication during the cell cycle (Rhind and Gilbert, 2013). The dense compaction of DNA in heterochromatin appears inconsistent with the ability of a large motor like DNA or RNA polymerase to access and move along the enclosed DNA strand. Consistent with this speculation, heterochromatic domains appear to decondense during S phase when replication is initiated (Yuan et al., 2014). The optical trap data presented here has interesting implications for the stability of heterochromatin against these motors. An individual motor attempting to access the DNA in a heterochromatic region by pulling would find an enormous force barrier of 40pN (Figure 2.3C) As RNA polymerase has been

demonstrated to stall at 5-20pN (Wang et al., 1998 and Galburt et al., 2007) this is likely sufficient force to inhibit access of the motor to the DNA within the condensate. However, the force clamping experiments at high force indicate sustained force on the HP1-DNA puncta is able to dissolve the stable structure (Figure 2.8F). If multiple motors were continuously pulling on a heterochromatic region, resulting in sustained force on the region, this might result in decompaction of the heterochromatic domain. Perhaps during replication, initially the DNA polymerase motors spread out along the genome and only regions that are easily replicated are successful. However, later in replication when much of the euchromatin is already replicated, a higher concentration of polymerase might be available to maintain attention on these heterochromatic regions resulting in sustained force on the region and therefore decompaction and replication can occur. Further, movement of HP1-DNA condensate to a high salt buffer disassembles the puncta, as similarly seen in the DNA curtains experiments (Figure 2.1D, 2.9E). This implies proteins that bind to the condensates and change the chemical nature within it might also provide a mechanism of heterochromatin dissolution. This potential mechanism will be further described in chapter 3.

Chapter 3: Dissecting the molecular mechanism of HP1-DNA compaction and droplet formation

3.1 Introduction

While the measured stability of HP1α-DNA condensates is consistent with a role for HP1α as a mediator of the positional stability and transcriptional silencing of heterochromatin, it is hard to reconcile this stability with the rapid reversibility heterochromatin necessitates. However, the dynamic binding of HP1α within condensates predicts proteins that compete with HP1 binding and DNA bridging could facilitate the dissolution of heterochromatic domains. In order to test this hypothesis, however, it is first important to determine an understanding of the molecular components important for HP1 condensation and whether there are specific regulatory regions of the protein that could be targeted by competitors. Therefore, I approach dissecting the mechanism of HP1-DNA condensation via two paths: first by determining the minimal protein components required for condensation activity and regulation and second by utilizing the intrinsic diversity of HP1 paralog sequences to determine how this affects condensation activity.

3.2 Results

The three HP1 paralogs share a common domain architecture: three disordered regions interspaced by a chromodomain (CD) and a chromoshadow domain (CSD) (Grewal and Elgin, 2002). The CD binds to H3K9me (Platero et al., 1995), the CSD mediates HP1 dimerization and interactions with other nuclear proteins (Brasher et al., 2000 and Thiru et al., 2004), and the disordered hinge mediates binding to DNA (Sugimoto et al., 1996 and Zhao et al., 2000). Interestingly, in cells all three HP1 paralogs display unique nuclear localization patterns despite all bearing a well conserved CD, with HP1β and HP1γ often localizing to euchromatic regions lacking H3K9 methylation entirely (Smothers et al., 2000 and Dialynas et al., 2007). However, the unstructured regions have diverged from one another. Therefore, I first characterize the

disordered regions of HP1α, then use this framework to describe the differential activities of the paralogs.

3.2.1 The hinge domain of HP1α is sufficient for DNA compaction and condensate formation

Given the net acidic isoelectric point of the full length HP1α protein, and particularly the acidic patches present in the disordered hinge and extensions, I speculated this DNA compaction and droplet formation might be driven by electrostatic binding of acidic residues within the disordered domains. DNA binding and cellular localization has been suggested to depend on two basic patches (BP_1 and BP_2) in the hinge region of HP1α (Figure 3.1A, 3.2A) (Sugimoto et al., 1996 and Zhao et al., 2000). Therefore, I investigated the behavior of the hinge peptide when isolated from the rest of the protein. Surprisingly, not only is the hinge peptide sufficient for DNA compaction (Figure 3.1B-C), it does so at a rate two-times faster than the full-length protein (Figure 3.1C, 3.2C). The hinge peptide was next tested for condensate formation with 147bp DNA and formed droplets down at a critical concentration of 12.5μM protein (Figure 3.1D), five times lower than the critical concentration for full length HP1α. Notably, as DNA concentration is varied the hinge peptide exhibits the same smooth transition of droplet formation as the full length protein (Figure 3.1E), suggesting that hinge-hinge interactions might also play a role in droplet formation. This could potentially occur via the multivalency of basic patches: if one basic patch of the HP1α hinge binds to DNA, the two other basic patches could either bridge another piece of DNA, tethering the two strands together (hinge-DNA contact), or interact with acidic residues in an adjacent hinge molecule (hinge-hinge contact). Given the highly potent activity of the hinge alone compared to full length HP1α, these results raise the possibility that the remaining portions of the protein act to regulate hinge behavior.

3.2.2 The disordered extensions of HP1α regulate hinge domain activity

Previous work has suggested that the N- and C-terminal extensions play opposing roles in controlling phase-separation by phosphorylated HP1α, with the CTE playing an auto-inhibitory

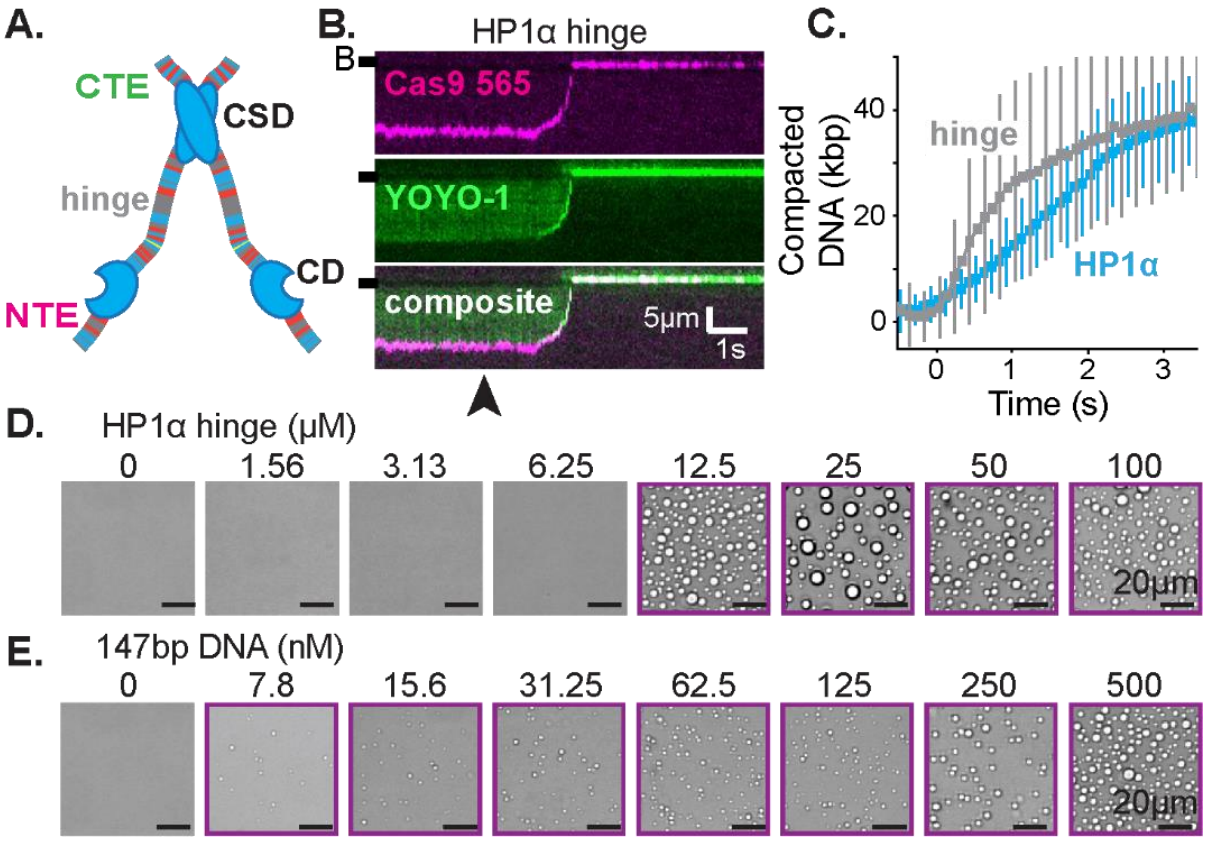

Figure 3.1. The hinge region of HP1α is sufficient for DNA compaction and condensate formation. **A.** Cartoon of HP1α with color-coded disordered regions: positive residues (K and R) blue, negative residues (E and D) red, proline yellow, and all other residues grey. Key HP1α domains are labeled: chromodomain (CD), chromoshadow domain (CSD), hinge, N-terminal extension (NTE), and C-terminal extension (CTE). **B.** Kymogram of DNA compaction by the hinge domain. DNA is labeled with dCas9 (top) and YOYO-1 (middle), also shown as composite image (bottom). Arrowhead represents approximate time of protein injection. (B-) or (-) specifies location of the barrier. **C.** Average DNA compaction by 5μM HP1α and 5μM HP1α-hinge. **D. and E.** Brightfield images of the HP1α-hinge and DNA. **D.** Titration of the HP1α-hinge with 500nM 147bp DNA. **E.** Titration of 147bp DNA with 12.5μM HP1α-hinge. Purple boxes indicate presence of condensates.

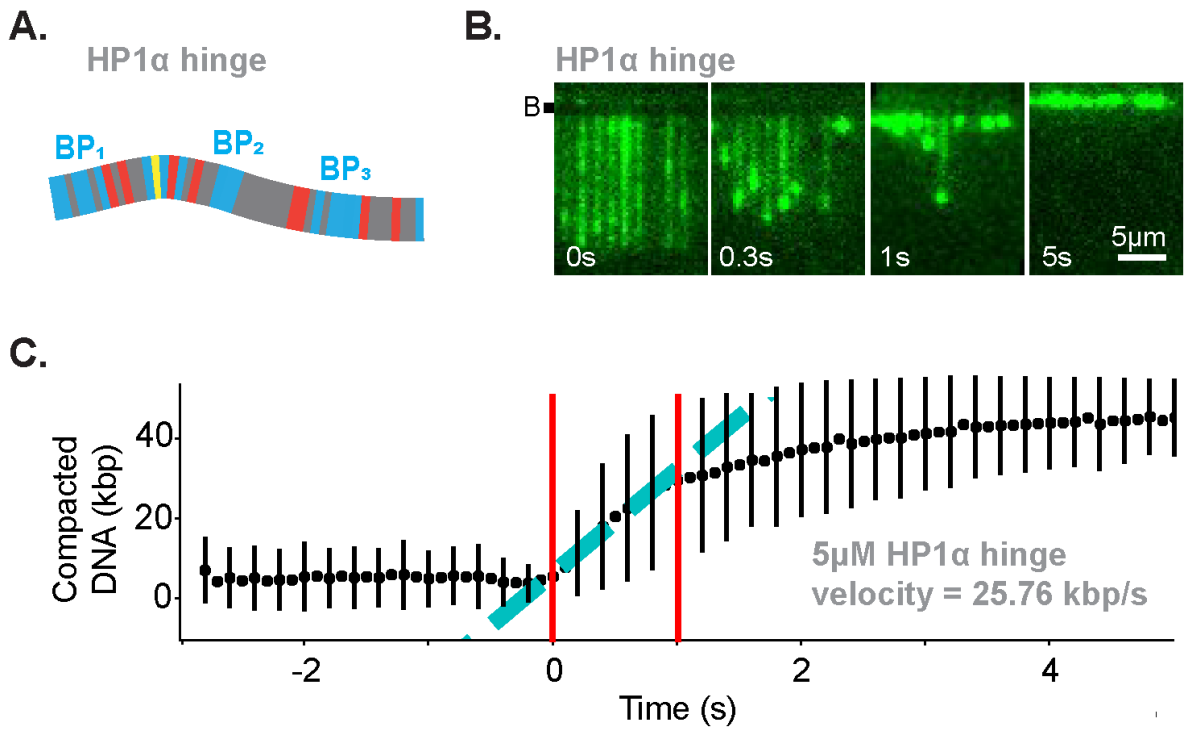

Figure 3.2. The hinge region of HP1 is sufficient for DNA compaction. **A.** Cartoon of HP1α hinge with color-coded disordered residues: positive residues (K and R) blue, negative residues (E and D) red, proline yellow, and all other residues grey. The HP1α hinge contains three basic patches (BP). **B.** Timestamped images of DNA labeled with YOYO-1 undergoing compaction by 5μM HP1α hinge (unlabeled) shown before, during, and after compaction. (B-) specifies location of the barrier. **C.** Average DNA compaction by the HP1α hinge. Compaction velocity estimated from linear fit to data (cyan). Fit constrained to the region within the two red lines.

role keeping the protein in a closed conformation and the NTE playing a positive role in which the N-terminal phosphates interact with the hinge of another dimer to promote oligomerization (Larson et al., 2017). I therefore hypothesized that these two disordered terminal extensions may similarly regulate hinge activity in the context of the HP1α-DNA condensates. To dissect the roles of these extensions, I deleted the extensions of HP1α, either separately or in tandem (Figure 3.4A). Removal of the NTE, (HP1α- ΔNTE), inhibited condensate formation with 147bp DNA (Figure 3.3A) and increased the critical concentration for condensate formation 2-fold with 9kb DNA (Figure 3.3B). Further, NTE deletion resulted in a 20-fold decrease in DNA compaction rate (Figure 3.3E, 3.4C). This inhibition of both DNA compaction and condensate formation upon NTE deletion suggested the NTE plays a positive role in each process. As NTE phosphorylation promotes higher-order oligomerization, it is possible even in the absence of phosphorylation acidic residues in the NTE could facilitate electrostatic interactions with the basic patch of adjacent dimers. I hypothesize that the NTE is involved in higher order oligomerization of HP1α post-DNA binding (Figure 3.5A). In contrast, deletion of the CTE (HP1α-ΔCTE) decreased the HP1α critical concentration an order of magnitude when mixed with 147bp DNA (Figure 3.3A) and 2-fold when mixed with 9kb DNA (Figure 3.3B). Further, HP1α-ΔCTE compacted DNA 2-times faster than WT HP1α (Figure3.3D, 3.4C). These results suggest the CTE is a negative regulator of the full-length protein, potentially by directly binding to the hinge in cis and thereby regulating the proteins accessibility to DNA (Figure 3.5F).

When both the NTE and the CTE are removed from HP1α (HP1α-ΔNTEΔCTE) I observe an intermediate phenotype, with a compaction rate similar to FL HP1α (Figure 3.3C-D, 3.4C) and a decrease in HP1α critical concentration for DNA (Figure 3.3A-B). This result is consistent with the model that the NTE and CTE play opposing roles in regulating HP1α activity. Dimerization via the CSD is a critical regulatory step for oligomerization of phosphorylated HP1α. I speculate the CSD and the CTE facilitate autoregulation of DNA hinge accessibility by maintaining a ‘closed dimer’ conformation, where hinge basic patches bind to the acidic residues of the CTE, as seen

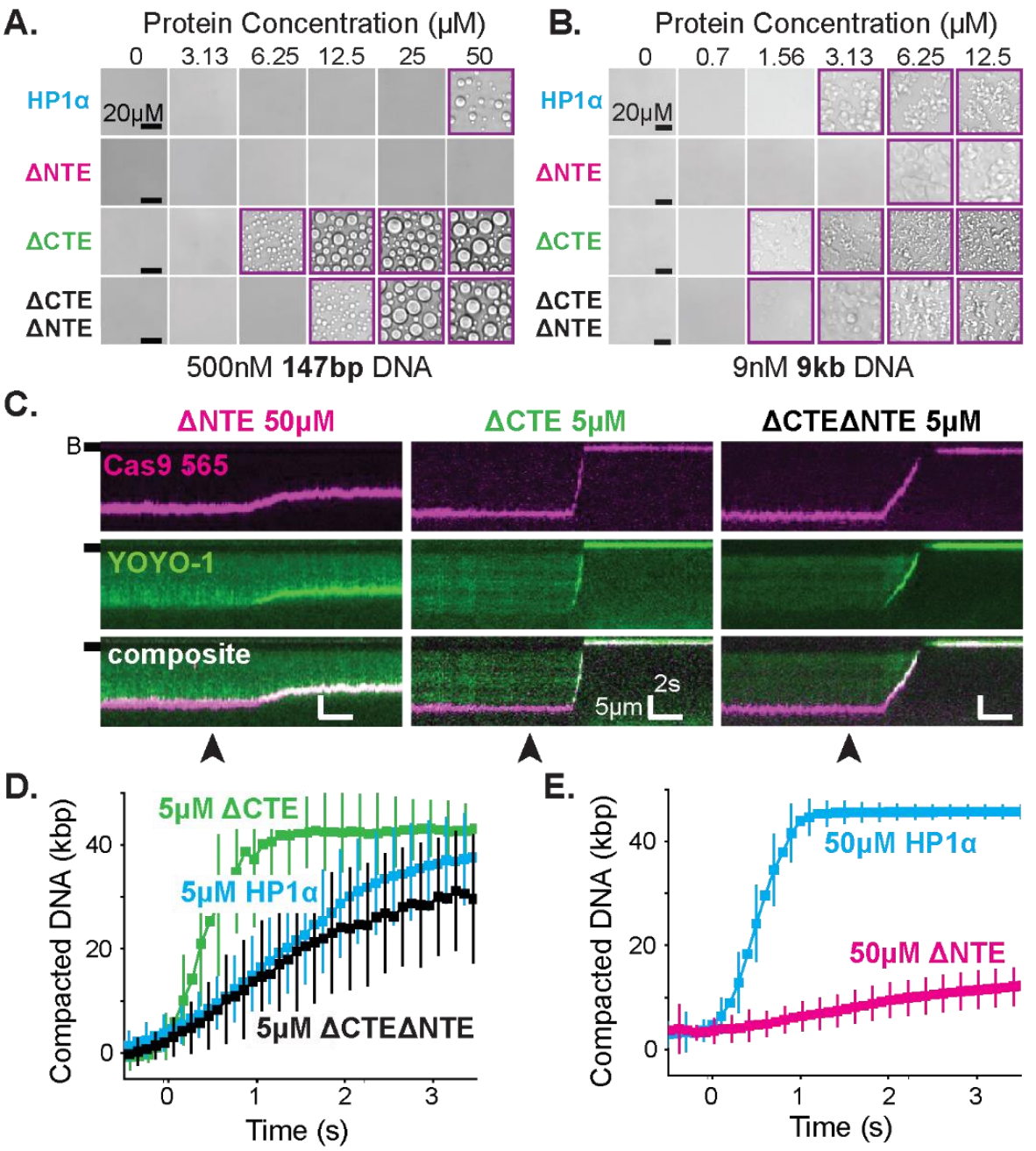

Figure 3.3. The disordered extensions of HP1α regulate DNA compaction and condensate formation **A. and B.** Brightfield images of HP1α domain mutants and DNA. **A.** Titration of HP1α domain mutants with 500nM 147bp DNA. **B.** Titration of HP1α domain mutants with 9nM 9kbp DNA. Purple boxes indicate presence of condensates. **C.** Kymograms of DNA compaction by HP1α domain mutants. DNA is labeled with dCas9 (top) and YOYO-1 (middle), also shown as composite image (bottom). Data shown for reactions including 50μM HP1αΔNTE, 5μM HP1αΔCTE, and 5μM HP1αΔNTEΔCTE, respectively. Arrowheads represent approximate time of protein injection. (B-) or (-) specifies location of the barrier. **D.** Average DNA compaction by 5μM HP1α, 5μM HP1αΔCTE, and 5μM HP1αΔCTEΔNTE. **E.** Average DNA compaction by 50μM HP1α and 50μM HP1αΔNTE.

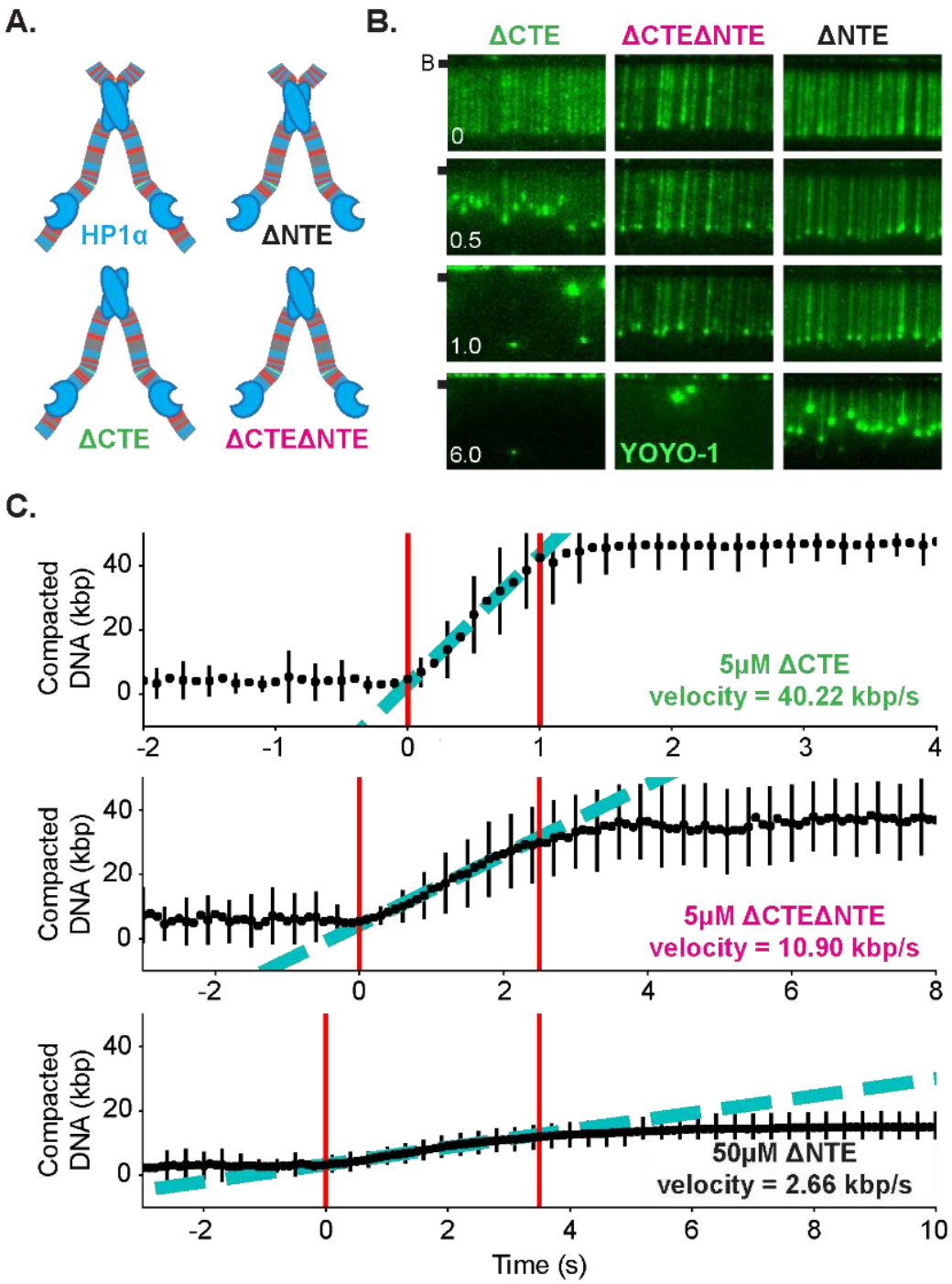

Figure 3.4. DNA compaction activity of HP1α domain mutants. **A.** Cartoon of HP1α extension mutants with color-coded disordered residues: positive residues (K and R) blue, negative residues (E and D) red, proline yellow, and all other residues grey. **B.** Timestamped images of DNA labeled with YOYO-1 undergoing compaction by 5μM HP1αΔCTE, 5μM HP1αΔNTEΔCTE, and 50μM HP1αΔNTE (unlabeled) shown before, during, and after compaction. (B-) or (-) specifies location of the barrier. **C.** Average DNA compaction by each HP1α mutant. Compaction velocity estimated from linear fit to data (cyan). Fit constrained to the region within the two red lines.

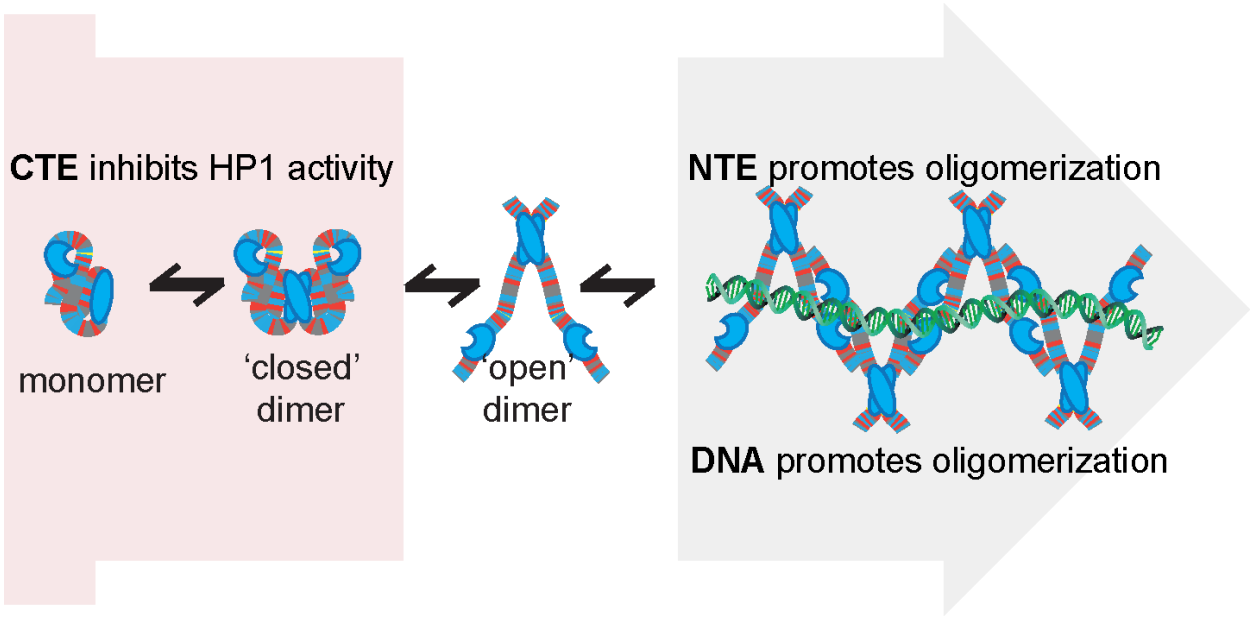

Figure 3.5. Proposed model of HP1α autoregulation and potential oligomerization.

previously (Larson et al., 2017, red arrow, Figure 3.5). Binding of DNA to the hinge basic patches could release the autoinhibited state, potentially facilitating an 'open conformation' of HP1α (grey arrow, Figure 3.5). As long as DNA does not saturate basic patch binding sites, I hypothesize a multivalent network of HP1α-HP1α oligomerization is formed, likely via electrostatic interactions provided by the negative and positive residues within the hinge and NTE (grey arrow, Figure 3.5), allowing both DNA compaction and condensate formation to occur. Fascinatingly, every mutation that affected droplet critical concentration proportionally altered compaction rates implying (1) HP1α contacts might similarly facilitate DNA compaction in the curtains experiments by tethering distal sites together and (2) DNA compaction and condensate formation by HP1α are linked phenomena driven by the same molecular components.

3.2.2 Divergence in the disordered regions of the HP1 paralogs drives differential function

The three HP1 paralogs display unique nuclear localization patterns in cells despite all bearing a well conserved CD and CSD, with HP1β and HP1γ often localizing to euchromatic regions lacking H3K9 methylation entirely (Smothers et al., 2000 and Dialynas et al., 2007). However, the unstructured regions have diverged significantly from one another (Figure 3.6A-B)). I hypothesized that a combination of charge topology and specific residue spacing within the disordered regions would result in differential DNA compaction and phase separation behavior and facilitate their differential activities seen *in vivo* (Canzio et al., 2014). To address this question, I first characterized the compaction phenotypes of HP1 paralogs. HP1β is only able to transiently bind to DNA when fluorescently labeled and compaction is severely reduced compared to HP1α (Figure 3.6C-D, 3.7A). Visualization of DNA with YOYO-1 indicates that several puncta appear throughout the DNA strand upon injection of HP1β, but these are dimmer and less localized than those seen with HP1α (Figure 3.7A). Further, HP1β did not phase separate with any of the DNA lengths tested (Figure 3.6G, 3.7D-E). While HP1β maintains both basic patches in its hinge, there is a 2-log decrease in its isoelectric point which I propose affects DNA binding, compaction, and co-condensate formation.

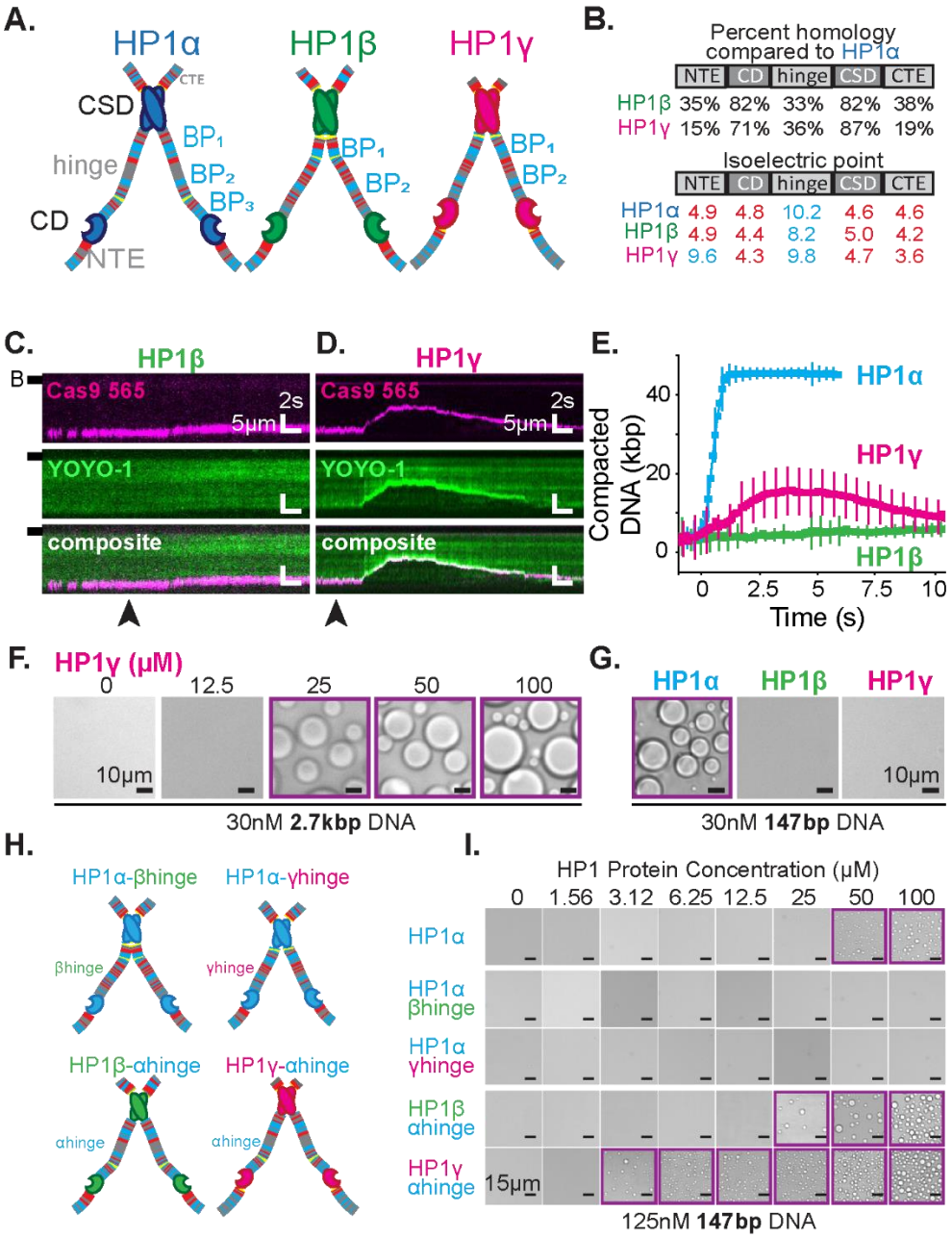

Figure 3.6. DNA compaction and condensate formation activity of HP1β and HP1γ. **A.** Cartoons of the three paralogs of human HP1 with color-coded disordered residues: positive residues (K and R) blue, negative residues (E and D) red, proline yellow, and all other residues grey. Basic patches (BP) for each paralog are labeled. **B.** Comparison of amino acid homology between HP1α and HP1β or HP1γ. **C. and D.** Kymograms of DNA compaction by **C.** HP1β and **D.** HP1γ. DNA is labeled with dCas9 (top) and YOYO-1 (middle), also shown as composite image (bottom). Arrowheads represent approximate time of protein injection. (B-) or (-) specifies location of the barrier. **E.** Average DNA compaction by 50μM HP1α, HP1β, and HP1γ. **F.** Brightfield images of HP1γ and 2.7kbp DNA. **G.** Brightfield images of 100μM HP1α, HP1β, or HP1γ and 147bp DNA. **H.** Cartoon of HP1 hinge domain swaps. **I.** Brightfield images of HP1 domain swap mutants and 147bp DNA. Purple boxes indicate presence of condensates.

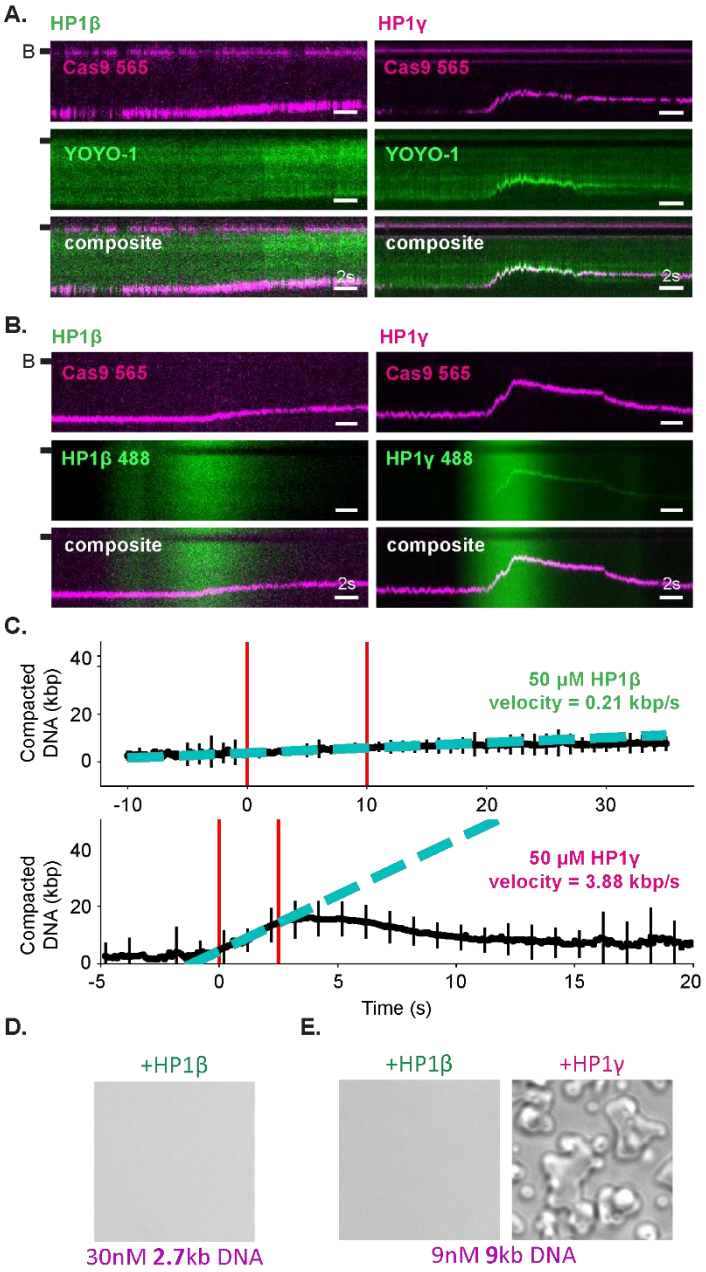

Figure 3.7. DNA compaction and condensate formation activity of HP1β and HP1γ. **A.** Cartoons of the three paralogs of human HP1 with color-coded disordered residues: positive residues (K and R) blue, negative residues (E and D) red, proline yellow, and all other residues grey. Basic patches (BP) for each paralog are labeled. **B.** Comparison of amino acid homology between HP1α and HP1β or HP1γ. **C. and D.** Kymograms of DNA compaction by **C.** HP1β and **D.** HP1γ. DNA is labeled with dCas9 (top) and YOYO-1 (middle), also shown as composite image (bottom). Arrowheads represent approximate time of protein injection. (B-) or (-) specifies location of the barrier. **E.** Average DNA compaction by 50μM HP1α, HP1β, and HP1γ. **F.** Brightfield images of HP1γ and 2.7kbp DNA. **G.** Brightfield images of 100μM HP1α, HP1β, or HP1γ and 147bp DNA. **H.** Cartoon of HP1 hinge domain swaps. **I.** Brightfield images of HP1 domain swap mutants and 147bp DNA. Purple boxes indicate presence of condensates.

When HP1γ is injected into the flowcell I see compaction of almost the full extent of DNA (Figure 3.6D-E, 3.7A-B). However, this compaction is much more transient than that seen with HP1α, immediately decompacting after the injected HP1γ leaves the flowcell and additional buffer is washed through (Figure 3.6D-E, 3.7A-B). This is consistent with HP1γ's weaker affinity for DNA. Consistent with an intermediate compaction phenotype, HP1γ induces droplet formation when mixed with 2.7kb DNA but with a ~10 fold increase in critical concentration when compared to HP1α (Figure 3.6F). Further, droplets were not formed when HP1γ was mixed with 147bp DNA (Figure 3.6G). Interestingly, the HP1γ hinge has a similar isoelectric point to HP1α so it remains uncertain whether it is the spacing between the basic patches in the hinge, placement of the negative hinge residues, autoregulation of the extensions, or decreased multivalency that contribute to the weakened DNA affinity, DNA compaction, and co-condensate formation observed for HP1γ and is an interesting avenue of future work.

Given the centrality of the hinge in all the DNA related activities of HP1α, I hypothesized that the divergence in hinge sequences of the HP1 paralogs resulted in their differential DNA activities. To directly test this possibility, I generated four hinge swapped mutants: HP1α-βhinge, HP1α-γhinge, HP1β-αhinge, and HP1γ-αhinge (Figure 3.6H). I found that replacing the hinge of HP1α with either the βhinge or γhinge (HP1α-βhinge and HP1α-γhinge) was insufficient to form DNA co-condensates with 147bp DNA (Figure 3.6I). This implies that the HP1α hinge is necessary for droplet formation in the context of the full length HP1α protein. While it might be expected for HP1α-γhinge to have an intermediate activity, it is worth noting that HP1γ lacks any appreciable CTE, and its NTE is remarkably different than that of HP1α with a 4-log increase in isoelectric point (Figure 3.6B). Therefore, in its native context the hinge domain of HP1γ may not have to mediate a competition between domains to facilitate interactions with DNA, whereas when placed within the HP1α molecule, it is possible that the hinge domain of HP1γ is unable to overcome the potent effect of HP1α's autoregulatory CTE extension. I then performed the compensatory domain swaps, placing the hinge domain from HP1α into HP1β (HP1β-αhinge) and HP1γ (HP1γ-

αhinge). I find both of these mutants form co-condensates with DNA, implying the HP1α hinge is sufficient for phase separation in the context of the other paralogs (Figure 3.6I). Intriguingly, the HP1 critical concentration was markedly lowered for both mutants, two-fold lower for HP1β-αhinge and ten-fold lower for HP1γ-αhinge. As HP1α exhibits robust autoregulation of the potent hinge activity, I propose HP1β and HP1γ have not evolved the same regulatory mechanisms and therefore exhibit decreased critical concentration upon the swapping of the α-hinge into the paralogs.

HP1 paralogs are often found in overlapping genomic regions in cells and have been suggested to heterodimerize. Given the differential DNA activities of the paralogs, I asked what role mixed populations might play on regulation of the potent HP1α co-condensate formation. To test this, I performed droplet assays in the presence of paralog competitors. When HP1β or HP1γ were premixed with HP1α and added to DNA to assess LLPS, both HP1β and HP1γ inhibited droplet formation in a concentration dependent fashion (Figure 3.8A-B). Notably, these experiments were performed with 147bp DNA in which HP1γ exhibits no co-condensate formation (Figure 3.6G). Interestingly, when HP1β is introduced to pre-formed HP1α co-condensates, HP1β is capable of invading and subsequently dissolving the droplets in real time (Figure 3.8B). As HP1β has a much weaker affinity for DNA than HP1α (Supplementary Figure 1A), the addition of HP1β to the co-condensates must either change the chemical characteristics of the droplets and indirectly change the HP1α-DNA interactions or directly bind to HP1α and inhibit either its binding to DNA or HP1α-HP1α interactions. In contrast, HP1γ enriches in the co-condensates but does not destabilize them suggesting it acts as a less potent inhibitor of HP1α. Together, these results suggest inter-paralog competition as a possible mechanism of cellular regulation.

Together, these results suggest inter-paralog competition as a possible mechanism of cellular regulation of HP1-mediated chromatin domains. Moreover, these experiments demonstrate the critical advantage of biological organization by liquid condensates—competition can be fast. Fast competition means that, regardless of domain stability, when the molecular

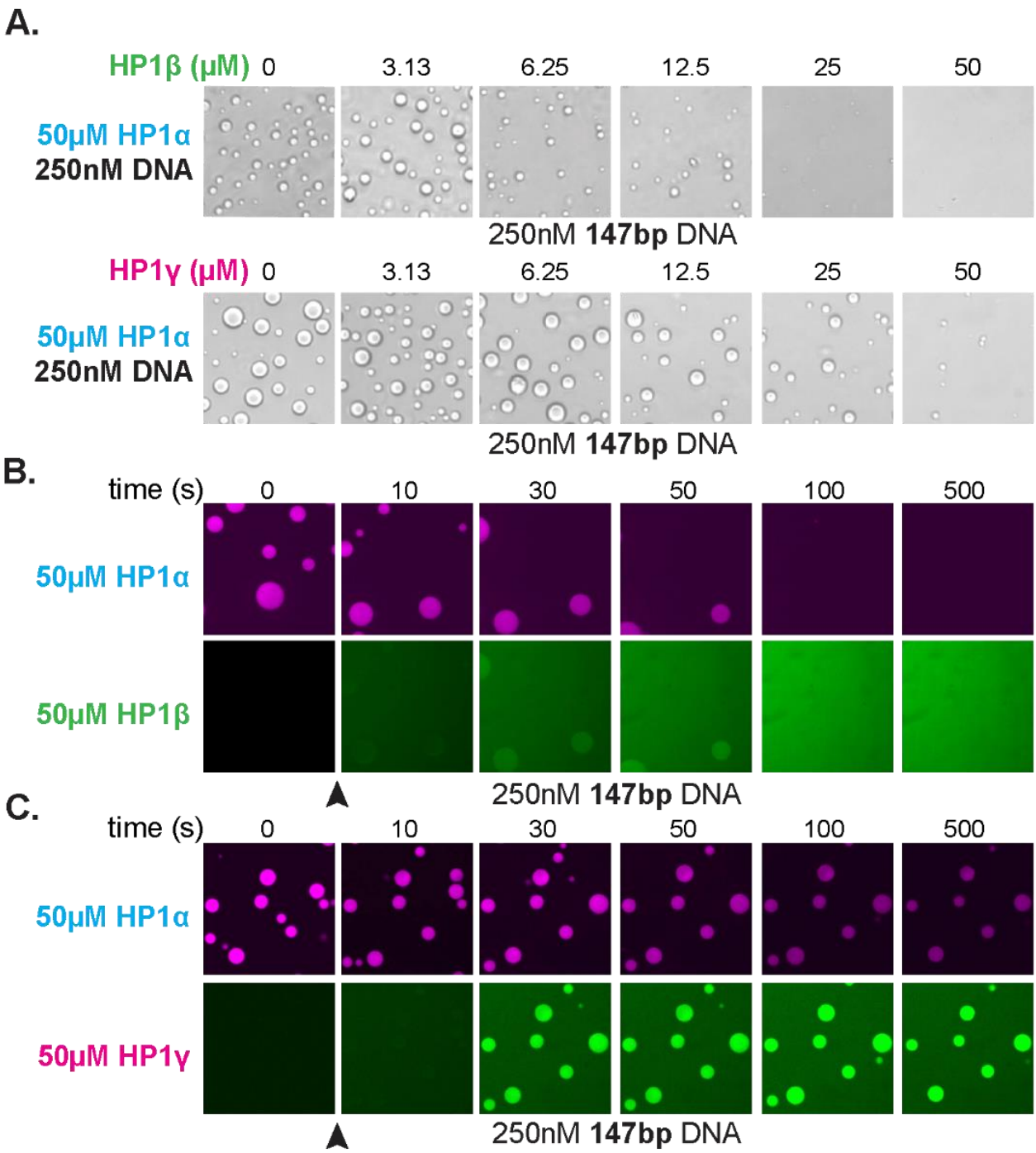

Figure 3.8. Effect of HP1β and HP1γ on HP1α-DNA condensate formation and stability. **A.** Brightfield images of DNA and pre-incubated mixtures of HP1α and HP1β (top) or HP1α and HP1γ (bottom). **B. and C.** Confocal images showing a time course of HP1α condensates after injection of **B.** HP1β or **C.** HP1γ.

environment changes, condensates can respond to those changes at the rate at which the organizing material exchanges. For condensation of DNA by HP1α, this means that even in the context of highly viscous, tangled DNA and large networks of protein-protein and protein-DNA interactions that resist mechanical disruption at steady state, domains can easily be disassembled in seconds due to the rapid exchange rate of individual HP1α molecules.

Discussion

The compaction of DNA in heterochromatin is thought to drive transcriptional silencing. While HP1 is an established driver of heterochromatin, limitations in *in vitro* assays that recapitulate compaction and *in vivo* resolution have hindered decoding the mechanism of HP1 compaction and transcriptional silencing. Therefore, we utilize two mesoscale approaches, DNA curtains and phase separation assays, to decipher a preliminary mechanistic understanding of HP1 activity. In short, I found the HP1α hinge is necessary and sufficient to drive DNA compaction and DNA-driven LLPS and the terminal extensions provide both positive and negative regulation of the hinge activity. Each of the HP1 paralogs exhibit distinct compaction and LLPS behavior in part due to sequence differences in the disordered hinge regions. And finally, the differences in the paralogs allow for the rapid invasion and dissolution of the stable HP1α-DNA condensates.

The results from Chapter 2 suggest a dynamic population of HP1α can stably condense DNA due to the bulk affect of enough HP1 molecules binding at any one time. In Chapter 3, I described how dynamic HP1 diffusion facilitates competition and dissolution of the condensates. Therefore, the contradictory necessity for heterochromatin to be both stable and rapidly reversible is preliminary explained by the rapid diffusion and phase separation of HP1. This lens brings to light many important considerations for heterochromatin biology, as is described below.

A potential mechanism of HP1-DNA phase separation and its implications

Complex coacervation describes when two oppositely charged polymers together form a polymer rich condensate due to preferential solvation by polymer-polymer interactions over those

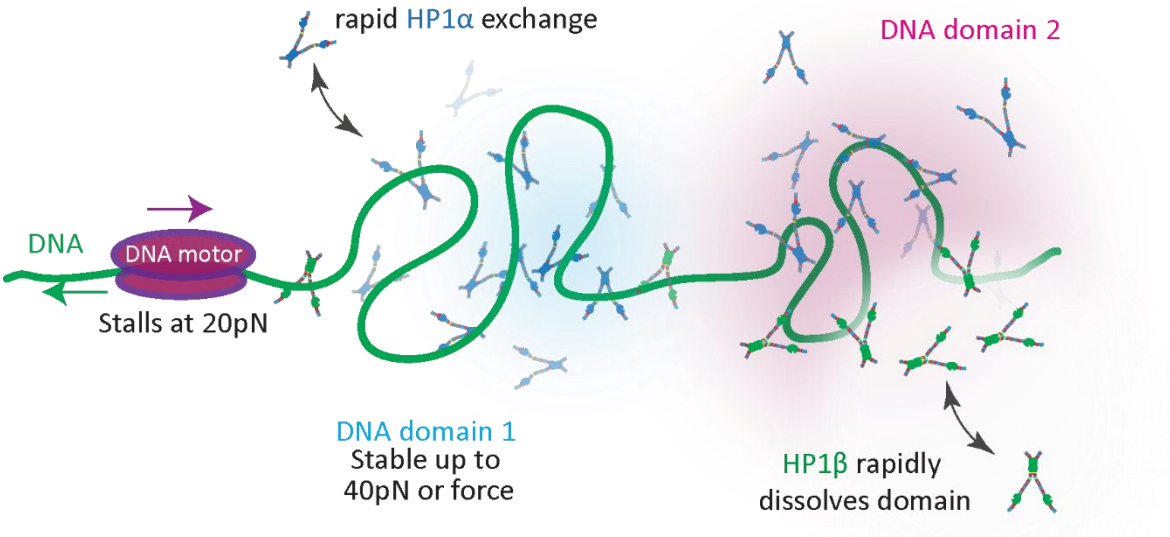

Figure 3.9. Cartoon scheme of HP1 domain regulation in cells. Dynamic HP1 binding can maintain stable domains resistant to up to 40pN of force, while simultaneously rapidly dissolving upon the addition of HP1β.

with the solvent. This is a remarkably different type of phase than those formed via an “incompatibility” with the solvent, such as hydrophobic polymers that are immiscible with the solvent because of the large enthalpic cost for mixing (Overbeek and Voorn, 1957). Given the negative character of a DNA polymer and the basic patches within the disordered regions of HP1 proteins, I hypothesize complex coacervation could be driving the condensate formation of HP1α and DNA. This has several important implications for the material properties of the HP1-DNA phases. First, phase separation caused by immiscibility has the almost total enrichment of the polymer into the concentrated phase, and this phase excludes solvent. In contrast, phase separation caused by coacervation has one phase with solvent and a high concentration of polymer, and another phase with solvent and a dilute concentration of the polymer. The ability of solvent to incorporate into both phases in coacervation would allow rapid sensing of salt and pH changes in the nucleus, and likely would allow the entrance auxiliary proteins into the phase as long as the charge balance between HP1 and DNA is dramatically disrupted. Further, the polymer does not need to be entirely enriched in the concentrated phase and can move between these two phases with ease. Phase separation caused by coacervation is therefore completely consistent with *in vivo* HP1 phenotypes of quick diffusion between phases (Cheutin et al., 2003, Festenstein et al., 2003) and does not require the field to remove the label of phase separation for HP1 in cells quite yet (Erdel et al., 2020).

Second, coacervation is dependent on both the charge density and the molecular weight of the polymer. Seen in this lens, the differences in condensation properties between the paralogs are easily explained. The hinge of both HP1β and HP1γ have one less basic patch than HP1α and a larger number of acidic residues (Figure 3.5A,B) which would lower the valency of interactions and the net charge of the region. Interestingly, while HP1γ cannot phase separate with the short 147bp piece of DNA, it can when the valency of the DNA is increased to 2.7kb (Figure 3.5F-G. Perhaps the increased molecular weight and valency of the 2.7kb DNA makes up for the lower charge density of HP1γ, allowing de-mixing of the solution to occur. The difference

in acidity between the HP1β and HP1γ hinges could also explain why HP1β can dissolve pre-formed HP1α-147bp DNA phases while HP1γ simply enriches (Figure 3.8C). While both can easily enter the phase, the increased acidity of HP1β might push the solution out of the two-phase regime while the acidity induced by HP1γ is not sufficient at these concentrations. Finally, post-translational modification of all proteins involved will influence the net charge and therefore whether a two-phase regime is favorable (Aumiller and Keating, 2015). This is likely a universal characteristic: the concentration, charge, and valency of molecules that enter into a heterochromatin region will determine whether disruption occurs.

Implications for transcriptional regulation

How does sequestering DNA into heterochromatin allow for transcriptional silencing? There are two non-mutually exclusive hypotheses: the first is heterochromatic compaction does not allow for free diffusion and binding of transcriptional machinery and the second is that RNA polymerase is unable to provide sufficient force to unwind compacted heterochromatin regions during transcription. My data in Chapter 2 suggests that force is a large barrier for de-condensation, as it is only when the force is sustained in the optical trap experiments that HP1-DNA condensates dissolve (Figure 2.8F). The experiments presented in Chapter 3 suggest, but by no way confirm, that diffusion of heterochromatic competitors into condensates might be free and fast due to the quick diffusion of HP1 paralogs into the pre-formed phases (Figure 3.8B-C). However, the entrance of competitors into the phase might be dependent on the size, charge, and binding partners these proteins have within heterochromatic regions. Further, the dense condensation of chromatin might limit the free diffusion of proteins large in size or densely charged that have already entered the phase. While my data suggests transcription will be limited by force, and not diffusion, future studies more carefully detailing both components will bring to light to what extent each is affected by the phase separation of HP1.

A conserved mechanism of heterochromatin condensation

Heterochromatin is mediated by the activity of both HP1 and the polycomb repressive complex (PRC) proteins, and the genomic regions each occupies typically does not overlap (Hathway et al., 2012). Interestingly, Cbx2 is a major mediator of chromatin condensation in the PRC1 complex and has a similar internal low complexity, disordered domain with multiple basic patches as the HP1 hinge. These basic patches are essential for chromatin compaction in vitro and cause axial patterning defects in mice (Grau et al., 2011 and Lau et al., 2017). Further, the Kingston lab recently showed that these very basic patches mediate both DNA and phosphorylation dependent Cbx2 phase separation (Plys et al., 2019). Further, the protamine proteins that tightly package the chromatin in sperm appear to be simply a low complexity domain with basic patches, with all the other regulatory domains of Cbx2 and HP1 removed, and also shows DNA-compaction activity *in vitro* (Brewer et al., 1999) Our conclusions are very similar that those seen with Cbx2 and protamine proteins: basic patches in a disordered region cause both chromatin condensation and phase separation, and therefore could present phase separation as a universal mechanism of heterochromatin organization in mammals.

Chapter 4: Initial characterization of HP1-chromatin phase separation properties

4.1 Introduction

Up until this chapter I have largely ignored the role nucleosome substrates play on heterochromatin organization by HP1. This was done for both practical and conceptual reasons. For the practical, in my early days characterizing HP1-DNA phase separation and compaction I really struggled with reproducibility of phenotypes due to the enormous number of variables I had not yet determined how to control. Small changes in buffer conditions, temperature, pH, and DNA length completely changed my phenotypes leading me to a level of methodical paranoia I did not know I had in me. Further, chromatin is sticky and difficult to make, and my assays often required exorbitant amounts of material. For the conceptual, it seemed necessary to do the control experiments with DNA alone first and then slowly increase complexity. But Chapter 2 and 3 of this thesis describe control experiments whose phenotypes were incredibly complex, and often contradictory, and required a lot of additional experiments to come up with a cohesive mechanism.

However, we know the majority of the DNA in the nucleus is wrapped with nucleosomes. These nucleosomes contain 147bp of DNA wrapped around a histone-octamer core. In the cell, HP1α is found at compacted heterochromatic regions bearing tri-methylation of histone 3 at lysine 9 (H3K9me3) and is thought to localize via direct recognition of histone methylation by the HP1 chromodomain (CD) (Platero et al., 1995). In drosophila HP1 recruitment to genomic domains can occur before the H3K9me3 modification is installed, implying that HP1 can respond to other molecular inputs (Yuan and O'Farrell 2016). Furthermore, HP1 mutations that abrogate both H3K9me3 recognition and the DNA binding disrupt genomic localization in cells (Muchardt et al., 2002 and Mishima et al., 2012). In fact, all three HP1 paralogs display unique nuclear localization patterns despite all bearing a well conserved CD, with HP1β and HP1γ often localizing to euchromatic regions lacking H3K9 methylation entirely (Smothers et al., 2000 and Dialynas et al.,

2007). These complexities in cellular phenotypes are fascinating: a wide array of inputs direct HP1 localization and function. But it also means detailed characterization of chromatin recognition by HP1 is complex and will take time and many patient souls in the field comfortable with uncertainty to characterize.

However, careful biochemical characterization has allowed the field to zoom in on three binding sites human HP1 has for the nucleosome. The chromodomain (CD) recognizes the tri-methylation of histone H3 (H3K9me3) (Platero et al., 1995 and Nielsen et al., 2002), the basic patches in the unstructured hinge bind to DNA (Sugimoto et al., 1996 and Zhao et al., 2000), and the chromoshadow domain (CSD) that mediates dimerization further binds to the H3 helix within the nucleosome core (Cowieson et al., 2000, Dawson et al., 2009 and Richart et al., 2011). Interestingly, despite this complexity of binding sites the field often contributes all HP1 paralog activity to the binding of the H3K9me3 mark *in vivo.* Weirdly, specificity for this mark on a mononucleosomes substrate was difficult to obtain *in vitro* (unpublished work by Adam Larson, Mishima et al., 2012, and Ryan et al., 2018). Mishima found, however, that increasing the linker length on a mono-nucleosome increases specificity for the H3K9me3 mark while Ryan found you can further increase methyl mark specificity by increasing the number of nucleosomes present on a DNA substrate. This suggests the binding sites in HP1 are linked: the DNA, octamer core, the H3K9me3 mark, and the valency of each all work together to correctly place HP1 on the nucleosome.

While not initially my intention, I have fallen into the same trap as many in the HP1 field and have limited my analysis to HP1α after being presented with the complexity of phenotypes found within the paralogs. Being first in the alphabet is certainly an unfair advantage, and I encourage any future students reading this to resist this same urge. In particular, I hope you to read the 2016 Hiragami-Hamada paper and speculate whether the mesoscale phase separation assays I utilize might not be the right fit to understand the function of HP1β (while not shown, HP1β has shown no evidence of phase separation with either unmodified or methylated arrays in

our hands). Further, the critical concentrations necessary to induce the phase separation of HP1γ with DNA alone may not be physiologically relevant, yet other substrates involved in euchromatin might be more potent inducers of multivalency.

Finally, it is essential to point out the work in this chapter is all a collaboration with Lucy Brennan and would not have been possible without her expertise in chromatin biology and biophysics.

Results

It is certainly fitting that as I attempted to increase complexity of my experimental system by adding in nucleosomes, salt conditions would again come to plague all of my results in the most beautiful way. Bryan Gibson had found that arrays assembled with 12-nucleosomes on a single strand of DNA could phase out of solution at specific salt conditions (Gibson et al., 2019). At 75mM KOAc, these arrays were miscible in solution but when moved to a buffer with 150mM KOAc and 1mM $Mg(OAc)_2$ macroscopic droplets emerged. Biochemical experiments with HP1 are also typically done in one of these two salt regimes (Mishima et al., 2012 and Kilic et al., 2015 were performed at ~50mM salt, while Kilic et al., 2015 and Canzio et al., 2013 utilize 150mM salt). These salt concentrations will have important implications for binding interactions: While electrostatic interactions are enhanced at lower salt concentrations (likely promoting DNA binding by the basic patches in the HP1 hinge), hydrophobic interactions are enhanced at higher salt conditions (likely promoting HP1 binding to the H3 helix and H3K9me3). The results below utilize both salt regimes to describe a preliminary picture of how DNA linker length and methylation state impact the ability of HP1α to form condensates.

Nucleosomes can induce the phase separation of HP1α

Increasing the linker length on mononucleosomes increases the affinity of HP1α to nucleosome substrates (Mishima et al., 2012 and Ryan et al., 2018). Therefore, I wished to determine first if nucleosomes were capable of inducing phase separation of HP1α and, if so, the role linker length played in this process. I utilized buffer conditions (70mM KCl, 20mM Hepes pH

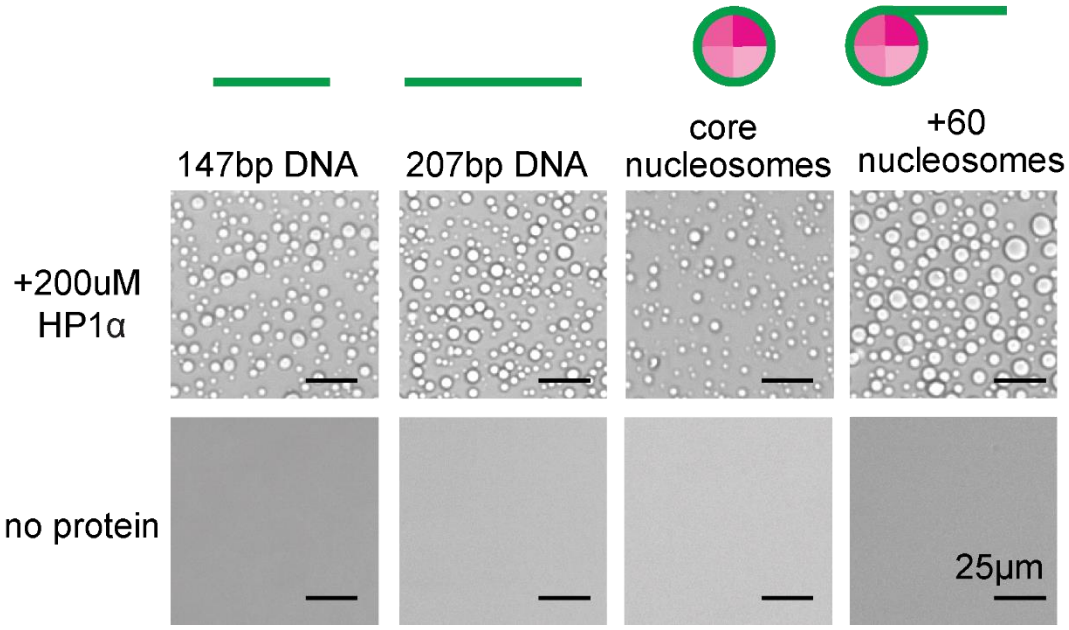

Figure 4.1. Droplet formation of HP1α and chromatin substrates. 200μM HP1α was mixed with each substrate at 70mM KCl and imaged with brightfield microscopy

7.5, 1mM DTT, 5mM Tris, 0.25mM EDTA, 5% glycerol) in which HP1α and the DNA/nucleosome substrates alone are miscible in solution. However, upon the addition of either DNA or nucleosome substrates to HP1α, macroscopic droplets emerge in solution indicating that nucleosomes are indeed capable of inducing the multivalent properties necessary for the phase separation of HP1α (Figure 4.1). Interestingly, the droplets created with core nucleosomes and HP1α appeared smaller in size than those made with either substrate DNA alone. I hypothesize the wrapping of the DNA around the histone octamer core limits the HP1α-DNA binding sites provided by the nucleosome substrate when compared to naked DNA.

I next tested the effect DNA linker length had on HP1α phase separation. If the nucleosome was simply blocking accessibility of HP1α to the DNA, I would expect droplet sizes to reduce with this substrate similar to the core nucleosome. In contrast, I saw the nucleosomes with 60bp of linker DNA formed droplets larger than those produced with either the core nucleosomes or the naked DNA substrates (Figure 4.1). A possible explanation for this phenotype is the extra 60bp linker length in these nucleosomes allows HP1α to dock in a conformation that promotes binding of the CSD to the H3 helix, thus the wrapping of the DNA around the nucleosome core does not inhibit binding as a new site is now accessible within the histone core. This model was similarly presented by Mishima, who showed that linker length increased specificity for the H3K9me3 mark. Another possibility is that both binding and the higher order HP1α-HP1α oligomerization is affected by linker length, leading to the larger droplet sizes. Future work delving into the influence linker length and the H3K9me3 mark have on the binding, oligomeric potential, and phase separation of HP1α are necessary to fully understand the mechanistic underpinning of these phenotypes.

Preferential enrichment of HP1 into arrays modified with H3K9me3

As increasing the linker length influenced droplet size, I next wished to determine how increasing the valency of the nucleosomes affected droplet formation. In particular, arrays assembled with 12-nucleosomes on a single strand of DNA increases the affinity of HP1α binding

over 2-fold when compared to a mononucleosomes (Ryan et al., 2018). I first utilized conditions were neither HP1α or the chromatin arrays phase separate individually and titrated the concentration of HP1α (Figure 4.2A). The 12-nucleosome arrays formed droplets down to 1.56μM of HP1α, two-fold lower than the critical concentration of naked 2.7kb DNA (Figure 2.3E), indicating that chromatin arrays serve as a more efficient multivalent substrate than DNA alone. Interestingly, this critical concentration still lies above the $K_{1/2}$ of dimerization for HP1α (1μM, Larson et al., 2017) despite the $K_{1/2}$ for HP1α binding to 12-nucleosome arrays being slightly below this (~700nM Ryan et al., 2018, gel shift assays). While this could report on technical differences between assays, it is intriguing to speculate that robust dimerization might be essential for droplet formation with chromatin arrays, but not the initial binding.

To test if HP1α would enrich into phases formed at buffer conditions where chromatin arrays phase separate, we utilized 12-nucleosome chromatin arrays with either unmodified wild-type chromatin or chromatin labeled at H3K9 with a methyl lysine analog (MLA) to mimic an H3K9me3 modification. These experiments were performed at the high salt conditions (150mM KOAc and 1mM $Mg(OAc)_2$), where phase separation of chromatin alone is induced (Figure 4.2B, 0μM HP1α). We found HP1α enriches into H3K9me3 chromatin phases at lower concentrations of HP1α (3.125μM) than that needed for unmodified nucleosome arrays (6.125μM). Further, H3K9me3 droplets exhibit higher fluorescence intensity for each HP1α concentration, indicating an increase in HP1α binding to H3K9me3 when compared to unmodified arrays (Figure 4.2B).

Interestingly, while unmodified chromatin phases with no HP1α have spherical morphologies, adding in HP1α at low concentrations caused aggregation of multiple drops with digitated morphologies (Figure 4.2B, 3.25-12.5μM HP1α), indicating a change in the surface tension and/or viscosity of the droplets. This digitated phenotype is concentration dependent, for as HP1α concentration increases the droplets return to spherical morphologies. Similar to the curtain's experiments in Chapter 2, I hypothesize HP1α is binding to the droplets and bridging adjacent DNA sites together. Fast HP1α diffusion might similarly contribute to the surface tension

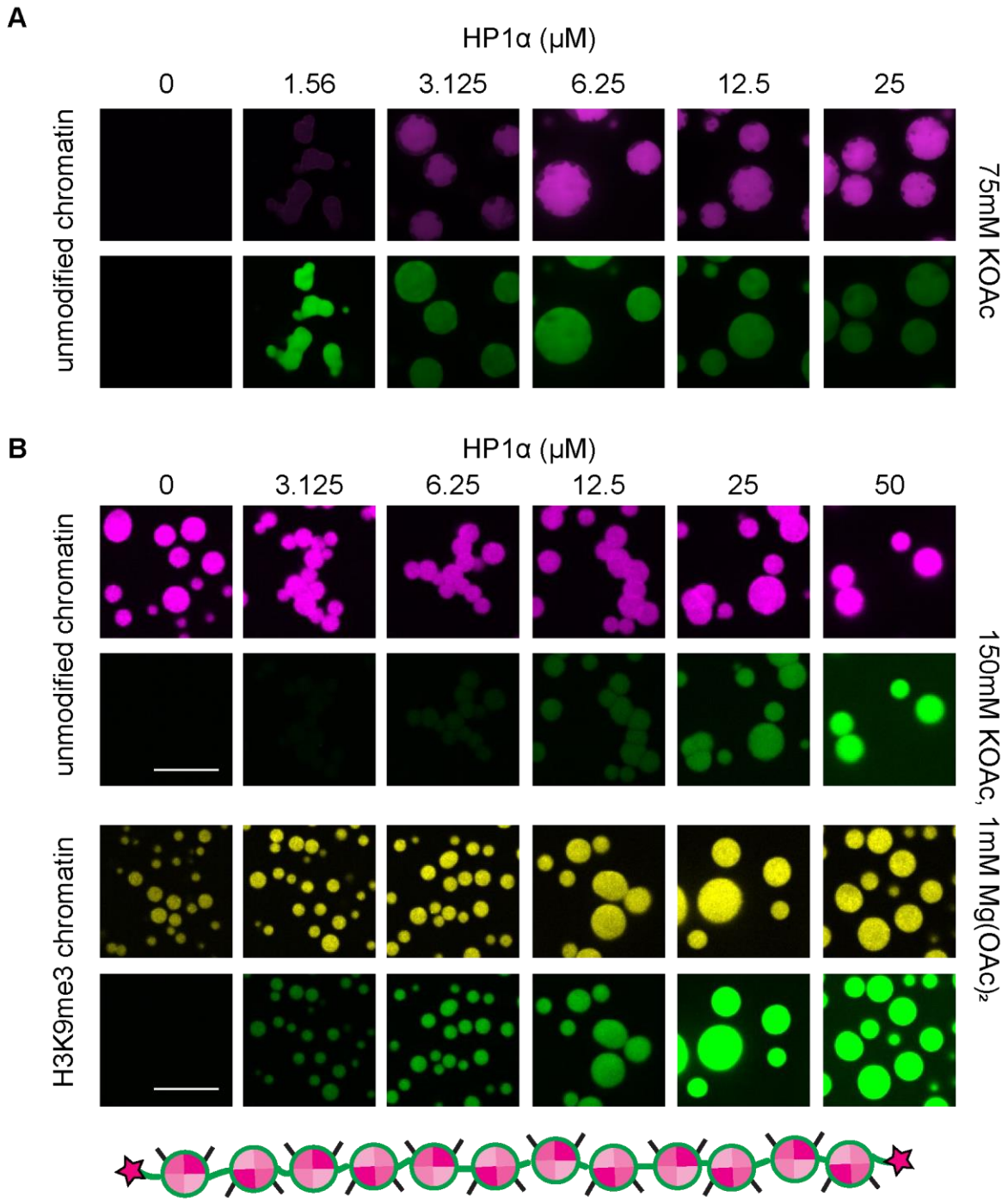

Figure 4.2. Mixing of HP1α and chromatin arrays. **A.** 12-nucleosome arrays were assembled with unmodified cy-5 octamer and unlabeled DNA (magenta) and incubated with stated concentration of HP1α and 250nM HP1α-488 (green). These experiments were performed at 75mM KOAc were arrays alone do not form droplets**. B.** 12-nucleosome arrays were assembled with either unmodified nucleosomes and cy5-end labeled DNA (magenta) or H3-MLA nucleosomes and cy3-DNA (yellow). Chromatin was incubated with the stated concentration of HP1α (μM) and 250nM HP1α-488 (green). These experiments were performed at 150mM KOAc and 1mM $Mg(OAc)_2$ were arrays alone do form droplets**.**

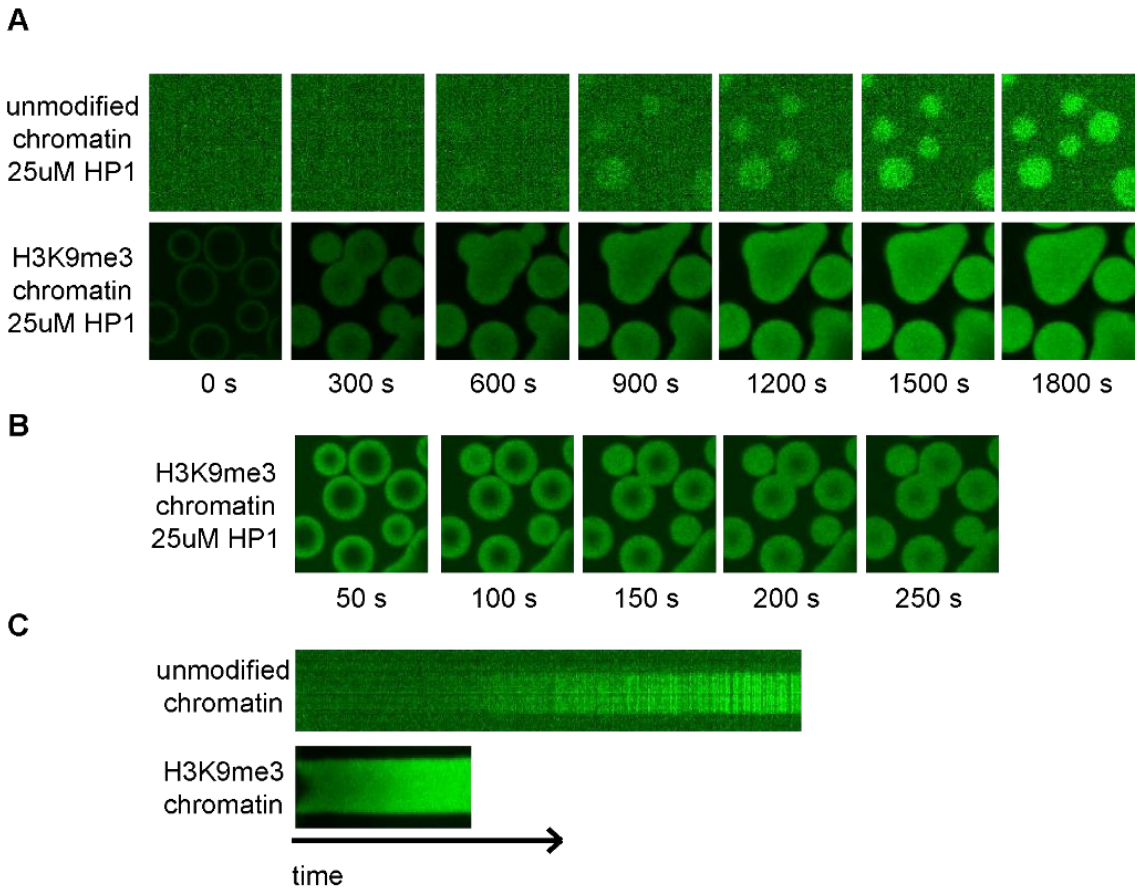

Figure 4.3. Enrichment of HP1α into pre-formed chromatin arrays. **A.** 12-nucleosome chromatin arrays were assembled either with unmodified nucleosomes or H3K9me3 nucleosomes (MLA modification) and mixed with 25μM HP1α and 200nM HP1α-488. **B.** Zoomed in time course of the methylated chromatin arrays with 25μM HP1α. **C.** Kymograph of HP1α incorporation into unmodified or H3K9me3 droplets.

of the droplets, but at low concentrations is insufficient to complete coalescence. Interestingly, this digitated morphology was also seen in droplets formed at low salt with 1.56μM HP1α but became spherical by 3.125μM protein. Whether this increased ability of HP1α to drive surface tension at low salt is due to differential chromatin arrangements in the droplets or an increase in the number of available electrostatic interactions remains to be determined.

Next, chromatin droplets were pre-formed at high salt conditions and HP1α was injected into the well and enrichment of HP1α into the droplet visualized in real time. Consistent with previous data, HP1α diffused into the droplets containing the H3K9me3 mark faster than it diffused into droplets with unmodified chromatin (Figure 4.3). Further, H3K9me3 chromatin resulted in interesting HP1α diffusion patterns. HP1α rapidly coated of the outer edge of the H3K9me3 droplets (Figure 4.3A-B, time 0 and 50s), but subsequent diffusion into the remaining area of the droplet was much slower and as it occurred nearby droplets began to fuse. In contrast, HP1α diffusion into unmodified chromatin appeared to occur at a constant rate, enriching at all locations in the droplet simultaneously over time (Figure 4.3A). A simple explanation is the chromatin phases are much denser in material and this results in longer diffusion times. However, this does not totally explain the divergence in phenotypes between the two chromatin types. Differences in binding affinity, oligomeric potential, HP1α docking orientations, and even potential distortions to the nuclear core might all take part in this differential phenotype (Sanulli et al., 2019). Interestingly, DNA compaction by HP1 proteins in the curtains experiments was dependent on the full coverage of protein along the length of the DNA strand. Fusion of the nearby H3K9me3 droplets could be initially mediated by the bridging of two droplets together, but a sufficient HP1α coating within the droplet would be required to overcome the internal viscosity and complete coalescence. The HP1α concentration necessary to undergo this process with unmodified chromatin would be higher, both due to a decrease in affinity and any other subsequent changes to HP1 activity when the methyl mark is not present.

De-mixing of chromatin phases with the addition of HP1

In cells, euchromatic genomic regions with active histone modifications are typically separate from both heterochromatic regions with inactive histone modifications and inert regions without these characteristic histone modifications. To determine if methylation status of chromatin influenced chromatin sequestration *in vitro*, we mixed unmodified and H3K9me3 chromatin together and saw robust mixing of the two chromatin types (Figure 4.4A, top panel). This indicates the methylation mark on its own does not change any material properties that would inhibit droplet fusion and mixing. However, when HP1α was added to each chromatin solution we saw distinct segregation of unmodified and H3K9me3 chromatin, with a significant enrichment of HP1α into the H3K9me3 phase (Figure 4.4A-B). Therefore, we have reconstituted a minimal system capable of segregating marks characteristic with heterochromatin (H3K9me3 and HP1) from unmodified chromatin, indicating the separation of heterochromatin and euchromatin in cells could be mediated by HP1α phase separation.

The previous experiment was performed at high salt concentrations where chromatin substrates phase separates on their own. We wished to determine whether salt conditions affect this segregation of chromatin domains based on methyl mark. Therefore, 75mM KOAc was used, where neither HP1 nor chromatin arrays phase separate alone, but when mixed form a two-phase solution. At these low salt conditions, we see no segregation of chromatin based on the presence of the methyl mark, and droplets are formed that are enriched for both unmodified chromatin, H3K9me3 chromatin, and HP1 (Figure 4.5, top panel). Lowering salt conditions decreases hydrophobic interactions, so this lack of sequestration could be due to a decreased affinity of HP1 for the methyl mark and increased charge of both the DNA and HP1 basic patches. We next injected the high salt buffer directly into the well containing these miscible droplets, and first visualized a complete dissolution of the droplets. As time went on the droplets re-emerged. Instead of the homogenous concentrations within droplets as seen at low salt, however, we saw HP1 was enriched into the H3K9me3 chromatin and depleted in the regions of unmodified

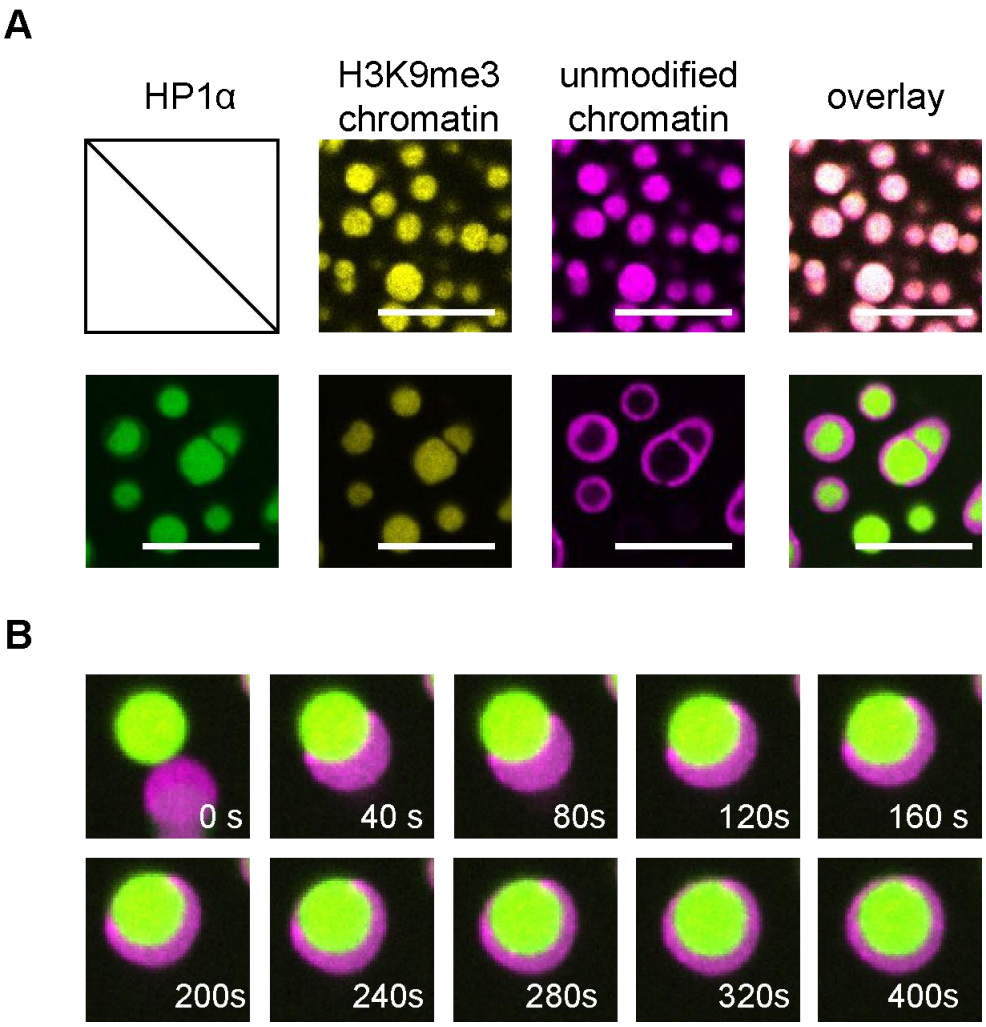

Figure 4.4. De-mixing of chromatin domains based on methylation state in the presence of HP1α. **A.** 12-nucleosome arrays were assembled with either unmodified nucleosomes and cy5-end labeled DNA (magenta) or H3-MLA nucleosomes and cy3-DNA (yellow). Chromatin was mixed in either the presence or absence of HP1α (μM) and 200nM HP1α-488 (green). **B.** Time course of droplet fusion with HP1α included.

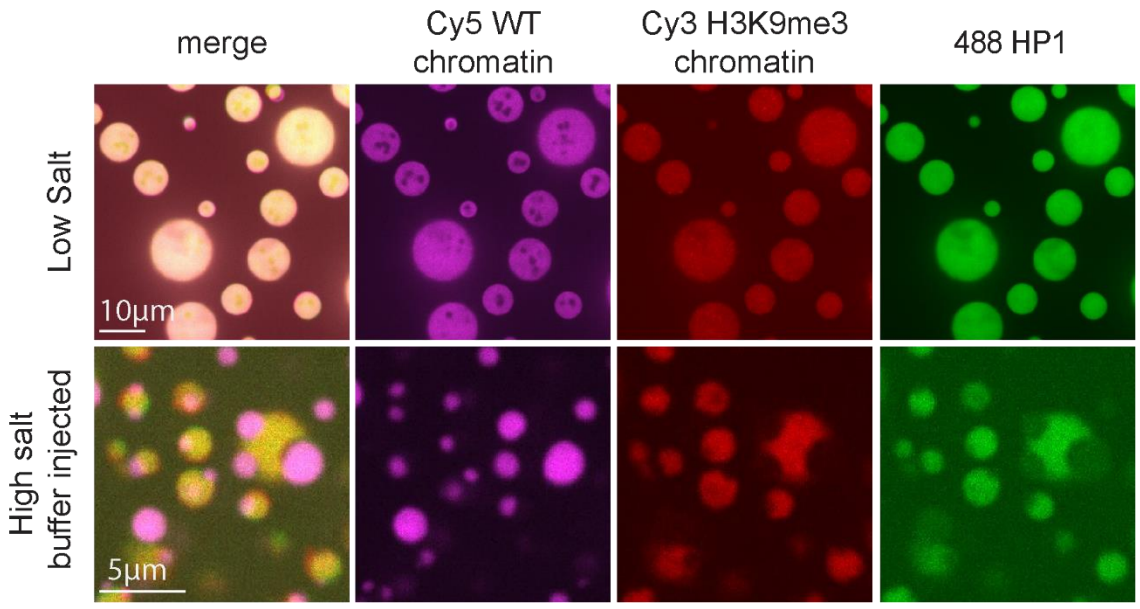

Figure 4.5. Miscibility of WT and H3K9me3 chromatin in the presence of HP1 is dependent on salt concentration. Droplets were initially formed with 1μM WT chromatin labeled with Cy5, 1μM H3K9me3 chromatin (MLA modified) labeled with cy3, 25μM HP1α, and 200nM HP1α-488 in low salt buffer (75mM KOAc). After droplets settled, high salt buffer was injected directly to the well (150mM KOAc, 1mM $Mg(OAc)_2$) and droplets were visualized after a one-hour incubation with high salt.

chromatin (Figure 4.5, bottom panel), similar to the droplets visualized in figure 4.4. This suggests that even on the exact same chromatin substrates and HP1 molecules, the salt concentrations directly impact 1-the preferential binding of HP1 to methylated chromatin and 2-the abrogation of fusion of these two disparate chromatin types. Both experiments demonstrate the HP1 is not entirely depleted in unmodified chromatin but is heavily enriched in the H3K9me3 droplets. Therefore, the same question remains: what does the binding of HP1 do to change the material properties of the methylated droplets such that fusion to unmodified chromatin droplets is now inhibited? It will be fascinating to see what future scientists in the field discover.

Discussion

Chromatin in the nucleus is a complex substrate with a huge variety of histone modifications, variations in DNA linker length and methylation, and the number of binding proteins that control transcriptional output. Further, the concentration of macromolecules is between 100-200mg/ml in the nucleus (Lampert et al., 1966, Viola and Puccinelli, 1965), creating an incredibly crowded nuclear milieu (Hanckock 2014). Yet within this complexity, transcriptional control must be carefully maintained. Just as sequestration of organelles allowed cells to begin specializing functions, creating molecular domains within the nucleus with different functions would be an efficient way to save energy and regulate transcriptional output. The cytological observations that heterochromatin and euchromatin occupy separate nuclear domains and have specialized functions in and of itself is evidence of the emergence of two phases. However, the discovery by Adam Larson and Amy Strom that HP1 phase separates out of solution gave the field new tools to dissect the molecular details of heterochromatic phase separation.

Within this chapter, I have presented evidence that chromatin substrates are capable of inducing the phase separation of HP1α at conditions were neither chromatin nor HP1α form droplets individually. Further, HP1α is preferentially enriched into chromatin with the H3K9me3 mark and is able to maintain the methylated chromatin in separate domains from unmodified chromatin in a salt dependent manner. Given the complexity of nuclear of chromatin substrates

in cells, I propose that this salt dependence could be mimicked in cells via changes in linker length and the binding of protein modulators that change local ionic conditions. Interestingly, the phosphorylation of the H3 helix has been shown to effect DNA binding *in vitro*, and I speculate will have effects on the enrichment of HP1α in chromatin phases as well. While multiple labs have detailed the effect H3K9me3 has on HP1α binding a detailed description of how DNA and chromatin substrates influence the higher-order oligomerization of HP1 proteins has not been examined with the human proteins. I speculate chromatin substrates will change the oligomeric potential differently than naked DNA. Future work delving into the biochemical and structural mechanism of HP1-chromatin phase separation will be essential to further dissect the different cellular cues that induce HP1 activity.

Chapter 5: Materials and Methods

Protein Purification:

General method: Rosetta competent cells (Millipore Sigma 70954) transformed with expression vectors for 6x-HIS tagged HP1 proteins were grown at 37C to an OD600 of 1.0-1.4 in 1 liter of 2xLB supplemented with 25µg/mL chloramphenicol and 50µg/mL carbenicillin. HP1 protein expression was induced by the addition of 0.3mM isopropy-βD-thiogalactopyranoside (IPTG). Cells were then grown for an additional 3 hours at 37C, before pelleting at 4,000xg for 30 minutes. Cell pellets were then resuspended in 30mL Lysis Buffer (20mM HEPES pH7.5, 300mM NaCl, 10% glycerol, 7.5mM Imidazole) supplemented with protease inhibitors (1mM phenylmethanesulfonyl fluoride (Millipore Sigma 78830), 1µg/mL pepstatin A (Millipore Sigma P5318), 2µg/mL aprotinin (Millipore Sigma A1153), and 3µg/mL leupeptin (Millipore Sigma L2884)). Cells were then lysed using a C3 Emulsiflex (ATA Scientific). Lysate was clarified by centrifugation at 25,000xg for 30 minutes. The supernatant was then added to 1mL of Talon cobalt resin (Takara 635652) and incubated with rotation for 1 hour at 4C. The resin-lysate mixture was then added to a gravity column and washed with 50mL of Lysis Buffer. Protein was then eluted in 10mL of elution buffer (20mM HEPES pH 7.5, 150mM KCl, 400mM Imidazole). Then, TEV protease was added to cleave off the 6x-HIS tag and the protein mixture was dialyzed overnight in TEV cleavage buffer (20mM HEPES pH 7.5, 150mM KCl, 3mM DTT) at 4C. The cleaved protein was then further purified by isoelectric focusing using a Mono-Q 4.6/100 PE column (GE Healthcare discontinued) and eluted by salt gradient from 150mM to 800mM KCl over 16 column volumes in buffer containing 20mM HEPES pH 7.5 and 1mM DTT. Protein containing fractions were collected and concentrated in a 10K spin concentrator (Amicon Z740171) to 500µL and then loaded onto a Superdex-75 Increase (GE Healthcare 29148721) sizing column in size exclusion chromatography (SEC) buffer (20mM HEPES pH7.5, 200mM KCl, 1mM DTT, 10% glycerol).

Protein containing fractions were again collected and concentrated to 500μM in a 10K spin concentrator. Finally, aliquots were flash frozen in liquid nitrogen and stored at -80C.

HP1α, HP1β, and HP1γ were all purified as described above. For the terminal extension deletes (HP1αΔNTE, HP1αΔCTE, and HP1αΔNTEΔCTE) minor changes to the ionic strength of buffers were made. Specifically, each protein was dialyzed into a low salt TEV protease buffer (20mM HEPES pH 7.5, 75mM KCl, and 3mM DTT) in the overnight cleavage step. Additionally, the salt gradient used in isoelectric focusing ranged from 75mM to 800mM KCl. The rest of the protocol followed as written above.

The HP1α hinge was purified as written until the overnight TEV cleavage step. After which, the protein was loaded onto a Hi-Trap SP HP column (GE Healthcare 17115201) and eluted in a salt gradient from 150mM to 800mM KCl over 16 column volumes in buffer containing 20mM HEPES and 1mM DTT. Protein containing fractions were collected and concentrated in a 10K spin concentrator to 500μL and then loaded onto a Superdex-30 10/300 increase (GE Healthcare 29219757) sizing column in size exclusion chromatography (SEC) buffer. Protein containing fractions were then collected and concentrated to 500μM in a 10K spin concentrator. Finally, aliquots were flash frozen in liquid nitrogen and stored at -80C.

Protein labelling:

Proteins constructs for fluorescent labelling were modified to contain a C-terminal GSKCK tag and to substitute native reactive cysteines to serine residues (HP1α-C133S and HP1γ-C176S). For labeling, HP1 proteins were dialyzed overnight into SEC buffer with 1mM TCEP substituted for DTT. Protein was then mixed at a 1:1 molar ratio with either maleimide Atto488 or maleimide Atto565 (Millipore Sigma 28562, 18507). The reaction was immediately quenched after mixing by addition of 10x molar excess of 2-mercaptoethanol. Labeled protein was then separated from free dye over a Hi-Trap desalting column ran with SEC buffer (GE Healthcare 17-1408-01). Labeled protein was then flash frozen in liquid nitrogen and stored at -80C.

DNA purification:

Plasmids containing DNA used in this study were amplified in DH5α cells (ThermoFisher 18265017) grown in TB. Plasmids were purified using a Qiagen Plasmid Giga kit (Qiagen 12191) Plasmids containing the “601” DNA sequence were digested with EcoRV (NEB R0195S) and the 147bp fragments were then isolated from the plasmid backbone by PAGE purification. Briefly, DNA was loaded into a 6% acrylamide gel and run at 100mV for ~2 hours in 1xTBE.The desired 147bp DNA band was cut out of the gel and soaked in TE (10mM Tris-HCL pH 7.5, 1mM ETDA) buffer overnight. The supernatant was then filtered, and DNA isolated by two sequential ethanol precipitations. The 2.7kbp DNA (Puc19) was linearized by HindIII (NEB R0104S) digestion and purified by two sequential ethanol precipitations. The 9kbp DNA (pBH4-SNF2h[1]) was linearized by BamHI (NEB R0136S) digestion and purified by two sequential ethanol precipitations.

DNA from bacteriophage λ (λ-DNA) (NEB N3011S) used in phasing and curtains experiments was prepared by heating to 60°C to release base pairing of the cohesive ends in the presence of complementary 12bp primers as previously described[2]. For curtain experiments, the primer targeted to the 3’ overhang of λ-DNA was modified to include a 5’ biotin. λ-DNA and primers were then allowed to slowly cool to room temperature and then incubated overnight with T4 DNA ligase (NEB M0202S). The λ-DNA was then precipitated in 30% PEG(MW 8000) + 10mM $MgCl_2$ to remove excess primers and washed 3 times in 70% ethanol before resuspension and storage in TE.

DNA labeling:

DNA was end-labeled with fluorescent dUTPs as follows. 50µg linear 2.7kbp and 9kbp plasmids were incubated with 12.5 units of Klenow 3´→ 5´ exo– (NEB M0212S), 33 µM dATP, dCTP, dGTP (Allstar scientific 471-5DN), and either 33µM of either ChromaTide™ Alexa Fluor™ 568-5-dUTP (ThermoFischer Scientific C11399) or ChromaTide™ Alexa Fluor™ 488-5-dUTP (ThermoFischer Scientific C11397) in 1x T4 DNA ligase buffer (NEB B0202S) at room temperature overnight.

Fluorescently labeled DNA was then purified by ethanol precipitation, resuspended in 1xTE, and dialyzed overnight in 1xTE to remove any residual nucleotides.

DNA was biotinylated by performing fill-in reactions with 5U Klenow exo- fragment (NEB M0212S) and 0.8 mM dTTP, 0.8 mM dGTP, 3.2 μM bio-dCTP, 8 μM bio-dATP (NEB N0446S, Thermo Fisher 19518018, R0081). The reaction was incubated at room temperature overnight and then DNA were purified by ethanol precipitation. Purified DNA were then resuspended in 1xTE to a working concentration of 4mg/mL.

Curtain Assays:

DNA curtain experiments were prepared and executed as described elsewhere[2,3]. Briefly, UV lithography was used to pattern chromium onto a quartz microscope slide, which was then assembled into a flowcell (Figure 1A). A lipid bilayer was established within the flowcell by injecting a lipids mix containing 400ug/mL DOPC, 40ug/mL PEG-2000 DOPE, and 20 ug/mL biotinylated DOPE (Avanti Polar Lipids 850375, 880130, and 870273) diluted in lipids buffer (100mM NaCl, 10mM Tris pH 7.5). Streptavidin, diluted in BSA buffer (20mM HEPES pH7.5, 70mM KCl, 20 μg/mL BSA, and 1mM DTT), was then injected into the flowcell at a concentration of 30 μg/mL. Biotinylated DNA from bacteriophage λ, prepared as described above, was then injected into the flowcell and anchored to the bilayer via a biotin-streptavidin linkage. Buffer flow was then used to align the DNA at the nanofabricated barriers and maintain the curtain in an extended conformation during experiments.

End-labeling of DNA was accomplished using dCas9 molecules. Specifically, dCas9 (IDT 1081066), Alt-R CRISPR-Cas9 tracrRNA (IDT 1072532), and an Alt-R CRISPR-Cas9 crRNA targeting bacteriophage λ at position 47,752 (AUCUGCUGAUGAUCCCUCCG) were purchased from IDT (Integrated DNA Technologies). Guide RNAs were generated by mixing 10μM crRNA and 10μM tracrRNA in in Nuclease-Free Duplex Buffer (IDT 11050112), heating to 95C for 5 min and then slowly cooling to room temperature. Guide RNAs were then aliquoted and stored at -20C.

To prepare Cas9 RNPs for labeling, 200nM of dCas9 was mixed with 1μM of guide RNA in dCas9 Hybridization Buffer (30mM HEPES pH 7.5 and 150mM KCl) and incubated for 10 minutes at room temperature. Next, 166nM of the dCas9-RNA mixture was incubated with 0.08mg/mL of 6x-His Tag Antibody conjugated with Alexa Fluor 555 (Invitrogen MA1-135-A555) on ice for 10 minutes. Labeled RNPs were then diluted in BSA buffer and injected into the flowcell at a final concentration of 4nM. Labeled dCas9 were allowed to incubate with DNA in the flowcell for 10 minutes before being washed out using imaging buffer (BSA Buffer supplemented with an oxygen scavenging system consisting of 50nM protocatechuate 3,4-dioxygenase (Fisher Scientific ICN15197505) and 31μM protocatechuic acid (Abcam ab142937)). Experiments where DNA are labeled, imaging buffer included 20pM YOYO-1 (Thermo Fisher Y3601).

For compaction experiments, HP1 proteins were diluted to the stated concentration in imaging buffer and injected into the flowcell at a rate of 0.7mL/min. The volume of protein injected was decided based on protein concentration: for experiments with 50μM protein, 100μL was injected, for 5μM protein, 200μL was injected, and for 500nM protein, 400μL was injected. For experiments utilizing fluorescent HP1, 200nM HP1α-488 was included in the injection 50μM HP1α, 100nM HP1α-488 was included in the injection 5μM HP1α, 400nM HP1β-488 was included in the injection of 50μM HP1β, and 400nM HP1γ-488 was included in the injection of 50μM HP1γ. After each experiment, HP1 was removed by washing 0.5M KCl, and replicates performed. Data was analyzed as described below.

HP1α binding site size:

The end to end distance of an HP1α dimer in the closed conformation is 12.9nm. The end to end distance of a phosphorylated HP1α dimer phosphorylated in the open conformation is 22.2nm[4]. Assuming 0.34nm/bp, we estimate the minimal binding unit of a HP1α dimer in the open conformation is ~65bp.

Phasing Assays:

HP1 condensates were imaged using microscopy grade 384 well plates (Sigma-Aldrich M4437). Prior to use, individual wells were washed with 100µL of 2% Hellmanex (Sigma-Aldrich Z805939) for 1 hour. Then wells were rinsed 3 times with water and 0.5M NaOH was added to each well for 30 minutes before again rinsing 3 times with water. Next, 100µL of 20mg/mL PEG-silane MW-5000 (Laysan Bio MPEG-SIL-5000) dissolved in 95% EtOH was pipetted into each well and left overnight at 4C protected from light. Next, wells were rinsed 3 times with water and 100mg/mL BSA (Fisher Scientific BP1600) was pipetted into each well and allowed to incubate for 30 minutes. Finally, wells were rinsed 3 times with water and 3 times with 1x phasing buffer (20mM HEPES pH 7.5, 70mM KCl, and 1mM DTT) was added to each well. Care was taken to maintain 10µL of volume at the bottom of the well in all steps to prevent drying of the PEG Silane coating of the bottom of the well.

In preparation of experiments, HP1 proteins and DNA substrates were dialyzed overnight into 1x phasing buffer. Then, Protein and DNA were added to a 1.5mL microcentrifuge tube at 1.5x of the final concentration stated in results. Excess phasing buffer was removed from cleaned wells and exactly 10µL of 1x phasing buffer was added to the bottom of the well. Then 20µL of the protein-DNA solution was then added to the well, resulting in a 30µL solution of DNA and protein at the concentrations reported in the results section.

To generate the phase diagram for HP1α (Figure 2.3A), determine condensate radius (Figure 2.3B, Figure 2.4A), and for general condensate assays in Figure 2.3 D-E, Figure2.4C-D, Figure 3.1D-E, Figure 3.3A-B, Figure 3.5F-G,I, Figure 3.7D-E, Figure 3.8A, and Figure 4.1, condensates were visualized by brightfield microscopy at 20X magnification. Condensates were prepared as described above and allowed to incubate for 1 hour at room temperature before imaging. However, for droplet coalescence assays (Figure 2.3D), droplets were visualized immediately after the reactions were added to the well. The assays in Figure 2.5A-F, Figure 2.6A,

Figure 2.7, Figure 3.8B-C, Figure 4.2, Figure 4.3, Figure 4.4, Figure 4.5 were imaged by spinning disk confocal microscopy at 100x Magnification.

For the mixing assays in Figure 2.5D and Figure 2.7D, 100μM HP1α was mixed with 50ng/μl 2.7kbp DNA in 1x phasing buffer for five minutes in two separate reactions with an additional 200nM HP1α-488 or 200nM HP1α-565 added to each reaction. Then, a single-color reaction was added to a well, briefly imaged, followed by addition of the remaining reaction. The DNA mixing experiments in Figure 2.5E and Figure 2.7E were experiments performed identically to above, except the reactions were prepared using either 50ng/μl 2.7kb-488 or 50ng/μl 2.7kb-565 and unlabeled protein.

For the MNase assays in Figure 2.5F, condensates were formed by incubating 50μM HP1α and either 12.5ng/μl 9kbp-488 or 12.5ng/μl 9kbp-565 for 5 minutes. Then individual reactions were mixed and incubated at room temperature for one hour prior to imaging. MNase digestion was initiated by the addition of 1mM $CaCl_2$ and 20U MNase (NEB M0247S) and mock reactions were initiated by addition of 1mM $CaCl_2$ alone.

For the competition experiments in Figure 3.8A, HP1α was first mixed with either HP1β or HP1γ to the stated final concentrations. This solution was then added to 147bp DNA (250nM final concentration) and allowed to incubate for 1 hour at room temperature prior to imaging.

For the competition experiments in Figure 3.8B-C, condensates were formed with 50μM HP1α, 200nM HP1α-565, and 250nM 147bp DNA and incubated for 1 hour at room temperature before briefly imaging. Then, either HP1β-488 or HP1γ-488 was added to the reaction to final concentrations of 50μM unlabeled protein and 200nM fluorescent protein.

Droplet Segmentation Analysis:

Many images of HP1-DNA condensates were collected by brightfield microscopy. Segmenting these droplets presented multiple challenges. For example, the rings of high and low intensity at the edges of the droplets and the fact that the intensity inside droplets is almost the same as background intensity. These factors made analysis with basic threshold segmentation

difficult. To overcome these difficulties, we created a custom approach utilizing edge detection and several filters (figure supplement 2.1B). We first high pass filter the image in Fourier space. Then we detect the edges of condensates with a Canny edge detector (scikit-image.org). Canny edge detection applies a Gaussian filter to smooth the image before taking the gradient. We found that larger condensates were detected more readily when larger values for the variance of the Gaussian filter were used and smaller condensates when smaller values were used. To implement adaptive smoothing, we calculated the edges across a range of sigma values before combining the segments into a single detected image. This method introduced a significant amount of noise. To remove this noise, we utilized two thresholds: one for condensate area (condensates must be larger than 3 pixels) and the other for condensate eccentricity (condensates must have eccentricity at or less than 0.94).

We segmented at least five separate images for each DNA and protein concentration tested and collected the radius of each detected condensate (Figure 2.3B-C). Then we determined the complementary cumulative distribution (CCD) for condensate radius at each condition (Figure 2.4). Confidence intervals for each CCD were determined by the Bootstrap method. Finally, each curve was integrated to determine the expectation value of the radius for each condition (Figure 2.3B-C).

FRAP Assays:

For HP1α FRAP experiments, condensates were formed with 100μM HP1α, 250nM HP1α-488, and 50ng/μl of either linear 147bp, 2.7kbp, 9kbp, or 48.5kbp DNA (see above, DNA purification). For DNA FRAP experiments, condensates were formed with 100μM HP1α, 100nM YOYO-1 (Thermo Fisher Y3601), and 50ng/μl of either linear 147bp, 2.7kbp, 9kbp, or 48.5kbp DNA. Samples were then imaged at room temperature (and 5% CO_2 for line FRAP experiments). For each photobleaching experiment, automatic focus was activated, pixel binning was set at 2x2, and exposure time was set at 300ms. For the line FRAP, a 3x512 pixel rectangle was irradiated with 7mW power at 476nm (Integrated Laser Engine, Andor) one time for 300ms between the

25th and 26th acquired frame. For the whole droplet FRAP, a custom rectangle surrounding a single condensate was irradiated five times with 7mW power at 476nm for 300ms between the 10th and 11th acquired frame. Recovery times to half max ($t_{1/2}$) were calculated using a biexponential fit.

Line FRAP analysis:

Line FRAP analysis was performed with a custom R-script. Unbleached condensates, used for normalization, were segmented by threshold. The ROI of bleached regions of condensates (FRAP ROI) was user-defined during imaging. The intensity of the bleached and unbleached condensates as well as background were measured over time. First, the background was subtracted from the FRAP ROI and the unbleached droplets. Then, the FRAP ROI was normalized via the following equation:

$$\frac{I_{FRAP}(t)}{I_{FRAP}(0)} \Big/ \frac{I_{unbleached}(t)}{I_{unbleached}(0)}$$

The normalized intensity was then plotted as a function of time (Figure 2.5B, Figure 2.7B) and fit to a bi-exponential fit to determine $t_{1/2}$ values (Figure 2.5C, Figure 2.7C).

Whole drop FRAP:

Droplets were formed with 100μM HP1α, 250nM HP1α-488, and 50ng/μl 2.7kbp DNA and imaged as described. A square ROI incorporating an entire droplet was photobleached and recovery visualized over ten minutes (Figure 2.6).

Unbleached condensates, used for normalization, were segmented by threshold. Due to diffusion and, potentially, the chemical environment of condensates, HP1α fluorescence decays differently inside of droplets relative to background. Therefore, we only use the signal from the fluorescent HP1α within droplets to correct for fluorescence recovery. Additionally, intensity values near the boundary of droplets were omitted from the analysis due to intensity fluctuations resulting from droplet motion. Furthermore, droplets local to the bleached condensate are affected

by the bleach strike and are removed from the analysis. Then, we fit the time-dependent decay of condensate fluorescence to a bi-exponential decay equation (figure supplement 3.2B-C).

$$y(t) = ae^{-k_1 t} + be^{-k_2 t}$$

We would then normalize the intensity of the bleached condensate by dividing through by the average decay of unbleached droplets from this equation. However, the intensity of the fluorescent HP1α also decays differently depending on its location within the field of view due to non-homogenous illumination of the sample (Figure 2.6D). We therefore scale the decay rates of the unbleached droplets in the following way to correct for spatial variation:

$$\bar{y}(t) = \langle a \rangle e^{-k_1(x,y)t} + \langle b \rangle e^{-k_2(x,y)t}$$

$$k_1(x,y) = k_1^0 + x\alpha_1 + y\beta_1$$

$$k_2(x,y) = k_2^0 + x\alpha_2 + y\beta_2$$

where α and β and k_1^0 and k_2^0 are the slopes and intercepts from a linear regression of decay rate versus position in the image, $\langle a \rangle$ and $\langle b \rangle$ are the average population factors, and $\bar{y}(t)$ is the adjusted intensity signal.

Next, we use the average corrected rate values from all of the unbleached condensates to normalize the intensity versus time for all the unbleached droplets. We then use the normalized unbleached intensity versus time to visualize the expected spread of the data, which we use as a visual measure of error (Figure 2.6E). Finally, we plot the normalized intensity of the bleached condensate against this unbleached distribution to visualize the extent of fluorescence recovery (Figure 2.6E).

Optical Trap:

Optical trapping experiments were performed on a Lumicks C-Trap G2 system (Lumicks) or a custom-built dual trap. Trapping experiments were performed in specialized flowcells with separate laminar flow channels. For each experiment, two streptavidin coated polystyrene beads (Spherotec SVP-40-5), diluted in HP1 buffer to 2.2nM (20mM HEPES pH 7.5, 70mM KOAc,

0.2mg/mL BSA, 1mM DTT), were captured. Then, the two beads were moved into a channel containing biotinylated λ-DNA diluted to ~0.5μg/mL in HP1 buffer. Then, using an automated "tether-finder" routine, a single strand of DNA was tethered between two beads. Each DNA strand was stretched at a rate of 0.1um per second to a maximal force of 40pN in the buffer-only channel two separate times to measure the force extension curve without HP1 present. Next, trapped DNA molecules were moved to a flow channel containing 10μM HP1α and 400nM HP1α-565 and incubated at 5-5.5μm extension for 30 seconds. We then perform stretch-relax cycles (SRC) either with or without waiting periods in the extended or relaxed configurations (Figure 2.9C).

For SRCs with no waiting periods (Figure 2.9C, Figure 2.9A), we performed fifteen SRCs to a maximal force of 40pN in HP1 buffer with 10μM HP1α and 400nM HP1α-565. For SRCs with waiting periods, we performed three consecutive SRCs to a maximal force of 25pN in HP1 buffer with 10μM HP1α and no additional fluorescent protein. We then moved the DNA tether into a channel containing either HP1 buffer or HP1 buffer supplemented with 500mM KCl and performed three additional SRCs (Figure 2.9D-E)

Anisotropy:

Prior to anisotropy experiments, HP1α, HP1β, and HP1γ were dialyzed overnight into binding buffer (20mM HEPES pH 7.5, 70mM KCl, and 1mM DTT) at 4C. 60bp DNA oligos containing a 5'FAM modification (supplementary table) were purchased from IDT (Integrated DNA technologies) and diluted to a final concentration of 10nM in reactions. Binding reactions were then performed in binding buffer supplemented with 0.1mg/mL BSA and variable amounts of HP1 proteins as indicated. Reactions were incubated for 30 minutes at room temperature in Corning Low Volume 384 well plates (Corning LCS3821) then measurements were performed on an Analyst HT (Molecular Devices). Data from three independent HP1 titrations were normalized by subtracting the anisotropy value of FAM-60bp DNA with no added HP1 from each concentration then fit to a one site binding curve and presented with standard errors.

Table 5.1. Protein sequences used in this study
Chromodomains (CD) and chromoshadow domains (CSD) are indicated in bold. A 6xHis tag followed by TEV cleavage site tag (MGHHHHHHDYDIPTTENLYFQGS) was appended to each construct for purification

HP1α	GKKTKRTADSSSSEDEE**EYVVEKVLDRRVVKGQVEYLLKWKGFSEEHNT WEPEKNLDCPELISEFM**KKYKKMKEGENNKPREKSESNKRKSNFSNSADDI KSKKKREQSNDIAR**GFERGLEPEKIIGATDSCGDLMFLMKWKDTDEADLVL AKEANVKCPQIVIAFYEERLTWHAY**PEDAENKEKETAKS
HP1β	MGKKQNKKKVEEVLEEEEE**EYVVEKVLDRRVVKGKVEYLLKWKGFSDED NTWEPEENLDCPDLIAEFL**QSQKTAHETDKSEGGKRKADSDSEDKGEESK PKKKKEESEKPR**GFARGLEPERIIGATDSSGELMFLMKWKNSDEADLVPA KEANVKCPQVVISFYEERLTWHSY**PSEDDDKKDDKN
HP1γ	ASNKTTLQKMGKKQNGKSKKVEEAEPE**EFVVEKVLDRRVVNGKVEYFLKW KGFTDADNTWEPEENLDCPELIEAFLNSQ**KAGKEKDGTKRKSLSDSESDD SKSKKKRDAADKPR**GFARGLDPERIIGATDSSGELMFLMKWKDSDEADLV LAKEANMKCPQIVIAFYEERLTWHSC**PEDEAQ
HP1α hinge	KKYKKMKEGENNKPREKSESNKRKSNFSNSADDIKSKKKREQSNDIAR
HP1α ΔNTE	**EYVVEKVLDRRVVKGQVEYLLKWKGFSEEHNTWEPEKNLDCPELISEFM**K KYKKMKEGENNKPREKSESNKRKSNFSNSADDIKSKKKREQSNDIAR**GFER GLEPEKIIGATDSCGDLMFLMKWKDTDEADLVLAKEANVKCPQIVIAFYEE RLTWHAY**PEDAENKEKETAKS
HP1α ΔCTE	GKKTKRTADSSSSEDEE**EYVVEKVLDRRVVKGQVEYLLKWKGFSEEHNT WEPEKNLDCPELISEFM**KKYKKMKEGENNKPREKSESNKRKSNFSNSADDI KSKKKREQSNDIAR**GFERGLEPEKIIGATDSCGDLMFLMKWKDTDEADLVL AKEANVKCPQIVIAFYEERLTWHAY**
HP1α ΔNTEΔCTE	**EYVVEKVLDRRVVKGQVEYLLKWKGFSEEHNTWEPEKNLDCPELISEFM**K KYKKMKEGENNKPREKSESNKRKSNFSNSADDIKSKKKREQSNDIAR**GFER GLEPEKIIGATDSCGDLMFLMKWKDTDEADLVLAKEANVKCPQIVIAFYEE RLTWHAY**
HP1α β-hinge	GKKTKRTADSSSSEDEE**EYVVEKVLDRRVVKGQVEYLLKWKGFSEEHNT WEPEKNLDCPELISEFM**QSQKTAHETDKSEGGKRKADSDSEDKGEESKPK KKKEESEKPR**GFERGLEPEKIIGATDSCGDLMFLMKWKDTDEADLVLAKE ANVKCPQIVIAFYEERLTWHAY**PEDAENKEKETAKS

HP1α γ-hinge	GKKTKRTADSSSSEDEE**EYVVEKVLDRRVVKGQVEYLLKWKGFSEEHNT WEPEKNLDCPELISEFM**KAGKEKDGTKRKSLSDSESDDSKSKKKRDAADK PR**GFERGLEPEKIIGATDSCGDLMFLMKWKDTDEADLVLAKEANVKCPQI VIAFYEERLTWHAY**PEDAENKEKETAKS
HP1β α-hinge	MGKKQNKKKVEEVLEEEEEE**EYVVEKVLDRRVVKGKVEYLLKWKGFSDED NTWEPEENLDCPDLIAEFL**KKYKKMKEGENNKPREKSESNKRKSNFSNSA DDIKSKKKREQSNDIAR**GFARGLEPERIIGATDSSGELMFLMKWKNSDEAD LVPAKEANVKCPQVVISFYEERLTWHSY**PSEDDDKKDDKN
HP1γ α-hinge	ASNKTTLQKMGKKQNGKSKKVEEAEPE**EFVVEKVLDRRVVNGKVEYFLKW KGFTDADNTWEPEENLDCPELIEAFLNSQ**KKYKKMKEGENNKPREKSESN KRKSNFSNSADDIKSKKKREQSNDIAR**GFARGLDPERIIGATDSSGELMFLM KWKDSDEADLVLAKEANMKCPQIVIAFYEERLTWHSC**PEDEAQ
DNA for anisotropy	5'FAM-TAGTCAATAAACCGGTAAACCAGCAATAGACATAAGCGGCTATTTAACGA CCCTGCCCTG

References

1.Zhao, T., Heyduk, T., Allis, C. D. & Eissenberg, J. C. Heterochromatin Protein 1 Binds to Nucleosomes and DNA in Vitro. *J Biol Chem* **275**, 28332–28338 (2000).

2.Yuan, K., Shermoen, A. W. & O'Farrell, P. H. Illuminating DNA replication during Drosophila development using TALE-lights. *Curr Biol* **24**, R144–R145 (2014).

3.Yuan, K. & O'Farrell, P. H. TALE-light imaging reveals maternally guided, H3K9me2/3-independent emergence of functional heterochromatin in Drosophila embryos. *Gene Dev* **30**, 579–593 (2016).

4.Wang, M. D. *et al.* Force and Velocity Measured for Single Molecules of RNA Polymerase. *Science* **282**, 902–907 (1998).

5.Wallrath, L. L. & Elgin, S. C. Position effect variegation in Drosophila is associated with an altered chromatin structure. *Gene Dev* **9**, 1263–1277 (1995).

6.Umbetova, G. H., Belyaeva, E. S., Baricheva, E. M. & Zhimulev, I. F. Cytogenetic and molecular aspects of position effect variegation in Drosophila melanogaster. *Chromosoma* **101**, 55–61 (1991).

7.Tartof, K. D., Hobbs, C. & Jones, M. A structural basis for variegating position effects. *Cell* **37**, 869–878 (1984).

8.Sun, X., Le, H. D., Wahlstrom, J. M. & Karpen, G. H. Sequence Analysis of a Functional Drosophila Centromere. *Genome Res* **13**, 182–194 (2003).

9.Sugimoto, K., Yamada, T., Muro, Y. & Himeno, M. Human Homolog of Drosophila Heterochromatin-Associated Protein 1 (HP1) Is a DNA-Binding Protein Which Possesses a DNA-Binding Motif with Weak Similarity to That of Human Centromere Protein C (CENP-C). *J Biochem* **120**, 153–159 (1996).

10.Shimada, J. & Yamakawa, H. Ring-closure probabilities for twisted wormlike chains. Application to DNA. *Macromolecules* **17**, 689–698 (1984).

11.Schultz, J. Variegation in Drosophila and the Inert Chromosome Regions. *Proc National Acad Sci* **22**, 27–33 (1936).

12.Sanulli, S. *et al.* HP1 reshapes nucleosome core to promote phase separation of heterochromatin. *Nature* **575**, 390–394 (2019).

13.Ryan, D. P. & Tremethick, D. J. The interplay between H2A.Z and H3K9 methylation in regulating HP1α binding to linker histone-containing chromatin. *Nucleic Acids Res* **46**, gky632-(2018).

14.Richart, A. N., Brunner, C. I. W., Stott, K., Murzina, N. V. & Thomas, J. O. Characterization of Chromoshadow Domain-mediated Binding of Heterochromatin Protein 1α (HP1α) to Histone H3*. *J Biological Chem* **287**, 18730–18737 (2012).

15.Rhind, N. & Gilbert, D. M. DNA Replication Timing. *Csh Perspect Biol* **5**, a010132 (2013).

16.Radic, M. Z., Lundgren, K. & Hamkalo, B. A. Curvature of mouse satellite DNA and condensation of heterochromatin. *Cell* **50**, 1101–1108 (1987).

17.Plys, A. J. *et al.* Phase separation of Polycomb-repressive complex 1 is governed by a charged disordered region of CBX2. *Gene Dev* **33**, 799–813 (2019).

18.Overbeek, J. T. G. & Voorn, M. J. Phase separation in polyelectrolyte solutions. Theory of complex coacervation. *J Cell Compar Physl* **49**, 7–26 (1957).

19.Ostrovsky, B. & Bar-Yam, Y. Motion of polymer ends in homopolymer and heteropolymer collapse. *Biophys J* **68**, 1694–1698 (1995).

20.Nielsen, P. R. *et al.* Structure of the HP1 chromodomain bound to histone H3 methylated at lysine 9. *Nature* **416**, 103–107 (2002).

21.Muller, H. J. Types of visible variations induced by X-rays inDrosophila. *J Genet* **22**, 299–334 (1930).

22.Mishima, Y. *et al.* Hinge and Chromoshadow of HP1α Participate in Recognition of K9 Methylated Histone H3 in Nucleosomes. *J Mol Biol* **425**, 54–70 (2013).

23.Mirny, L. A. The fractal globule as a model of chromatin architecture in the cell. *Chromosome Res* **19**, 37–51 (2011).

24.Martinez-Balbas, A. *et al.* Satellite DNAs contain sequences that induce curvature. *Biochemistry-us* **29**, 2342–2348 (1990).

25.Marsano, R. M., Giordano, E., Messina, G. & Dimitri, P. A New Portrait of Constitutive Heterochromatin: Lessons from Drosophila melanogaster. *Trends Genet* **35**, 615–631 (2019).

26.Lau, M. S. *et al.* Mutation of a nucleosome compaction region disrupts Polycomb-mediated axial patterning. *Science* **355**, 1081–1084 (2017).

27.Kilic, S., Bachmann, A. L., Bryan, L. C. & Fierz, B. Multivalency governs HP1α association dynamics with the silent chromatin state. *Nat Commun* **6**, 7313 (2015).

28.Jr, W. M. A. & Keating, C. D. Phosphorylation-mediated RNA/peptide complex coacervation as a model for intracellular liquid organelles. *Nat Chem* **8**, 129–137 (2016).

29.James, T. C. & Elgin, S. C. Identification of a nonhistone chromosomal protein associated with heterochromatin in Drosophila melanogaster and its gene. *Mol Cell Biol* **6**, 3862–3872 (1986).

30.Hiragami-Hamada, K. *et al.* Dynamic and flexible H3K9me3 bridging via HP1β dimerization establishes a plastic state of condensed chromatin. *Nat Commun* **7**, 11310 (2016).

31.Henikoff, S. Position-effect variegation and chromosome structure of a heat shock puff in Drosophila. *Chromosoma* **83**, 381–393 (1981).

32.Hathaway, N. A. *et al.* Dynamics and Memory of Heterochromatin in Living Cells. *Cell* **149**, 1447–1460 (2012).

33.Grigoryev, S. A. & Woodcock, C. L. Chromatin organization — The 30nm fiber. *Exp Cell Res* **318**, 1448–1455 (2012).

34.Grau, D. J. *et al.* Compaction of chromatin by diverse Polycomb group proteins requires localized regions of high charge. *Gene Dev* **25**, 2210–2221 (2011).

35.Gibson, B. A. *et al.* Organization of Chromatin by Intrinsic and Regulated Phase Separation. *Cell* **179**, 470-484.e21 (2019).

36.Galburt, E. A. *et al.* Backtracking determines the force sensitivity of RNAP II in a factor-dependent manner. *Nature* **446**, 820–823 (2007).

37.Funk, M., Hegemann, J. H. & Philippsen, P. Chromatin digestion with restriction endonucleases reveals 150–160 bp of protected DNA in the centromere of chromosome XIV in Saccharomyces cerevisiae. *Mol Gen Genetics Mgg* **219**, 153–160 (1989).

38.Francis, N. J., Kingston, R. E. & Woodcock, C. L. Chromatin Compaction by a Polycomb Group Protein Complex. *Science* **306**, 1574–1577 (2004).

39.Fitzgerald, D. J., Dryden, G. L., Bronson, E. C., Williams, J. S. & Anderson, J. N. Conserved patterns of bending in satellite and nucleosome positioning DNA. *J Biological Chem* **269**, 21303–14 (1994).

40.Erdel, F. *et al.* Mouse Heterochromatin Adopts Digital Compaction States without Showing Hallmarks of HP1-Driven Liquid-Liquid Phase Separation. *Mol Cell* **78**, 236-249.e7 (2020).

41.Elgin, S. C. R. & Reuter, G. Position-Effect Variegation, Heterochromatin Formation, and Gene Silencing in Drosophila. *Csh Perspect Biol* **5**, a017780 (2013).

42.Eissenberg, J. C. *et al.* Mutation in a heterochromatin-specific chromosomal protein is associated with suppression of position-effect variegation in Drosophila melanogaster. *Proc National Acad Sci* **87**, 9923–9927 (1990).

43.Demerec, M. & Slizynska, H. Mottled White 258-18 of Drosophila Melanogaster. *Genetics* **22**, 641–9 (1937).

44.Dawson, M. A. *et al.* JAK2 phosphorylates histone H3Y41 and excludes HP1α from chromatin. *Nature* **461**, 819 (2009).

45.Cowieson, N. P., Partridge, J. F., Allshire, R. C. & McLaughlin, P. J. Dimerisation of a chromo shadow domain and distinctions from the chromodomain as revealed by structural analysis. *Curr Biol* **10**, 517–525 (2000).

46.Cartwright, I. L., Hertzberg, R. P., Dervan, P. B. & Elgin, S. C. Cleavage of chromatin with methidiumpropyl-EDTA . iron(II). *Proc National Acad Sci* **80**, 3213–3217 (1983).

47.Canzio, D. *et al.* A conformational switch in HP1 releases auto-inhibition to drive heterochromatin assembly. *Nature* **496**, 377 (2013).

48.Canzio, D. *et al.* Chromodomain-Mediated Oligomerization of HP1 Suggests a Nucleosome-Bridging Mechanism for Heterochromatin Assembly. *Mol Cell* **41**, 67–81 (2011).

49.Canzio, D., Larson, A. & Narlikar, G. J. Mechanisms of functional promiscuity by HP1 proteins. *Trends Cell Biol* **24**, 377–386 (2014).

50.Brewer, L. R., Corzett, M. & Balhorn, R. Protamine-Induced Condensation and Decondensation of the Same DNA Molecule. *Science* **286**, 120–123 (1999).

51.Boettiger, A. N. *et al.* Super-resolution imaging reveals distinct chromatin folding for different epigenetic states. *Nature* **529**, 418–422 (2016).

52.Bloom, K. S. & Carbon, J. Yeast centromere DNA is in a unique and highly ordered structure in chromosomes and small circular minichromosomes. *Cell* **29**, 305–317 (1982).

53.Benfante, R., Landsberger, N., Tubiello, G. & Badaracco, G. Sequence-directed curvature of repetitive AluI DNA in constitutive heterochromatin of Artemia franciscana. *Nucleic Acids Res* **17**, 8273–8282 (1989).

54.Becker, H. J. Genetic Mosaics and Cell Differentiation. *Results Problems Cell Differ* 29–49 (1978) doi:10.1007/978-3-540-35803-9_2.

55.Allshire, R. C. & Madhani, H. D. Ten principles of heterochromatin formation and function. *Nat Rev Mol Cell Bio* **19**, 229–244 (2018).

56.Alberti, S., Gladfelter, A. & Mittag, T. Considerations and Challenges in Studying Liquid-Liquid Phase Separation and Biomolecular Condensates. *Cell* **176**, 419–434 (2019).

Publishing Agreement

It is the policy of the University to encourage open access and broad distribution of all theses, dissertations, and manuscripts. The Graduate Division will facilitate the distribution of UCSF theses, dissertations, and manuscripts to the UCSF Library for open access and distribution. UCSF will make such theses, dissertations, and manuscripts accessible to the public and will take reasonable steps to preserve these works in perpetuity.

I hereby grant the non-exclusive, perpetual right to The Regents of the University of California to reproduce, publicly display, distribute, preserve, and publish copies of my thesis, dissertation, or manuscript in any form or media, now existing or later derived, including access online for teaching, research, and public service purposes.

DocuSigned by:
522767A658814CB...
Author Signature

12/15/2020
Date